102p

N64-15879
CODE-1
CR-55409

Methodology of Mission and Systems Synthesis of Manned Planetary Flights with Particular Emphasis on Venus and Mars as Target Planets

by

K. A. Ehricke
Director, Advanced Studies
General Dynamics/Astronautics

1 Jul. 1963

OTS PRICE

XEROX $ 9.10 ph

MICROFILM $ 3.26 mf.

GENERAL DYNAMICS
ASTRONAUTICS

A2136-1 (REV. 6-61)

(NASA CR-55499, AOK63-019) OTS: $

1 July 1963

Methodology of Mission and Systems Synthesis of Manned Planetary Flights with Particular Emphasis on Venus and Mars as Target Planets

by

K. A. Ehricke 1 Jul. 1963 102 p refs
Director, Advanced Studies
General Dynamics/Astronautics, San Diego, Calif.

09741 62

A Study of Early Manned Planetary-Interplanetary Roundtrip Missions, NASA Contract No. NAS8-5026

Prepared for

National Aeronautics and Space Administration
George C. Marshall Space Flight Center
(Future Projects Office)
Huntsville, Alabama

1. INTRODUCTION

This report contains a description of a method for the parametric analysis of planetary roundtrip missions using high acceleration propulsion systems.

The method consists of two parts. The principal difference between these is that in the first part the flight mechanics is based on impulse, maneuvers and the weight estimates are based on the use of the mass fraction x, defined as the sum of propellant weight and wet inert weight divided by the propellant weight.

The second part which is of higher accuracy is based on finite propulsion periods and on the use of scaling coefficients which in the first part were implicitly contained in the definition of the mass fraction. In addition to the tie between performance and weight analyses, the correlations between conceptual or preliminary design and operations analysis and between operations analysis and program analysis are discussed. Program analysis includes the determination of critical development problems, the establishment of development schedules, cost analyses and value analyses.

In the last section of the report, a number of equations and graphs are presented which are of practical value in applying the described methods. The graphs refer to Venus and Mars as target planets.

2. GENERAL APPROACH

Fig. 2-1 shows schematically the evolution of a mission and systems synthesis by progressive development of information in a systematic pattern of interrelation of flight dynamics, design, operations analysis and program analysis. These four principal study areas are outlined in Fig. 2-2.

As seen from this point in time (1963) there are certain fundamental inputs and constraints which must be adopted, since one talks about a state-of-the-art which, as a whole, does not yet exist. Therefore, particular consideration must be given to the following items.

2.1 Mission Objectives

Mission objectives must be defined carefully, so as not to impose unrealistic requirements on technology, funding or manpower. Even within these limits there remains quite a variety of objectives which can be summarized in the following main groups

MO-1 Target Planet: Venus or Mars

MO-2 Mission Profile: Fly-By or Capture

MO-3 Planet Exploration: Orbital or Orbital & Landing

MO-4 Level of Effort: Small or Large Crew Size, Number of Auxiliary Vehicles Information Absorption Density (e.g. average bits/second)

MO-5 Mission Duration: Short Capture Periods (30-50 d)
Long Capture Period (300-400 d)

These groups, either directly or through a number of associated considerations (e.g. crew shielding) affect the payload requirements.

Like the mission objectives, particularly sensitive constraints imposed by the state-of-the-art in the area of Earth launch vehicles (ELV) and propulsion systems must be considered at the outset.

2.2 Earth Launch Vehicles

In the case of planetary flight during the seventies the ELV alternatives are as follows:

(A) Limitation to Apollo-type Saturn V

(B) Uprated Saturn V with Increased Payload
F-1 uprated in S-IC
5 J-2 engines in S-II

(C) Uprated Saturn V with Configuration Changes
Larger diameter of S-IC and S-II

(D) Cluster of Saturn V to one Larger ELV

(E) Post-Saturn

Alternative (A) offers a payload weight into near-Earth orbit of 230,000 to 250,000 lb (104.5 to 113.5 t), a maximum payload volume of 125,000 ft^3 and a maximum payload diameter of approximately 33 ft. The lowest permissible payload density is, therefore, approximately 2 lb/ft^3 for 250,000 lb and 1.8 lb/ft^3 for 230,000 lb.

Alternative (B) offers a payload weight of the order of 280,000 to 300,000 lb while retaining the previous limitations on volume and diameter, resulting in minimum permissible payload densities for the full load of 2.2 and 2.4 lb/ft^3, respectively.

Alternative (C) does not necessarily offer a payload increase over (A), since the effect of higher thrust may largely be compensated for by weight increases associated with the configuration changes (although this is probably a conservative assumption). This alternative, however, offers a larger payload volume which

itself can enhance greatly the usefulness of the Saturn V as ELV for planetary missions. If the diameter is increased to 50 ft, the length of the first two stages is reduced from 216 ft to 112 ft. This fact and the larger diameter increase the available payload volume by a factor of four, to 500,000 ft^3 at the same overall height as the previous versions (370 ft). For a full load of 250,000 lb, the range of permissible payload densities is lowered to 0.5 lb/ft^3. This opening of the permissible density range is important because of the large volumetric requirements for planetary vehicles using liquid hydrogen with nuclear engines and having often odd shapes. Larger payload volume, in terms of larger diameter and greater length of payload section, reduces the amount of matings and other orbital operations involving attachment and detachment of sections. Thereby, in turn, the probability of success in readying this particular space vehicle for orbital departure is increased. Moreover, the procurement level of spare parts, spare modules and spare ELV's, which varies inversely with the probability of successful orbital preparations, is reduced at corresponding reduction in overall operational cost. In enabling the selection of larger tank diameters for the orbital vehicle, the potential for clustering increasing numbers of nuclear engines becomes possible. The importance of this is discussed below in connection with the propulsion system selection.

Alternative (D) involves major changes not only in Saturn V, but also in test and launch facilities. Herein will probably lie the major causes of funding expenditures and delay of operational availability. Nevertheless, a cluster of two or three Saturn V's would raise the payload to some 500,000 to 750,000 lb, at less initial investment than required for a Post-Saturn vehicle, but higher direct operating cost, if compared with a Post-Saturn vehicle which offers the possibility of

reusability not too long after it has become operational.

Alternative (E) involves a completely new vehicle. In the simplest case, it can be a super-Saturn, i.e. use a Lox-RP-1 first stage with a larger number of F-1 engines and an O_2/H_2 second stage with a larger number of J-2 engines or with M-1 engines. This version would be very similar to alternative (D) (except that it would contain larger single tanks), inasmuch as its stages would not be recoverable and similar expenditures for new test and launch facilities would be involved. Taking a somewhat larger step, the first stage can be designed for recovery, thereby making this vehicle partially reusable. This case would correspond to alternative (D), only on a larger scale. Finally, a more advanced concept could be applied, designed to reduce future operating cost. Almost invariably, this will raise required development funds and time; operational availability will be postponed correspondingly. The more advanced the Post-Saturn ELV design, the more important it becomes to understand fully the extent and purpose of its future deployment as well as to obtain reasonable confidence in the repetitiveness of the deep space missions which it is to serve. If a few exploratory manned flights to Venus and Mars were to be the extent of planetary venctures between 10 and 20 years from now, the most modest versions of Post-Saturn or alternative (E) alone would be justifiable, since they will not be used often enough and long enough to amortize higher initial investments, even if their direct operating cost were fairly high. In any case, as far as manned planetary mission and systems synthesis is concerned, the Post-Saturn vehicle offers no significant restrictions. Its payload is to be at least 10^6 lb. The volume of its payload section can be made large enough to be compatible with the shapes of lunar cargo or planetary vehicle requirements.

It is assumed that Post-Saturn can transport complete planetary vehicles, dry or partially fueled, into the initial Earth orbit, thereby removing the need for mating large modules, but retaining the requirement for orbital fueling.

2.3 Propulsion Systems

In the case of propulsion systems the alternatives assumed to exist for manned planetary missions, the seventies are

Chemical (O_2/H_2)

Solid Core Nuclear.

The likely characteristic data for the latter family are classified and therefore not mentioned here. If nuclear engines are considered, a greater amount of vehicle-engine integration work is involved from the outset.

In considering the choice between chemical and nuclear propulsion system, not only I_{sp} and associated orbital departure weights are involved. In addition, the operational life time of the nuclear engine is a most decisive parameter. If this period is short, say 30 to 60 minutes, thrust acceleration rates are required which are higher than those dictated by consideration of gravitational losses versus gain in payload from larger and larger propellant quantities. The higher the specific impulse, the higher can be the gravitational velocity loss before further payload growth is inhibited. This fact by itself provides a possibility of using relatively low-thrust nuclear engines on large vehicles for orbital departure, either singly or in clusters of up to 4 engines. If greater numbers are to be assumed, special minimum diameter requirements may have to be specified for the ELV; or tank + engine clustering must be adopted for the planetary vehicle; this is an example for the interplay between propulsion system selection and vehicle-engine integration with

the vehicle configuration studies in Fig. 2-1. In cases where, due to operational life limitations, the required thrust acceleration rates exceed those which single, or certain clusters of available engines are able to provide, chemical engines, which are less likely to display such limitations, may permit the attainment of larger payloads at the same initial stage weight. Finally, cost is a sensitive parameter in the selection of chemical versus nuclear propulsion systems. The use of nuclear engines for 1973 to 1977 missions is assumed to be charged to the manned planetary program, because this would be the pace setter and their principal "customer". If planetary missions in the 1979 and beyond period are contemplated, this probably is no longer true, because by then general advancements in the state-of-the-art of nuclear engines (since their development would not be discontinued if plans for planetary missions were abandoned) as well as presumably growing demand for advanced cislunar transportation systems would provide engines anyway. For the 1973/77 period, therefore, it is, from the narrower viewpoint of the manned planetary program alone, much less expensive to use chemical engines, as far as development costs are concerned. All-chemically powered planetary vehicles, however, have a much higher orbital departure weight--everything else being the same--than their nuclear or chemo-nuclear counterparts. This, in turn, has repercussions on the ELV; the more so, the relatively smaller the available ELV. Operationally, this reflects itself in a larger number of launchings required, more orbital fueling flights and to some extent more orbital matings. Up to a certain point (by a factor of 2 to 3), the chemical vehicle can be heavier than the nuclear vehicle (because of its higher density) without requiring more orbital matings, since it would essentially fit into the same transportation volume atop the ELV as one out of two or three

modules of the nuclear planetary vehicle. In this case, the chemical vehicle would require more orbital fuelings, the nuclear more orbital matings. As long as orbital matings are (or should be) assumed to have a comparatively lower probability of success than fueling (e.g. 0.95 as compared to 0.98) and--most importantly--as long as failure of a mating process may result in a loss of both modules involved (as compared to the loss of the tanker only in case of failure to fuel), the resulting number of launches that may be required for either vehicle is less different than the difference in orbital departure weight implies. As a result, the direct operating cost for the nuclear vehicle are not decisively lower, if they are lower at all, than for the chemical vehicle. This conclusion, however is no longer correct if improved techniques are available which make the mating process comparable to orbital fueling, because in this case the larger minimum number of flights for the chemical vehicle makes itself felt cost-wise (for 100% reliability for delivery and all orbital operations, the direct operating costs (except for procurement) would differ in direct proportion to the orbital departure weight); or, if the chemical vehicle is so much larger that it, too, requires significant amounts of orbital mating in addition to fueling.

2.4 Mission Modes

The mission mode defines the manner in which the mission is conducted as far as the planetary vehicles are concerned. The three basic mission modes are

Convoy

Single Vehicle

Multiplex Vehicle.

In the convoy mode the various loads are distributed over a number of separate vehicles. In the single vehicle mode, all loads are carried by one vehicle, designed as an integral unit. In the multiplex vehicle mode the individual convoy vehicles are clustered to form one vehicle which can be taken apart, if portions are damaged and must be abandoned, without impeding the capability of the remaining system to function as crew vehicle. The vehicle can be conceived as duplex or as triplex. In the duplex, two larger vehicles are coupled; in the triplex three smaller vehicles are combined. The triplex is less advantageous from the standpoint of crew module integration and associated crew protection against radiation from nuclear reactors; but it shows superior flexibility over the duplex at certain mission energy levels when only small engines (Nerva) are available. In other cases the duplex is superior weightwise.

The single vehicle mode is unsatisfactory from the viewpoint of reliability and crew safety, since this approach denies the crew members the opportunity to save themselves in a secondary vehicle in case the original crew vehicle is incapacitated. The convoy and the multiplex vehicle modes each have a number of characteristics in their favor. These are listed in Tabs. 2-3 and 2-4. It is not the subject of this particular report to analyze the relative weight of the pros and cons of each approach; but rather to characterize the choice between these two principal alternatives as one of the initial inputs in the scheme of Fig. 2-1.

If the convoy mode is adopted, another group of alternatives may require specification, in order to avoid ambiguity.

Fig. 2-3 shows six different modes distinguished by their method of assembling the individual convoy vehicle and/or convoy. In the DFM the fully fueled, operational vehicle is launched into the parking orbit. After it is joined by its

Tab. 2-3 Convoy Versus Multiplex Vehicle

Arguments in favor of convoy:

1. Low overall vulnerability; destructive events which incapacitate one ship not likely to affect the companion ship.

2. Because of 1., convoy offers high insurance that back-up ship will be available to crew in emergency.

3. In case of loss of one vehicle, problems of vehicle separation are avoided.

4. Flexibility in orbital departure weight distribution.

5. No inherent limitations as far as total orbital departure weight is concerned.

6. Freedom in selecting different types of main propulsion systems, if advantageous for any reason.

7. Orbital departure weight is not penalized by need for connecting structure between vehicles.

8. If vehicle spin is required for artificial g, weight penalty associated with spinning the larger mass of a multiplex vehicle is avoided.

9. Simplification of orbital operations by avoiding necessity to couple two large systems. Coupling would have to be in parallel which is inherently more difficult than coupling in series.

10. Higher probability of successful departure, since it is easier to provide a single back-up convoy ship than a back-up duplex.

11. Because of 9., higher success probability of departure on time at lower cost, since procurement need not consider potential failure and damages in the final coupling process of a duplex vehicle.

Tab. 2-4 Multiplex Vehicle Versus Convoy

Arguments in favor of multiplex vehicle:

1. Simplified engine start control and flight control during powered maneuvers.

2. Crew module transfer from one ship to another in case of emergency is avoided.

3. Good accessibility of auxiliary vehicles; this facilitates their checkout and launch preparations.

4. Because of 3., need for taxi capsules may be eliminated.

5. Lighter weight of meteoroid and heat shield for tanks, since multiplex tanks partially shield each other)it is assumed that damaged tanks are not jettisoned; in case of engine failure, only the engine and a small tank section are jettisoned)

6. Because of 5, easier access to tanks and easier propellant transfer if needed.

7. Transfer of individual tanks and associated demating and mating processes are avoided (Note: this can be avoided also for convoy vehicles by carrying empty spare tanks on board at moderate weight penalty).

8. Problems of intra-convoy vehicle maneuvering (path alignment with lead vehicle) are avoided.

9. Because of 8., superior safety that crew will not accidentally be irradiated by nuclear reactors of the companion ship.

10. Because of 8., lower propulsion weight required for attitude and path control during transfer and capture.

companion vehicles the convoy departs. In OVAM, the vehicles are assembled in Earth orbit. This can be done either by deliverying vehicle and payload separately; or by mating a number (two or three) of fueled modules; or, by transporting the entire vehicle unfueled into orbit where it is fueled by separate tanks; or it can be done in a combination of the two latter alternatives, i.e. either by mating two dry modules in orbit and then fuel or by sending the assembled vehicle into orbit partially fueled and complete the fueling process in orbit. The latter two cases depend on whether the launch vehicle has enough payload weight capability and volume in its payload section to carry the fully assembled dry convoy vehicle into orbit or; whether the launch vehicle has adequate volume and enough payload capability for the convoy vehicle to be delivered in partially fueled condition.

In IVAM and COVAM the departing vehicles are lighter but they are not self-sufficient. Therefore, two vehicles are required for each self-sufficient one as it would result from OVAM. Modules have to be mated or fuel transferred either during interorbital transfer or in the target planet capture orbit to make the return flight possible. In the combined IVAM/COVAM, four vehicles are needed for every OVAM vehicle; but their weight is considerably lower. Finally, in the modified IVAM, three vehicles are needed in orbit for every OVAM vehicle, of which the second and third (counting from left to right in Fig. 2-3) have the same orbital departure weights as the COVAM vehicles, while the third is of lower weight. This mode is distinguished from IVAM in that only the crew ship payload (primarily the crew modules, Earth entry module and life support system) needs to be transferred, rather than two larger masses to be mated as in IVAM. It is postulated that transfer of the crew ship apyload is a mandatory technological and operational state-of-

the-art requirement in a planetary convoy, to be able to use another ship as crew vehicle, in case the original crew vehicle is incapacitated. The other alternative, namely, carrying another shielded crew module system and life support system along on the back-up vehicle and distributing the crew over both vehicles imposes a considerable weight penalty, inasmuch as the crew modules are heavy and the scientific payload (in terms of various auxiliary vehicles for exploration of the target planet and its environment) is reduced correspondingly. On this premise, therefore, it is assumed that transfer of the crew vehicle payload, as in the modified IVAM or in COVAM involves only an operation which must be perfected anyhow for other reasons; whereas module mating in the depth of interplanetary space, just by the crew alone, implies a comparatively more risky operation; which is one of the draw-backs of IVAM, COVAM and IVAM/COVAM. In the concept of the modified IVAM this draw-back is avoided, albeit at the penalty of a third vehicle; the latter is comparatively small, however, and in most cases does not require orbital mating or fueling, but more likely is a case of DFM.

As an indication of the vehicle weight variations, the effect of the various mission modes is illustrated in Fig. 2-4 for a specific mission profile. The example contains certain simplifications, such as constancy of the crew vehicle payload and of certain mass fraction values, in spite of considerable variations in vehicle weight. This mission is not particularly energetic, because no Earth capture maneuver (M-4) was included (unless it is assumed to be contained in the 10^5 lb); and yet the chemical vehicle weights are so high with any mode that orbital assembly and/or fueling appears necessary, even if a Post-Saturn vehicle were available. In the case of even a comparatively modest nuclear capability, on the other hand,

substitution of OVAM by either mode permits use of the DFM for each individual vehicle. Even with Saturn V many of the vehicles can be delivered either via DFM or in one piece, though only partly, or not at all, fueled.

In addition to ELV limitations, OVAM may lead to orbital departure weights which exceed during one maneuver the permissible operational life of the available nuclear engines, even if arranged in an open cluster. In this case, the smaller departure weights obtained with the other mission modes could be more compatible with available nuclear propulsion capability. Furthermore, OVAM involves the mating of very large and massive modules if a Nova type launch vehicle is used. The other modes involve mating of considerably smaller modules, but mating must occur en route with a smaller crew and fewer resources than in the vicinity of Earth; and with more severe consequences in the event of a failure. Modes other than OVAM are, therefore, of particular interest in cases where nuclear engine thrust magnitude is a limiting factor, and where mating procedures are sufficiently well developed to assume safe handling by the crew en route. The only (favorable) exception is the modified IVAM for reasons stated above.

Again, it is not the objective of this report to evaluate the relative merits of each of these modes. For the methodology, however, the example shows that the considerable variations in orbital departure weight make it necessary to specify the mission mode as one of the significant initial inputs in Fig. 2-1.

2.5 Mission Requirements

The mission requirements are specified by the selection of target planet, departure date, outbound transfer time, capture period and capture orbit, if any, and return transfer time. From the transfer time and the known positions of

departure and target planet at the beginning and termination of the heliocentric transfer, the transfer orbit elements and the hyperbolic excess velocity, i.e. the velocity of the vehicle relative to the planet, are determined. This hyperbolic velocity, v_∞, is the generalized interface between transfer orbit mechanics and performance analysis. All other data, derived from it, such as the characteristics of planetocentric hyperbola and planetocentric velocity changes are, in addition, dependent on specific conditions, namely the periapsis of the planetocentric hyperbola and the eccentricity of the initial or terminal planetocentric orbit. The hyperbolic excess velocity is therefore used here as the common reference for all further computations. Fig. 2-5 surveys the sum of hyperbolic excess velocities at Earth departure and target planet arrival for missions to the planets Mercury through Saturn for Earth departure windows between 1972 and 1999. They show the magnitudes for the planets relative to each other and also show the approximate "bandwidth" connected with each planet between "good" and "poor" mission years. Only transfer in one direction is shown. Return flights, if selected properly are on a comparable or slightly higher level.

The planetary capture round-trip mission consists of two, comparatively independent transfer orbits which are connected by a specified capture period. Figs. 2-6 to 2-11 **show plots of hyperbolic excess velocities connected with outbound and return transfer orbits to and from Mars in 1973/74, 1975/76, 1977/78 and 1981/83. These** plots are separated by a center graph which correlates the Earth departure date with the Mars arrival date, capture period, Mars departure date and Earth arrival date. Any mission window to and from any target planet can be presented in the same manner, together with other possibly significant parameters, such as peri-

helion distance of the transfer orbits. For a selected mission profile, the associated hyperbolic excess velocities then provide an important preliminary indication of the overall mission performance requirement involved.

3. PRELIMINARY MISSION AND SYSTEMS SYNTHESIS

The approach to the preliminary mission and systems synthesis outlined in Fig. 2-1 consists of three main phases.

Phase I consists of performance estimates, vehicle-engine integration and vehicle configuration studies, based on the initial inputs discussed in the preceding section, regarding payload and mission requirements, ELV and propulsion system specifications and selection of the mission mode.

Phase II, based on the results of the first phase, includes a preliminary weight analysis whose main purpose it is to establish scaling coefficients for the engines, propellant quantities and a first estimate of constant weights involved in every stage of the vehicle configurations. These numbers are needed in a preliminary performance analysis and they are useful in varying the size of configurations with varying mission requirements as part of the evaluation of different configurations relative to each others merits. A preliminary operations analysis and program analysis tie aspects of ELV-vehicle integration, operational aspects, success analyses, development problems and cost into the configuration comparison to the extent this is meaningful and needed at that particular phase. Of special significance can be the value analysis whose purpose is twofold:

(a) comparison of the worthwhileness of concepts or of specific improvements (e.g. topping vs. bleed cycle in nuclear engines) as to their immediate operational objectives ("short-term") in terms of technological (failure analysis, success probability, operational characteristics) economical, schedule or mission objective related criteria,

(b) comparison as to their more long-range usefulness under conditions of rapidly changing technological conditions and mission objectives in terms of appropriate criteria (such as growth potential, rate of obsolescence, mission versatility, long-range direct operational cost, etc.).

The value analysis has the purpose of providing a rational check (rejection or justification) on technological or operational concepts which appear highly attractive for one or a few specific reasons, but may be less attractive from a broader aspect.

The second phase should lead to a selection of specific vehicle configurations, mission modes, mission periods and other basic decision items.

Phase III basically a more refined iteration of the second phase and typically will lead to refined mission profile specifications, performance analysis, flight navigation analysis, venicle-engine integration, operations analysis, program analysis and to a preliminary design of the selected configuration. These, in turn, form the basis for a preliminary mission and systems synthesis which, to a sufficient degree of detail, correlates those seven principal areas and displays the proper error and perturbation analyses from the selected standard conditions.

4. METHODOLOGY

In this section the methods of approach to the previously discussed Phases I through III are discussed qualitatively.

4.1 Phase I

A flow chart of the first of three approaches to be discussed is shown in Fig. Selection of a mission window and of a mission profile specifies the following initial inputs:

Mission window: Earth departure window dates D_1 (involving a period of 20, 30 or 40 days) and outgoing transfer time or times T_1 specify a series of values of the hyperbolic excess velocity $v^*_{\infty_1}$ (Earth departure) and $v^*_{\infty_2}$ (target planet arrival).

Target planet departure window dates D_3 and return transfer times T_2 specify a series of values of $v^*_{\infty_3}$ (target planet departure) and $v^*_{\infty_4}$ (Earth arrival).

Mission profile: The heliocentric mission profiles (perihelion distance; inclination of transfer orbit relative to ecliptic and orbit plane of target planet; path angle at departure and destination; transfer angle and other data) are specified by the mission windows above.

The planetocentric mission profiles involve specification of the departure or arrival hyperbola, of the initial Earth satellite orbit, of the capture orbit and of the terminal orbit at Earth return.

The shape of the hyperbolas is fixed by the associated hyperbolic excess velocity (already determined) and by specifying a periapsis distance $r_P = r_1, r_2, r_3$ or r_4 from the planet. This is the information needed to compute the velocity v_1, v_2, v_3 or v_4 at the periapsis, (numerical eccentricity and flight time from periapsis to the limit of the planet's activity sphere (termination of the nominal planetocentric flight

path) or vice versa.

The shape of the capture orbit is fixed by specifying its ellipticity (if any). This can be done in various ways. The most practical and lucid one is to specify the ratio of apoapsis to periapsis distance, $n = r_A/r_P$, where r_P generally will agree with the associated value of $r_1 \ldots r_4$. If the capture orbit is circular, $n=1$. Therewith the periapsis and apoapsis velocity v_P and v_A can be determined and the actual impulsive velocity change $\Delta v_1 = v_1 - v_{P1}$, $\Delta v_2 = v_2 - v_{P2}$, etc. found for the case of a planar maneuver. If a plane change is to anticipated, this will be combined with the main maneuver and the specification of the value of the plane change must be added.

If the capture orbit is elliptic, the departure maneuver (M-3) should occur at the periapsis, just as the capture maneuver (M-2), in order to take advantage of the reduced performance requirement offered by the elliptic capture orbit over a circular orbit. It is practically certain that in no case will the peri-apsis, established by the capture maneuver, be at the correct position for departure. Thus the major axis must be rotated. This is best done by adding two small maneuvers. The first is an impulsive velocity change at apogee from elliptic to circular orbit, Δv_A. The second maneuver is the reversal of the first one and is executed after the vehicle has flown through an appropriate arc in the circular orbit. The vehicle returns to the corrected periapsis position and there executes the departure maneuver proper (Δv_3). In this case, then, the overall departure maneuver M-3 consists of the velocity changes $2(\Delta v_A) + \Delta v_3$.

With the impulsive velocity changes known and multiplied with a contingency factor (for example 1.03), the specific impulse of the engines to be used in M-1

through M-4 must be defined, $I_{sp1,2,3,4}$, so that the mass ratios μ_1 through μ_4 for the four main maneuvers can be computed and plotted against D_1 and D_3 (Fig. 4-1). From the mass ratios, the propellant load fraction Λ (propellant weight W_p expended during given maneuver divided by ignition weight W_A) can be found immediately and plotted likewise against D_1 and D_3 (Fig. 4-1).

The remaining task is to determine the wet inert weight fraction $b = W_b/W_A$ so that the gross payload weight fraction $\lambda = W_\lambda / W_A$ is known, since, by definition, $\lambda + b + \Lambda = 1$.

At this point a difficulty is encountered. The wet inert weight fraction b is a function not only of μ, but also of the mass fraction $x = W_p/(W_b + W_p)$, by the relation $b = \frac{1-x}{x} \frac{\mu - 1}{\mu} = \frac{W_b}{W_p} \frac{\mu - 1}{\mu}$

The mass fraction, being a design constant depends on the absolute size, propellant weight (and design philosophy) of the vehicle or stage, none of which is known at this stage. In fact, x must be specified to eventually determine W_A. Even if a given design philosophy is assumed and a curve (or analytical relation) for the estimated variation of x with W_p developed, the value of x which must be picked at this point may turn out to be in error. In this case the process must be repeated until, by iteration, satisfactory agreement is reached between the selected value of x and the one derived later from W_A.

One way of proceeding is by adopting this iteration. A likely value of x is selected and b and λ determined and plotted against D_1 and D_2 (Fig. 4-1). In order to arrive at the absolute weights, the preliminary payload weights and preliminary weight variations between principal maneuvers must be specified. After this has been done, the weights can be computed, beginning with the terminal point of the mission. Thus,

with the payload $W_{\lambda 4}$ following M-4 given, the M-4 ignition weight W_{A4} follows from $W_{A4} = \lambda_4 W_{\lambda 4}$ and the other data from $W_{b4} = W_{A4} b_4$ and $W_{p4} = W_{A4} \Lambda_4$. It is assumed that just prior to M-4 ignition, the meteoroid and thermal shield of the M-4 tanks and other weights have been jettisoned to minimize the dead weight subjected to a velocity change. This jettison weight, W_{j4}, must now be added to yield the weight W_{C4} at termination of return coast. Additional postulated weight losses W_{j34} during return coast must then be added to establish the weight at beginning of the return coast, $W_{C3} = W_{C4} + W_{j34}$. This weight is the gross payload weight $W_{\lambda 3}$ of M-3, whence the ignition weight of M-3 becomes $W_{A3} = \lambda_3 W_{\lambda 3}$ and $W_{b3} = b_3 W_{A3}$, $W_{p3} = \Lambda_3 W_{A3}$. In this fashion, the Earth orbital departure weight W_{A1} will eventually be obtained and can be plotted against D_i (Fig. 4-2) together with additional plots of other weights as desired. For nomenclature see Fig. 4-3.

At each W_A it becomes necessary to check the selected value of x and iterate if required, rendering this method laborious and cumbersome, if done by hand, whereas on the computer it would be acceptable. This has been done during the first phase of the EMPIRE study.

It seems to be impossible to avoid the amount of labor involved, unless one wants to be more or less arbitrary and not iterate at all. It is possible, however, to put this work to better use by parametric variation of x, instead of iteration. This approach is shown in the flow chart, Fig. 4-4. Now the hyperbolic excess velocities (rather than calendar dates) are taken as independent variables, the range of each so selected as to be representative for the mission window(s) under consideration. Then Δv, μ and Λ are determined as function of their respective v_∞; and b is determined likewise, but with x as parameter, where a representative range of mass

fractions is used for each maneuver. Finally, the payload weight fraction is determined and plotted as function of v_∞ and x. Curves showing the estimated variation of x with W_p are constructed for each maneuver. Subsequently, mission windows are introduced, replacing v_∞ by D_1 and D_3 as independent variables for Δ v. At this point one introduced again the absolute weight inputs $W_{\lambda 4}$, W_{j4}, etc., and starts determining the absolute vehicle weights as function of D_3 and T_2. To a given D_3, T_2 belongs a value $v^*_{\infty 4}$. Now one goes back to the $\lambda_4 (v^*_{\infty 4}, x_4)$ chart from which a $\lambda_4(v^*_4)$ value is selected for a plausible x_4. The iteration process must now be resumed (indicated by $\rightleftharpoons$), but it is faster and less laborious with the aid of the $\lambda_4 (v^*_4, x_4)$ and $x_4 (W_{p4})$ charts. From the selected W_{A4} one obtains immediately W_{p4}, checks the selected x_4 against the value of x_4 in the chart $x_4(W_{p4})$, uses the discrepancy for improving the estimate of x_4, reads the corresponding new value of λ_4 from the $\lambda_4 (v^*_4, x_4)$ chart and repeats the process. Since the iteration cycle is now shorter (Fig. 4-5) and the correction requirement for the re-estimate of x_4 more readily assessed, the iteration converges quickly. There is no need for the initial and final value of x_4 in a given iteration cycle to agree more closely than the accuracy with which $x_4(W_{p4})$ is known at that stage. In this manner the four principal ignition weights are found failry rapidly and the orbital departure weight determined as function of the Earth departure date D_1.

Instead of starting out with v^*_∞ as independent variable, it would have been possible to apply the second approach (namely parametric variation of x) to the case where the mission window dates are the independent variables (Fig. 4-6). This approach has a slight edge over the second one in terms of simplicity; but the difference is small and it is bought at the expense of generality. In the second case, if

the ranges of v_∞ are selected reasonably broadly, the resulting plots of $\mu(v_\infty)$ through $\lambda(v_\infty, x)$ can be used in connection with a variety of mission windows. Therefore, preference is given to the second approach (Fig. 4-4), especially since in Phase I of the mission and systems synthesis, mission windows usually are not yet firmly established.

4.2 Phases II and III

Since these two phases differ only as to the degree of detail rather than in concept, they can be treated jointly as to their method of approach.

The two main factors contributing to the higher accuracy of either one of these phases are the breakdown of the mass fraction term x into a number of scaling coefficients and the replacement of impulsive velocity changes by finite periods of powered flight, whereby gravitational losses are automatically accounted for and refinements can be introduced, where appropriate, such as a distinction between tangential, azimuthal or variable thrust vector orientation. A wide range of initial thrust-to-weight ratios can be investigated; and the foundation is laid for the flight navigation analysis in Phase III.

As the result of repeated weight analyses and critical evaluation of structures, engines and engine integration, tank arrangements, payload integration, etc., the mass fraction $x = W_p/(W_b + W_p)$ can be replaced by an equation of the following type,

$$\frac{W_b}{W_p} = \frac{1 - x}{x} = k_f \frac{F}{W_p} + k_p + \frac{W_c}{W_p}$$

where k_f is the thrust dependent scaling coefficient,

$k_f \frac{F}{W_p}$ = the thrust dependent weight fraction of the wet inert weight,

k_p is the propellant-dependent scaling coefficient which, in turn is broken down

into the following coefficients

$$k_p = k_{p,s} + k_{p,m} + k_{p,h} + k_{resid}$$

where

$k_{p,s}$ = propellant dependent structural coefficient

$k_{p,m}$ = coefficient of meteoroid shield structure

$k_{p,h}$ = coefficient of heat protection systems for the propellant conservation (insulation, re-liquefaction, shadow shields, etc., where variety of heat protection systems is involved, $k_{p,h}$ must be broken down further)

k_{resid} = residual propellant weight coefficient; also coefficient of propellant contingency.

The powered flight path calculations were programmed on the IBM 7090 computer for tangential thrust for departure and approach to the target planet. The program was arranged in such a manner that the printouts provide a direct correlation between time of flight velocity, altitude, flight path angle, thrust-to-weight ratio, true anomaly of the osculating orbit, center angle swept by the radius vector and hyperbolic excess velocity. In the approach case, the terminal thrust acceleration (F/W_1), in local g's was specified; in the departure case the initial thrust acceleration (F/W_o) was fixed. Both were varied parametrically and a range of specific impulses selected for nuclear and chemical engines.

The method of approach adopted for the performance and parametric weight determination in Phases II and III is outlined in Figs. 4-7 and 4-8. The studies of vehicle configuration, engines, vehicle-engine integration, crew modules, Earth entry modules and associated integration requirements result in a functional correlation $k_f(F)$ of the thrust dependent scaling coefficient with the number of engines, N_E, in the cluster as parameter; and in a correlation k_p (W_p) for a number of prin-

cipal configurations, A. . . . D. In this form, k_f and k_p are injected as known quantities into the performance analysis cycle.

Computer data furnish the data for plotting mass ratio, powered flight time and cut-off altitude as function of hyperbolic excess velocity for given values of F/W_o (or F/W_1), I_{sp} and ϵ, the relative orbital energy of the initial or capture satellite orbit, determining the before mentioned distance ratio $n = r_A/r_P$ (graph (1), Fig.4-8a). A series of supplementary graphs can be constructed, as indicated in Fig.4-8a, plotting the ideal velocity increment Δv_{id}, the initial or terminal hyperbolic velocity v_1 (v_2, v_3, v_4), the actual velocity change Δv_1 ($\Delta v_2 \ldots \Delta v_4$), defined as the difference between hyperbolic velocity and velocity v_o in the satellite orbit, and the gravitational velocity loss $\Delta v_g = \Delta v_{id} - \Delta v_1$, as function of v_∞^*. Graph (1) of Fig.4-8a can be cross-plotted to give mass ratio and powered flight time (as well as cut-off altitude if desired) as function of F/W_o for given values of v_∞^*, I_{sp} and ϵ. This is indicated schematically in graph (2) of Fig.4-8a. Plots (1) and (2) can be modified to show the propellant loading factor Λ instead of mass ratio, because $\Lambda = (\mu - 1)/\mu$ (graphs (3) and (8), Fig.4-8a,b).

At this point either thrust F or gross weight W_o (or W_1) (which is identical with W_A in Par. 4.1) must be specified to correlate the results in graphs (1) and (2) with the scaling coefficients and in order to avoid iteration processes which in Phases II and III would be still much more involved than in Phase I, because of the non-impulsive character of the powered flight analysis. Generally, thrust is a less sensitive parameter from an overall point of view (payload weights, for example, vary less with variations in thrust than in gross weight, for comparable variations). Moreover, if nuclear engines are considered, there are going to be fewer

choices among thrust levels in the next 10-15 years.

Proceeding then in the left hand column of the performance analysis (Fig.4-7), where v_∞^* is the independent variable, one selects a suitable initial (terminal) thrust/weight ratio, F/W_o (F/W_1). Therewith W_o (v_∞^*) is fixed. With the aid of $\Lambda(v^*)$ one obtains now the propellant weight W_p (v_∞^*) and also the important correlation F/W_p (v_∞^*) which must be known to link the thrust dependent scaling coefficient k_f with the mass fraction x, as shown in the equation for W_b/W_p given earlier in this paragraph.

In the right hand side column of the performance analysis (Fig. 4-7) where F/W_o (or F/W_1) is the independent variable, the analogous process is carried out, selecting a value of v_∞^*, obtaining W_o (F/W_o), W_p (F/W_o) and F/W_p (F/W_o) for given values of v_∞^*, I_{sp}, ϵ and F.

With the selection of F, the value of k_f is fixed also, for given engines and engine clusters. With W_p specified as function of v_∞^* or F/W_o, one obtains now k_p (v_∞^*) and k_p (F/W_o). With k_f, F/W_p and k_p given, one can construct plots of $W_b/W_p = (1 - x)/x$ as function of v_∞^* and F/W_o as shown schematically in graphs (4) and (9) of Fig. 4-8 ; and plots of mass fraction x (v_∞^*) for given F/W_o, ϵ, F, N_E and I_{sp}, where N_E is the number of engines in a cluster. The way is now open to determine the wet inert weight fraction b (v_∞^*) and b (F/W_o) as well as the payload weight fraction λ (v_∞^*) and λ (F/W_o). As indicated in Fig. 4-7 , the results Λ (v_∞^*), b (v_∞^*), λ (v_∞^*) and Λ (F/W_o), b (F/W_o), λ (F/W_o) can now be correlated with mission profiles to evaluate the effect of mission, that is, of mission windows and mission years as well, on the vehicle weight at given stages of maneuvering including the orbital departure weight for given payload weights and to assess

the effect of changes in payload weight, specific impulse and thrust acceleration. From the then available data $W_p(v_\infty^*)$, $W_p(F/W_o)$, $k_f(F)$ and $k_p(v_\infty^*)$, $k_p(F/W_o)$ it is also possible to construct plots of $x(W_p)$ for given F/W_o. This graph, in turn, can be used to refine the determination of x or to assess uncertainties and establish an x-band rather than a single x-curve and to feed these refinements back into the main cycle of the performance analysis.

4.3 Correlation of Mission Performance Analysis and Vehicle Configuration Studies with Operations and Cost Analysis

Fig. 4-9 surveys the interaction between the principal elements of operations and cost analysis. The information flow begins where it ended in the preceding paragraph, namely, with the linking of the configuration-dependent generalized performance data and the performance requirements based on mission window and mission profile. From these, the launch requirements and orbital operations requirements are derived. Concurrently, from launch requirements and the ELV specifications the required ground operations are derived. Launch requirements and orbital operations provide the basis for a success analysis of the orbital preparations, i.e. the phase between the first ELV launch and orbital departure of the expedition.

Ground operations, orbital operations together with the implications of the success analysis of the orbital preparations, and the manufacturing cost provide the inputs for determination of the direct operating cost.

Two additional areas are indicated in Fig. 4-9 which lie outside the sequence outlined above. The first is the mission success analysis which, for a given mission profile, depends essentially on the vehicle configuration and on the operations to be performed during the mission. These operations are determined primarily by mission profile and mission mode. The second area pertains to the development cost which is strongly influenced by the vehicle configuration, primarily by the difference between nuclear and chemically powered configurations and by ground and orbital

test programs and associated facility requirements. Direct operating cost and development cost of the mission vehicles represent the overall mission cost if the development of a modified or new ELV and the cost of extra launch facilities either are not involved or are not charged to the planetary mission program.

Fig. 4-10 illustrates a typical flow chart showing principal results. By applying the general results of the performance analysis described in the preceding Paragraph to a particular mission, the variation of W_{A4} and W_{A3} with the date D_3 of departure from the target planet is obtained for a given return flight time T_2 (or for several values of T_2). It is assumed in the present example, that a retro-maneuver M-4 is executed. Based on the variation of W_{A3}, a suitable time interval $D'_3 - D''_3$ is selected (10-30 days) as the most favorable departure window from the target planet. Based on the first and last day of this period W_{A2} and W_{A1} are determined versus Earth departure dates D_1 for a given transfer period T_1. For given T_1 and D'_3 the capture period T_{cpt} is a function of D_1 only and T_{cpt} is positive as long as the arrival date D_2 precedes D'_3. It is desirable and realistic to provide a target planet departure window following the nominal capture period $T_{cpt} = D'_3 - D_2$, to allow a cushion for troubles which may arise during the capture period. The vehicle must be laid out for D''_3 if this date required the higher mission energy. The penalty, if any, in terms of Earth departure weight is assessed by determining W_{A1} for D'_3 and D''_3. The Earth departure window (EDW), $D'_1 - D''_1$, some 30 or 40 days, is selected for the low values of W_{A1}. The date D'_1 should be so selected that delays in departure require a minimum of additional launches due to changes in propellant requirements. This is not always realizable for all maneuvers. In the present example of Fig. 4-10, only the fuel requirement for M-4 is seen to increase.

Following determination of the EDW an ELV-space vehicle integration study is carried out to determine the best arrangement for transporting the total load into orbit. This results in establishment of the basic launch requirements, i.e. the total number of successful launchings. The success probability of the orbital preparations is affected by the Earth-to-orbit delivery success probability and the probability of successful mating or fueling. Selecting an acceptable success probability of orbital preparations yields the actual number of launchings which form the basis for analyzing the orbital and ground operations and determines the duration of the pre-departure operations.

The factors determining the overall mission cost are shown in Fig. 4-11. The mission cost can be broken down into three principal groups. In each group there are cost factors which are dominant. It is apparent that for the first few missions the development cost of the planetary vehicles (meant to comprise the interplanetary ships as well as all auxiliary vehicles, Earth entry module, Mars landing vehicle, Returners, Landers, Floaters, Mappers, etc.) far exceeds the direct costs. The development cost, in turn, hinges primarily on the degree to which nuclear engine development programs are directly involved. For chemical vehicles no significant advancement in engine technology is required, because, under space conditions and at the thrust levels of the individual engines (1-3 million lb), high pressure engines (pc 1000 psia) are not required. The direct operating cost is determined by the production cost. Here the difference between the production cost of nuclear and chemical vehicles is comparatively less significant than in the development area. The greater production cost of the nuclear space vehicle is in many cases overcompensated by the much larger departure weight of the chemical space vehicle and the

associated higher delivery cost. However, the question of whether the direct cost is higher for the nuclear or the chemical space vehicle depends on specific assumptions regarding the available ELV, probability of successful delivery into the assembly orbit and the assumptions made regarding the probability of successful orbital mating of fueled modules on the one hand and of successful orbital fueling of mated modules on the other. Reliability assumptions and required probabilities of success, as well as the interchangeability (or the lack thereof) of modules affect the procurement requirements and therewith exert an important influence on the direct cost.

The logistic cost depends primarily on the number of launches, N_{op} required for the pre-departure operations and on the total cost effectiveness. The former is again controlled by reliability and success probability considerations. The latter is decisively affected by whether or not major modifications of an existing ELV or the development of a new ELV are involved. The direct cost effectiveness is dominated by the ELV production cost. The cost of orbital labor is determined primarily by the cost of special training for the crew which, if the training costs are changed to a single period of orbital departure preparations of, say 100 days, can amount to more than all other orbital labor cost factors taken together. The cost of the orbital (launch) facilities are more difficult to determine on a general basis, because their specification depends on the number, size and propulsion system of the planetary vehicles involved.

5. ANALYSIS

In this Section, analytical relations anf plots are presented which are useful for the previously discussed methodology.

5.1 Phase I

1. Mission Profile Selection - Specification of departure date D_1, outbound transfer time T_1, capture period T_{cpt} and return transfer time T_2 automatically specifies arrival date D_2, target planet departure date D_3, Earth arrival date D_4, the associated hyperbolic excess velocities $v^*_{\infty 1}$ through $v^*_{\infty 4}$ (cf. Figs. 2-6 to 2-10), as well as all elements of the heliocentric outbound and return transfer orbits.

capture and departure distances from Earth or target planet are always meant to coincide with the periapsis of the satellite orbit where impulse maneuvers are concerned. An exception is Earth return (cf. below). These distances are designated as r_1, r_2 and r_3, where it is further assumed that capture and departure distance from the target planet are the same, i.e. $r_2 = r_3$. These distances also coincide with the periapsis of the arrival or departure hyperbola in an impulse maneuver.

Specification of r_i (i = 1, 2, 3), together with $v_{\infty i}$ specifies the planar elements of the planetocentric hyperbola. Specification of relative orbital energy ϵ and $n = r_A/r_P = r_A/r_i$ of the planetocentric satellite orbit specifies the required impulsive velocity changes. The absolute orbital energy constant (vis viva integration constant) is

$$h = v^2 - \frac{2K}{r} = \epsilon \frac{K}{r} \tag{5-1}$$

where the relative orbital energy constant

$$\epsilon = \frac{h}{K/r} = \frac{v^2}{K/r} - 2 \qquad \begin{pmatrix} \epsilon < 0 \text{ for closed orbits} \\ \epsilon = -1 \text{ for circle} \\ \epsilon = 0 \text{ for parabola} \\ \epsilon > 0 \text{ for hyperbola} \end{pmatrix} \tag{5-2}$$

has been introduced by this author because of its convenience, being independent of the differences in strength of the various planetary fields. Other important parameters are defined in terms of ϵ by the following relations, ratio of apsides (plotted in Fig. 5-1),

$$n = -\frac{2+\epsilon}{\epsilon} \tag{5-3}$$

since, for closed orbits

$$\epsilon = -\frac{2}{n+1} \tag{5-4}$$

periapsis velocity

$$v_P = \sqrt{(2+\epsilon)\,K/r} \tag{5-5}$$

numerical eccentricity,

$$e = 1 + \epsilon \tag{5-6}$$

semi-major axis,

$$a = -\frac{r_P}{\epsilon} \quad \text{(ellipse)} \tag{5-7}$$

$$|a| = \frac{K}{v_\infty^2} = \frac{r_P}{\epsilon} \quad \text{(hyperbola)} \tag{5-8}$$

periapsis distance,

$$r_P = (2+\epsilon)\frac{K}{v_P^2} \quad \text{(ellipse)} \tag{5-9}$$

$$r_P = \frac{K}{v_\infty^2}\,\epsilon \quad \text{(hyperbola)} \tag{5-10}$$

semilatus rectum,

$$p = r_P\,(2+\epsilon) \tag{5-11}$$

Tab. 5-1 Auxiliary Data

Body	K (km^3/sec^2)	U (km/sec)	U (10^4ft/sec)	r_{act} (Planet Radii)	Parabolic Velocity at r* (km/sec)	$Q = \frac{r_{oo}}{K/U_{\oplus}^2}$ (-)	$S = K/U_{\oplus}^3$ (sec)
Sun	$1.327154 \cdot 10^{11}$	--	--	--	--	--	--
Mercury	$2.1694 \cdot 10^4$	47.8724	15.7052	44.6	$4.166/\sqrt{r^*}$	102.377	0.8198
Venus	$3.2423 \cdot 10^5$	35.0209	11.4898	99.2	$10.726/\sqrt{r^*}$	16.9532	12.2778
Earth	$3.9858 \cdot 10^5$	29.7849	9.7719	144.9	$11.186/\sqrt{r^*}$	14.1865	15.0943
Mars	$4.2906 \cdot 10^4$	24.1295	7.9165	174.4	$5.092/\sqrt{r^*}$	68.39	1.6244
Jupiter	$1.26498 \cdot 10^8$	13.0580	4.2841	640.7	$60.19/\sqrt{r^*}$	0.0490	4790.2109
Saturn	$3.78811 \cdot 10^7$	9.6438	3.1640	743.1	$36.28/\sqrt{r^*}$	0.1347	1434.4801
Uranus	$5.79364 \cdot 10^6$	6.8006	2.2312	2027.4	$32.13/\sqrt{r^*}$	0.3902	219.3915
Neptune	$6.86004 \cdot 10^6$	5.4327	1.7824	3471.6	$23.43/\sqrt{r^*}$	0.3231	259.7743
Pluto	$3.31237 \cdot 10^5$	4.7380	1.5545	--	$10.51/\sqrt{r^*}$	--	12.5432

K = gravitational parameter

U = mean orbital velocity of planet

r_{act} = radius of planet's activity sphere

Q is a dimensionless term

$U_{\oplus}$ = mean orbital velocity of Earth

r^* = radial distance from planet in planet radii

apoapsis velocity,

$$v_A = \sqrt{-\frac{K}{r_A}\epsilon} \tag{5-12}$$

local path velocity at distance r,

$$v = \sqrt{\frac{K}{r}(2+\epsilon)} \tag{5-13}$$

eccentric anomaly,

$$\cos E = \frac{1 + \frac{r}{r_P}\epsilon}{1+\epsilon} \tag{5-14}$$

flight time from periapsis to distance r in an elliptic orbit

$$t_{Pr} = \sqrt{-\frac{r_P^3}{K\epsilon^3}}\,(E - (1+\epsilon)\sin E) \tag{5-15}$$

hyperbolic auxiliary angle (Fig. 5-2)

$$\cos H = \frac{1+\epsilon}{1+\frac{r}{r_P}\epsilon} = \frac{e}{1+\frac{r}{a}} \tag{5-16}$$

Since v_∞ and r_P are two key parameters of the hyperbola, it is useful to express the auxiliary angle H, the flight time t_{Pr} from periapsis to distance r and the true anomaly η at distance r in terms of these parameters, were, for the sake of convenience, v_∞^* (i.e. v_∞ in EMOS units) instead of v_∞ is used, since interplanetary flight charts usually provide the hyperbolic excess velocity in these units,

$$\cos H = \frac{1 + r^* Q v_\infty^{*2}}{1 + \frac{r}{r_P} r^* Q v_\infty^{*2}} \tag{5-17}$$

where

$$Q = \frac{r_{oo}}{K/U_\oplus^2} = \frac{r_{oo}/R_\oplus}{K/K_\odot} \tag{5-18}$$

$R_{\oplus}$ = mean distance of Earth from Sun

r_{oo} = surface radius of planet

$U_{\oplus}$ = Earth mean orbital speed

K = gravitational parameter of the planet

$K_{\odot}$ = gravitational parameter of Sun

r_P^* = periapsis distance in units of the planet's surface radius

r^* = distance from planet in units of planet's radius

The values of Q are listed in Tab. 5-1 together with other relevant constants.

Flight time between periapsis and distance r in hyperbolic orbit,

$$T_{Pr} = \frac{S}{v_{\infty}^{*3}} \left(\frac{r_P^*}{r^*}\right)^{3/2} \left[(1 + r^* Q v_{\infty}^{*2}) \tan H - \ln \tan\left(45^\circ + \frac{H}{2}\right)\right] \tag{5-19}$$

where

$$S = \frac{K}{U_{\oplus}^3} \tag{5-20}$$

also listed in Tab. 5-1. True anomaly at distance r in hyperbolic orbit

$$\cos \eta = \frac{1 - \frac{r_P}{r}\left(2 + \frac{v_{\infty}^{*2}}{Q} r_P^*\right)}{1 + \frac{v_{\infty}^{*2}}{Q} r_P^*} \tag{5-21}$$

The equations (5-17), (5-19) and (5-21) are plotted in Figs. 5-2 through 5-10 for the planets Venus, Earth and Mars for several values of r_P. The distance of the activity sphere, r_{act}, of the planet has been used as the limiting distance where the planetocentric hyperbola merges with the heliocentric orbit. This distance (cf. Tab. 5-1) is given by the relation

$$r_{act} = R \left(\frac{m}{M}\right)^{2/5} \tag{5-22}$$

where R is the mean heliocentric distance of the planet and m/M the ratio of planetary to solar mass.

The planar impulsive velocity change at the distance r_i (i = 1, 2, 3) becomes then

$$\Delta v_i = v_i - v_{o,i} = \sqrt{\frac{2K}{r_i} + v_\infty^2} - \sqrt{\frac{K}{r_i}(2+\epsilon)} \tag{5-23}$$

or, more conveniently,

$$\frac{\Delta v_i}{v_\infty} \equiv \frac{\Delta v_i^*}{v_\infty^*} = \sqrt{1 + \frac{2K/r_{oo}}{v_\infty^2} r_i^*} - \sqrt{(2+\epsilon)\frac{K/r_{oo}}{v_\infty^2} r_i^*} \tag{5-24}$$

where $2K/r_{oo}$ is the square of the parabolic velocity at the planet's surface (Tab. 5-1) and r_i^* is the periapsis distance of the hyperbola and of the satellite orbit in units of the planet's radius. Eq. (5-24) which applies equally to an escape or capture impulse is plotted in Figs. 5-11 through 5-14 for Earth departure from circular orbit ($\epsilon = -1$), capture and escape Venus and Mars, for circular satellite orbits and for Earth return with reduction to slightly sub-parabolic speed into an $\epsilon = -0.04$ (n = 49) ellipse. At this speed the entry module would enter the Earth atmosphere essentially at Apollo conditions.

If the capture orbit is elliptic, it is most convenient to express the ellipticity in terms of the ratio of the apsides, $n = r_A/r_P$, because this parameter is most directly meaningful in a mission analysis where factors such as mapping, deployment of instrumented vehicles to the planet and surface excursion impose certain constraints on the ellipticity, governed primarily by the effect of the distance ratio. From n one finds ϵ directly and for a given $r_P = r_i$, finds Δv_i from Eq. (5-24).

The primary reason for selecting an elliptic capture orbit is to reduce the overall mission energy requirement. This advantage, however, can be realized only if both, capture and departure, take place at or near the periapsis. If the departure would have to occur at the apoapsis, most of the advantage gained by the

periapsidal capture maneuver (and more, if v_∞^* is sufficiently large) would be lost. Fig. 5-15 illustrates that situation for $v_\infty^* = 0.1$ and 0.5 EMOS at Mars. The lower curves show the individual variation of $(\Delta v^*/v_\infty^*)_{r_P}$ and $(\Delta v^*/v_\infty^*)_{r_A}$ as function of n. It is seen that for higher v_∞^* the periapsis value drops off with n more strongly than for lower values of v_∞^*. On the other hand, the value of v_∞^* has little effect on the increase of the apoapsis maneuver with n. As a result, the upper curves show that for an r_P - r_A combination the maneuver becomes steadily more expensive with n if v_∞^* is small; whereas this is not the case for large v_∞^*. Here a moderate gain could still be realized even for an r_P - r_A combination, if n is sufficiently large, because of the large decrease in the r_P-maneuver. Much larger energy reductions would, however, be realized with an r_P- r_P combination. The graph also illustrates the fact that elliptic orbits yield greater energy savings when the hyperbolic excess velocities $v_{\infty 2}^*$ and $v_{\infty 3}^*$ are large. Comparison of the effect of elliptic orbits around Venus and Mars shows that they provide more effective relief in stronger gravity fields. Finally, it should be noted that most of the performance relief is gained during the initial increase of n. At large values of n, the gains diminish. These facts are, of course, consistent with the characteristics of a central force field and can easily be derived therefrom.

When capturing, the position of the periapsis is fixed by the space vehicle's direction of approach to the target planet. The departure conditions, however, may require a different position of the periapsis. An extreme case, namely, departure from a point 180° off the arrival point is shown in Fig. 5-16. The vehicle approaches the target planet along hyperbola H-2, executes maneuver Δv_2 and enters an elliptic capture orbit. Assume the required orientation of the asymptote for departure

is so oriented that the departure impulse has to occur 180° off the original periapsis. Without an intermediate maneuver the maneuver Δv_3 would have to be executed at the apoapsis given by

$$\left(\frac{\Delta v}{v_\infty}\right)_A \equiv \left(\frac{\Delta v^*}{v_\infty^*}\right)_A = \sqrt{1 + \frac{K/r_{oo}}{v_\infty^2}\,\frac{r_{oo}}{h\,r_P}} - \frac{1}{n}\sqrt{\frac{(2+\epsilon)\,K/r_{oo}}{v_\infty^2}\,\frac{r_{oo}}{r_P}} \qquad (5\text{-}25)$$

Preferably, two intermediate maneuvers are carried out whose purpose it is to rotate the major axis of the ellipse by 180°. The vehicle enters a circular orbit at r_A with the impulse Δv_A, coasts 180° and slows down by Δv_A, falling now towards a correctly located r_P where the desired departure hyperbola can be entered at an impulse $\Delta v_3' < \Delta v_3$. The cost of the two apoapsis maneuvers cause a penalty which generally is far smaller than the penalty associated with departure from the apoapsis. The requirement for an impulsive apoapsis maneuver is

$$\Delta v_A = \sqrt{\frac{K}{r_A}}\,\left(1 - \sqrt{-\epsilon}\right) \qquad (\epsilon < 0) \qquad (5\text{-}26)$$

Fig. 5-17 depicts the variation of v_P and v_A with n for elliptic orbits around Mars at $r_P^* = 1.3$. Fig. 5-18 shows the corresponding values of Δv_A and Fig. 5-19 presents the associated mass ratios for three specific impulses.

Also for Mars are shown in Figs. 5-21 through 5-23 the values of $\Delta v^*/v_\infty^*$, Δv and associated mass ratios for three specific impulses, all as function of v_∞^* and for $r^* = 1.3$. The curves for $\Delta v^*/v_\infty^*$ were computed with Eq. (5-24); Δv follows from

$$\Delta v = \frac{\Delta v^*}{v_\infty^*} \cdot v_\infty^* \cdot 97{,}700 \text{ (ft/sec)} \qquad (5\text{-}27)$$

and the mass ratios from

$$\mu = \exp\left(\Delta v / g\, I_{sp}\right) \qquad (5\text{-}28)$$

Thus, in the case of capture in an elliptic orbit, the capture maneuver is Δv_2

whereas the total departure maneuver is $2\,\Delta v_A + \Delta v_3$.

For hyperbolic capture or entry at Earth return and for hyperbolic capture at Venus or Mars, Figs. 5-24 through 5-26 show the variation of entry velocity (i. e. the hyperbolic velocity at the distances indicated) with the hyperbolic excess velocity, both in EMOS. It is worthwhile to note that at Mars the hyperbolic excess velocity can be as high as 0. 35 before the entry speed reaches values comparable with Apollo (parabolic) entry speeds in the Earth's field.

2. Weight Fraction Determination - A single-stage vehicle or a given stage of a multi-stage vehicle is assumed to consist of three basic weight groups. These can be expressed conveniently as fractions of the initial weight (at the beginning of the powered maneuver in which the propellant of the given vehicle or stage is to be used),

gross payload fraction, λ

wet inert weight fraction (i. e. burnout fraction minus λ), b

useful propellant weight fraction, Λ

Thus, by definition, $\lambda + b + \Lambda = 1$. The two most important variables determining λ are the mass ratio μ , defined as the ratio of mass at ignition to mass at burn-out (or cut-off) and the ratio of burnout weight to propellant weight, W_b/W_p. The first is a performance parameter the latter a design parameter. It is

$$\mu = \exp\left(\Delta v_{id}/g\, I_{sp}\right) = 1 + \frac{\Lambda}{\lambda + b} \tag{5-29}$$

where $\Delta v_{id} = \Delta v + \Delta v_g$ at non-impulsive propulsion, and

$$\frac{W_b}{W_p} = \frac{1 - x}{x} \tag{5-30}$$

where

$$x = \frac{W_b}{W_p + W_b} \tag{5-31}$$

is referred to as mass fraction. Estimating W_b/W_p, therefore, results in an estimate of x. A correlation between λ and μ with x as parameter is shown in Fig. 5-27. It is

$$\lambda = \frac{1}{x}\left(\frac{1}{\mu} - 1\right) + 1 = 1 - \frac{\Lambda}{x} \tag{5-33}$$

$$b = \frac{1-x}{x}\,\frac{\mu - 1}{\mu} \tag{5-34}$$

$$\Lambda = \frac{\mu - 1}{\mu} \tag{5-35}$$

Furthermore, the mass ratio is related to

$$b + \lambda = \Lambda \tag{5-36}$$

by the relation

$$\mu = \frac{1+\zeta}{\zeta} \tag{5-37}$$

The variation of ζ as function of v_{id} with I_{sp} as parameter is shown in Figs. 5-28 through 5-31. Given the ideal velocity (increment) and the specific impulse, ζ can be read from, whence μ is immediately obtained from Eq. (5-37) and Λ from (5-35). The associated sum $b + \lambda$ follows then from (5-36) The value of λ can now be read from Fig. 5-27 for a given x whence b is found from

$$b = (b + \lambda) - \lambda \tag{5-38}$$

The sensitivity of the payload fraction to small changes in mass ratio, in specific impulse, mass fraction or ideal velocity is given by the following relations,

$$\frac{\partial \lambda}{\partial \mu} = -\frac{1}{\mu^2}\,\frac{1}{x} \tag{5-39}$$

$$\frac{\partial \lambda}{\partial I_{sp}} = \frac{\tau}{I_{sp}^2}\,\frac{1}{\mu}\,\frac{1}{x} = \frac{\tau}{I_{sp}^2}\left(\lambda + \frac{1}{x} - 1\right) \tag{5-40}$$

$$\tau = \Delta v_{id}/g \tag{5-41}$$

$$\frac{\partial \lambda}{\partial x} = \frac{1}{x^2}\left(1 - \frac{1}{\mu}\right) = \frac{\Lambda}{x^2} = \frac{1-\lambda}{x} \tag{5-42}$$

$$\frac{\partial \lambda}{\partial (\Delta v_{id})} = \frac{1}{g\, I_{sp}} \frac{1}{\mu} \frac{1}{x} \tag{5-43}$$

With aid of these partials, the loss or gain in payload fraction is quickly found, e.g. for a change in I_{sp} by ΔI_{sp},

$$\lambda' = \lambda \pm \Delta\lambda = \lambda \pm \frac{\partial \lambda}{\partial I_{sp}} \Delta I_{sp} \tag{5-44}$$

5.2 Phases II and III

In these phases the impulsive maneuvers are replaced by finite powered flight periods whose duration is given by,

for departure (given initial thrust/weight ratio F/W_o),

$$t = \frac{I_{sp}\, \Lambda}{F/W_o} \tag{5-45}$$

for capture (given cut-off thrust/weight ratio F/W_1)

$$t = \frac{I_{sp}\, \Lambda}{\mu\, F/W_1} \tag{5-46}$$

Mass ratio and propellant fraction are a function of I_{sp} and the ideal velocity

$$v_{id} = \int_o^t f(t)\, dt \tag{5-47}$$

where

$$f(t) = \frac{F}{m(t)} \quad (\text{length/time}^2) \tag{5-48}$$

is the instantaneous thrust acceleration. Designating the angle between the path velocity vector and the local azimuth direction (line normal to the radius vector) as

the flight path angle θ and designating the planar angle between the thrust acceleration vector and the azimuth direction as φ, the relations for the radial and the azimuthal components of the thrust acceleration can be written as

$$f_r = \pm f \sin \varphi \tag{5-49}$$

$$f = \pm f \cos \varphi \tag{5-50}$$

where f_r is taken positive if directed away from the center of attraction and f_η is positive when accelerating in the direction of motion. The angle φ is counted from azimuth direction, seen in flight direction, and is positive if measured counterclockwise. The angle between thrust vector $\vec{f}$ and path velocity vector $\vec{v}$ is always $|\varphi - \theta|$. Both φ and θ are zero when their respective vector coincides with the local azimuth direction and are positive when their vector is pointing away from the center of attraction. Eqs. (5-49) and (5-50) apply to arbitrary thrust vector orientation in the orbit plane. For tangential thrust in an accelerating, outgoing ($\dot{r} > 0$) orbit

$$\varphi = \theta \tag{5-51}$$

hence,

$$f_r = f \sin \theta \tag{5-52}$$

$$f_\eta = f \cos \theta \tag{5-53}$$

and for tangential thrust in an incoming ($\dot{r} < 0$) decelerating path,

$$\varphi = 180 - \theta \tag{5-54}$$

$$f_r = f \sin \theta \tag{5-55}$$

$$f_\eta = -f \cos \theta \tag{5-56}$$

The instantaneous velocity vectors and simultaneous position coordinates of the space vehicle are

$$\dot{r} = \dot{r}_o + r\dot{\eta} - \frac{K}{r^2} \pm \int_o^t f_r \, dt \tag{5-57}$$

$$r = r_o \pm \int_o^t \dot{r} \, dt \tag{5-58}$$

$$\dot{\eta} = \dot{\eta}_o \mp \frac{\dot{r}}{r}\eta \pm \frac{1}{r} \int_o^t f_\eta \, dt \tag{5-59}$$

$$\eta = \eta_o + \int_o^t \dot{\eta} \, dt \tag{5-60}$$

the last integral being positive only, because the center angle η will always be counted positive in the direction of motion. The instantaneous path velocity in the planetocentric coordinate system is

$$v = \sqrt{\dot{r}^2 + (r\dot{\eta})^2} \tag{5-61}$$

and, for $v > 2\,K/r$, the associated hyperbolic excess velocity is

$$v_\infty = \sqrt{v^2 - \frac{2K}{r}} \tag{5-62}$$

In the above equations, subscript zero designates initial values (start of thrust power on). The instantaneous path angle and the instantaneous rate of change of the path angle are given by

$$\theta = \sin^{-1}\left(\frac{\dot{r}}{v}\right) \tag{5-63}$$

$$\dot{\theta} = \frac{r\dot{\eta}\,\ddot{r} - \dot{r}^2 \cdot - r\dot{r}\,\ddot{\eta}}{v^2} \tag{5-64}$$

where $r\dot{\eta}$ is the instantaneous azimuthal velocity component, $\ddot{r}$ the instantaneous radial acceleration, $\dot{\eta}$ the instantaneous angular velocity of the radius vector connecting the space ship with the center of attraction and $\dot{r}$ the instantaneous radial velocity.

Putting these relations on the IBM 7090 computer and evaluating them resulted in a number of graphs which, for relevant ranges of I_{sp}, F/W and v , show the variation of mass ratio and burning time for Earth departure, arrival and departure for Venus and Mars and Earth arrival. Earth departure is assumed to occur from a circular orbit. For the satellite orbits of Venus and Mars various values of were used, including $\epsilon = -1$ for circular orbits. For Earth arrival the retro-maneuver reduces the relative energy of the vehicle orbit to $\epsilon = -0.04$ at an altitude of 1000 km such that the unperturbed osculating orbit following cut-off leads to a perigee altitude of 60 km. These graphs were published in Rep. AOK63-0001, 31 January 1963, A Study of Early Manned Interplanetary Missions, Final Summary Report, NASA Contract No. NAS8-5026. They are also available in Part II of this report.

For a more detailed weight analysis the mass fraction is determined from the relation

$$x = \frac{W_p}{k_f F + W_p (1 + k_p)} \tag{5-65}$$

where k_f and k_p are defined in Par. 4.3. For given values of k_f and k_p, the propellant weight is given by

$$W_p = \frac{(\mu - 1)(W_\lambda + k_f)}{1 - k_p(\mu - 1)} \tag{5-66}$$

and the wet inert weight by

$$W_b = k_f F + k_p W_p = W_p \left(\frac{1 - x}{x}\right) \tag{5-67}$$

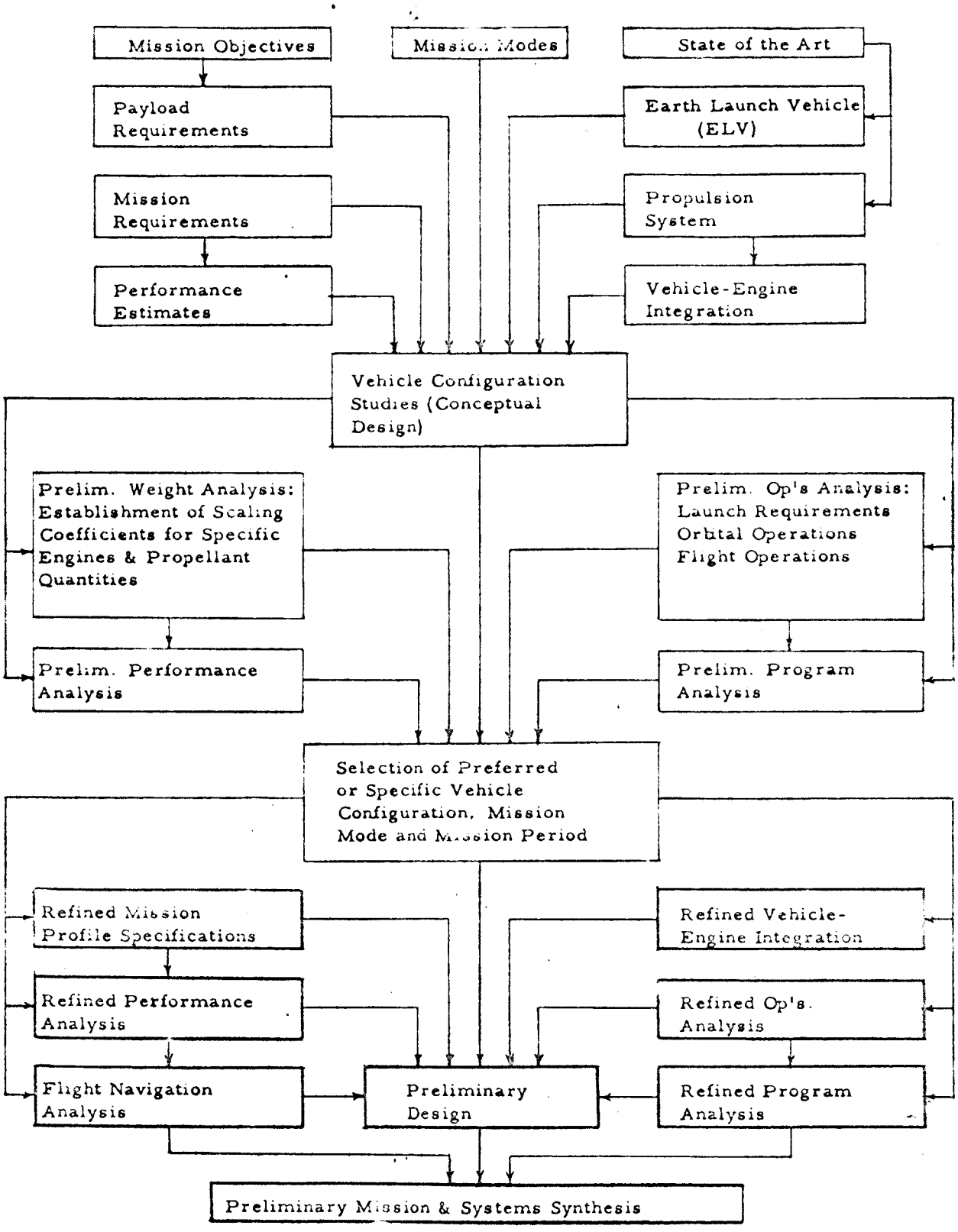

Fig. 2-1. Evolution of Mission & Systems Synthesis.

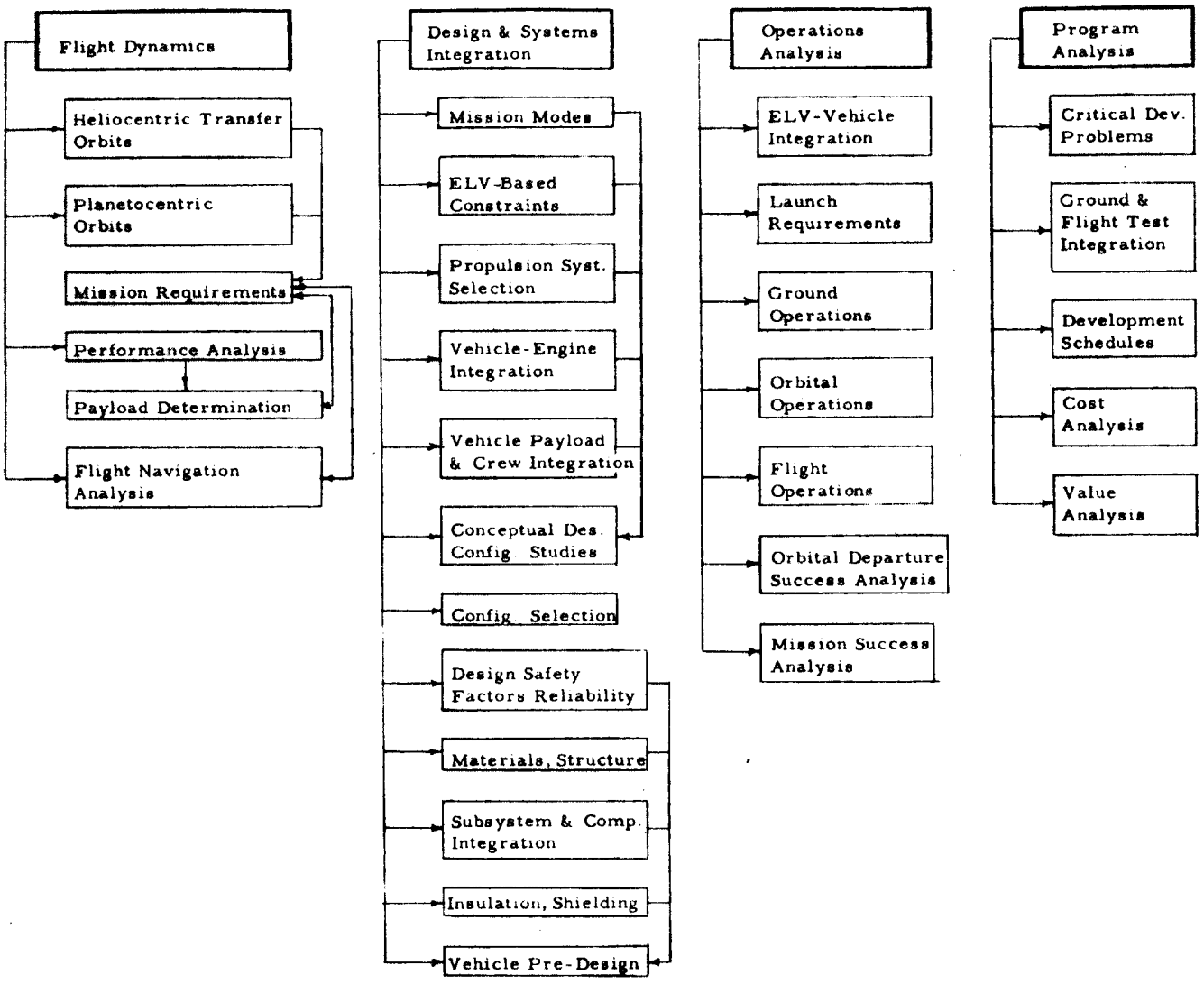

Fig. 2-2. Definition of Main Study Areas.

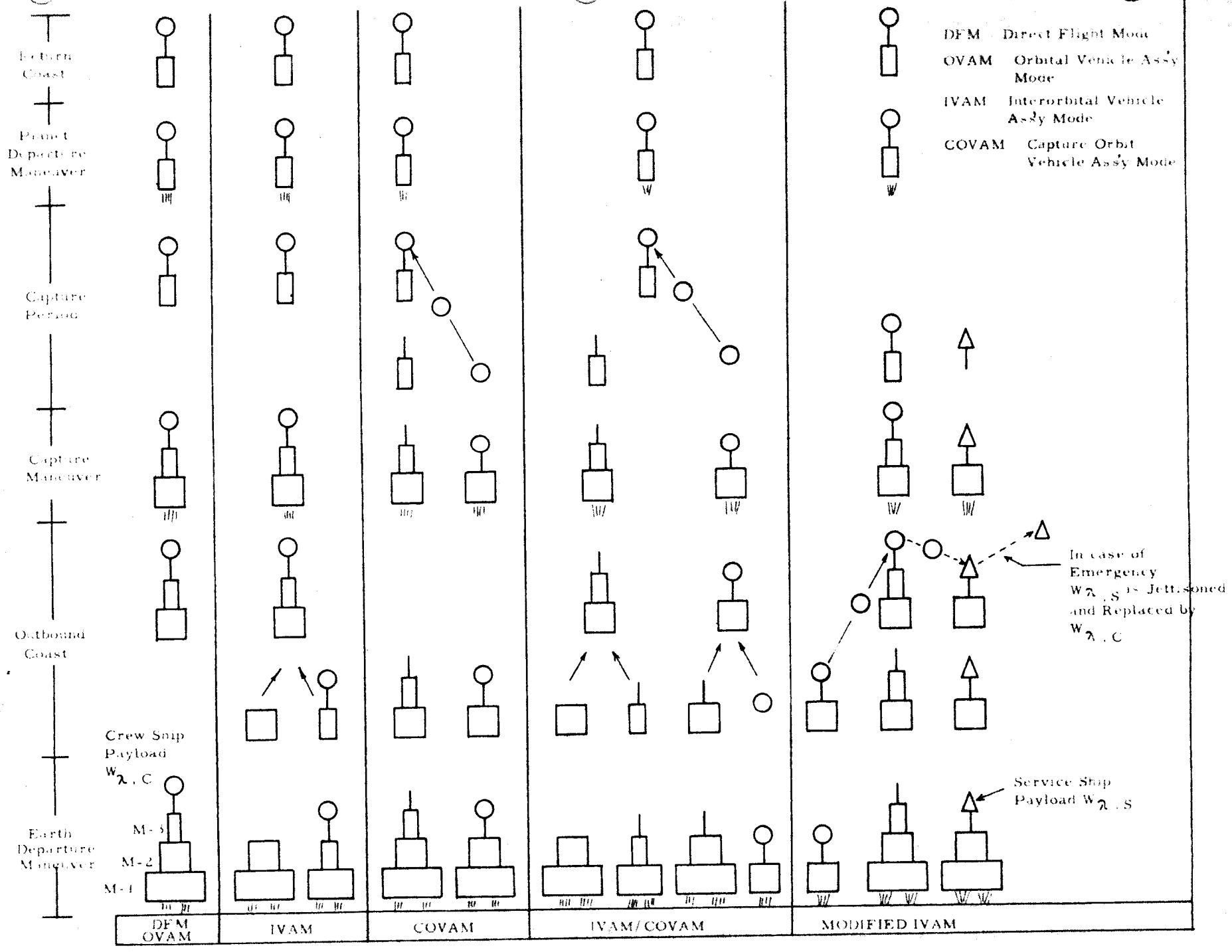

Fig. 2-3 Mission Modes for Planetary Convoy

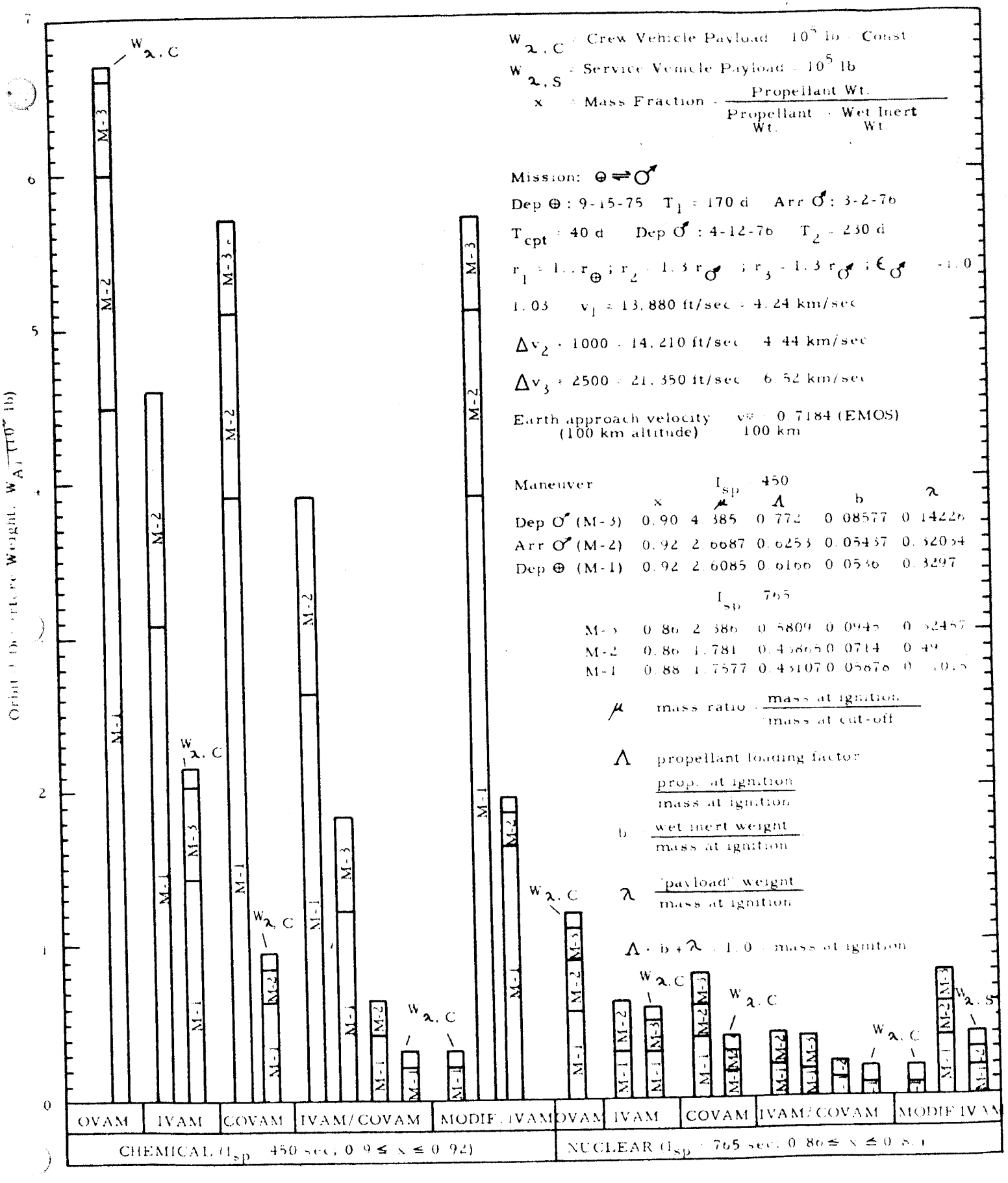

Fig. 2-4 Effect of Various Mission Modes on Orbital Departure Weight of Individual Vehicles for a Specific Mission Profile

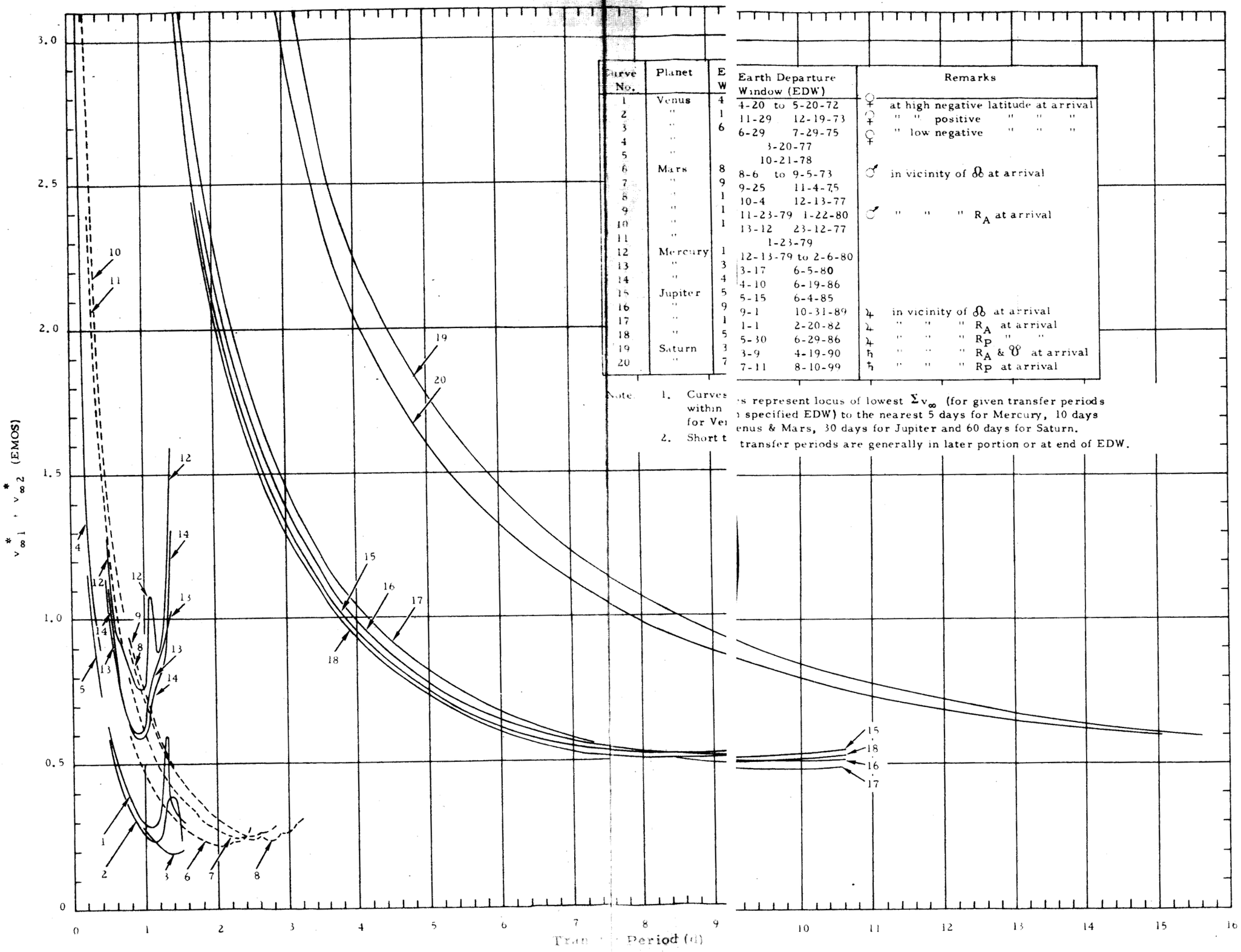

Curve No.	Planet	Earth Departure Window (EDW)	Remarks
1	Venus	4-20 to 5-20-72	♀ at high negative latitude at arrival
2	"	11-29 12-19-73	♀ " " positive " " "
3	"	6-29 7-29-75	♀ " low negative " " "
4	"	3-20-77	
5	"	10-21-78	
6	Mars	8-6 to 9-5-73	♂ in vicinity of ☊ at arrival
7	"	9-25 11-4-75	
8	"	10-4 12-13-77	
9	"	11-23-79 1-22-80	♂ " " " R_A at arrival
10	"	13-12 23-12-77	
11	"	1-23-79	
12	Mercury	12-13-79 to 2-6-80	
13	"	3-17 6-5-80	
14	"	4-10 6-19-86	
15	Jupiter	5-15 6-4-85	
16	"	9-1 10-31-89	♃ in vicinity of ☊ at arrival
17	"	1-1 2-20-82	♃ " " " R_A at arrival
18	"	5-30 6-29-86	♃ " " " R_P " "
19	Saturn	3-9 4-19-90	♄ " " " R_A & ☋ at arrival
20	"	7-11 8-10-99	♄ " " " R_P at arrival

Note: 1. Curves represent locus of lowest Σv_∞ (for given transfer periods within specified EDW) to the nearest 5 days for Mercury, 10 days for Venus & Mars, 30 days for Jupiter and 60 days for Saturn.

2. Short transfer periods are generally in later portion or at end of EDW.

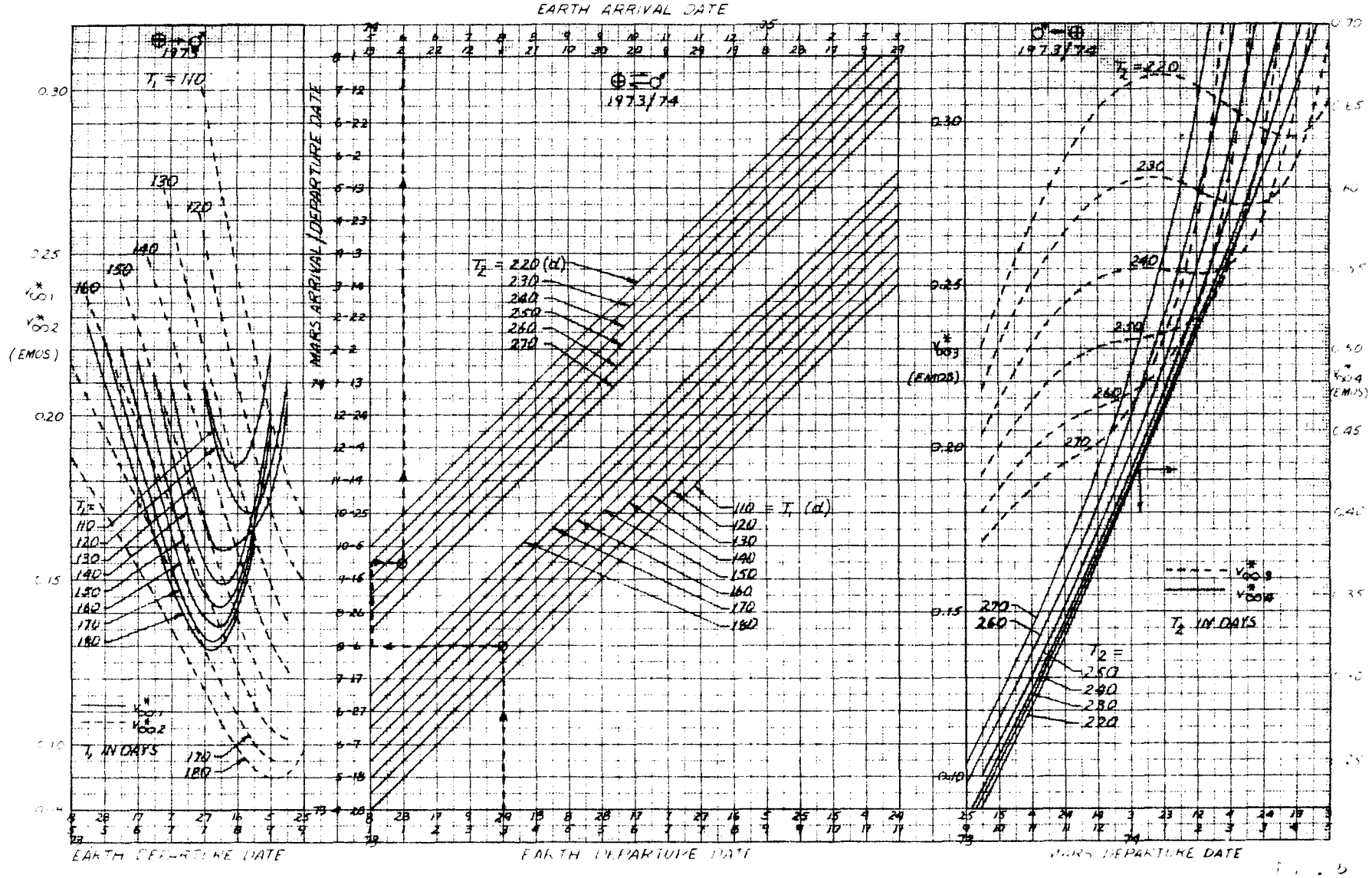
EARTH ARRIVAL DATE
MARS ARRIVAL / DEPARTURE DATE
EARTH DEPARTURE DATE
EARTH DEPARTURE DATE
MARS DEPARTURE DATE
1973/74
1973/74
T_1 = 110
T_2 = 220
T_2 (d) = 220, 230, 240, 250, 260, 270
T_1 (d) = 110, 120, 130, 140, 150, 160, 170, 180
T_1 IN DAYS
T_2 IN DAYS
(EMOS)
0.30
0.25
0.20
0.15
0.10
0.70
0.65
0.60
0.55
0.50
0.45
0.40
0.35
0.30
0.25

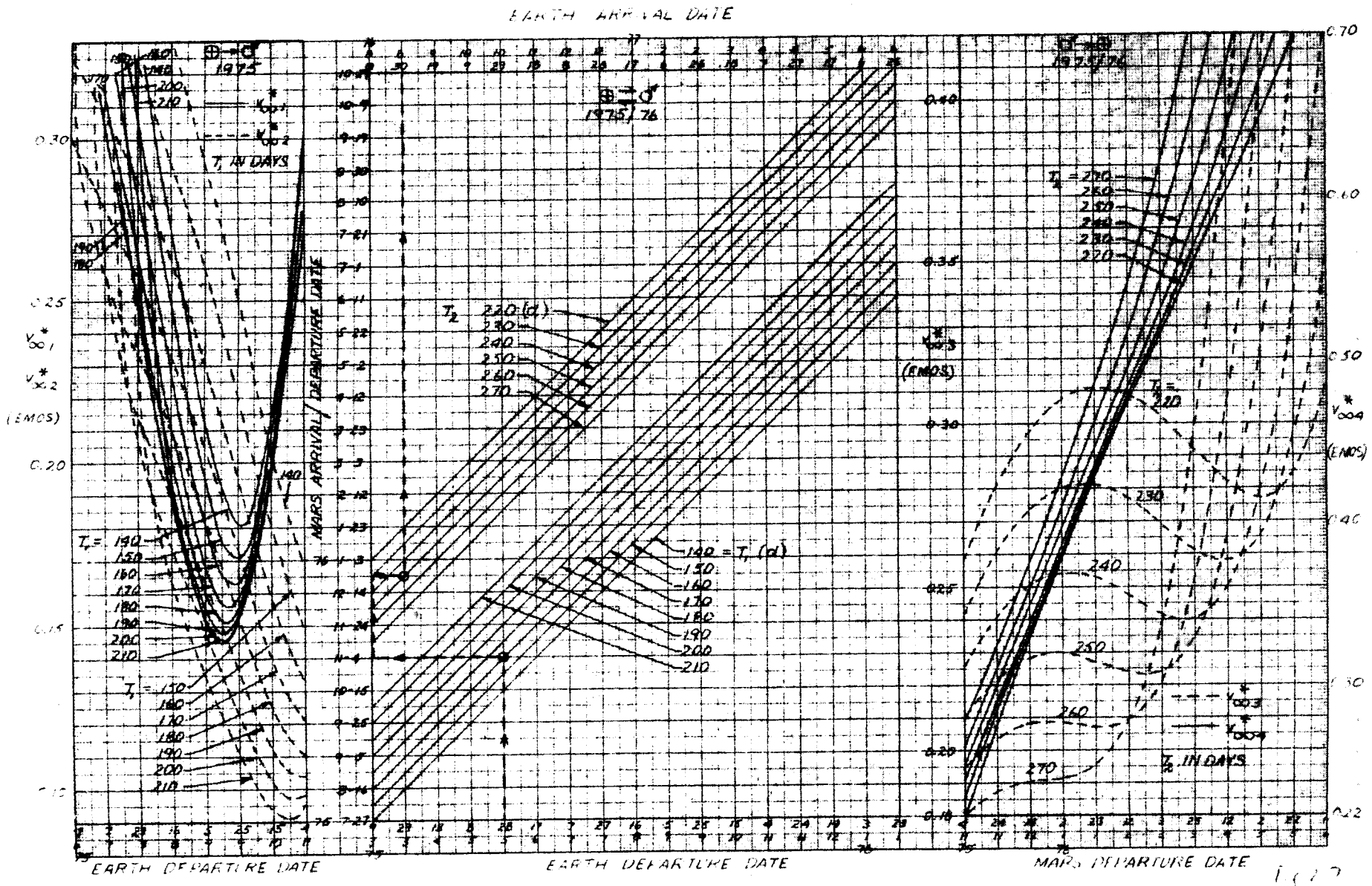
EARTH ARRIVAL DATE
EARTH DEPARTURE DATE
EARTH DEPARTURE DATE
MARS DEPARTURE DATE
MARS ARRIVAL / DEPARTURE DATE
T1 IN DAYS
T2 IN DAYS
(EMOS)
1975
1975/76

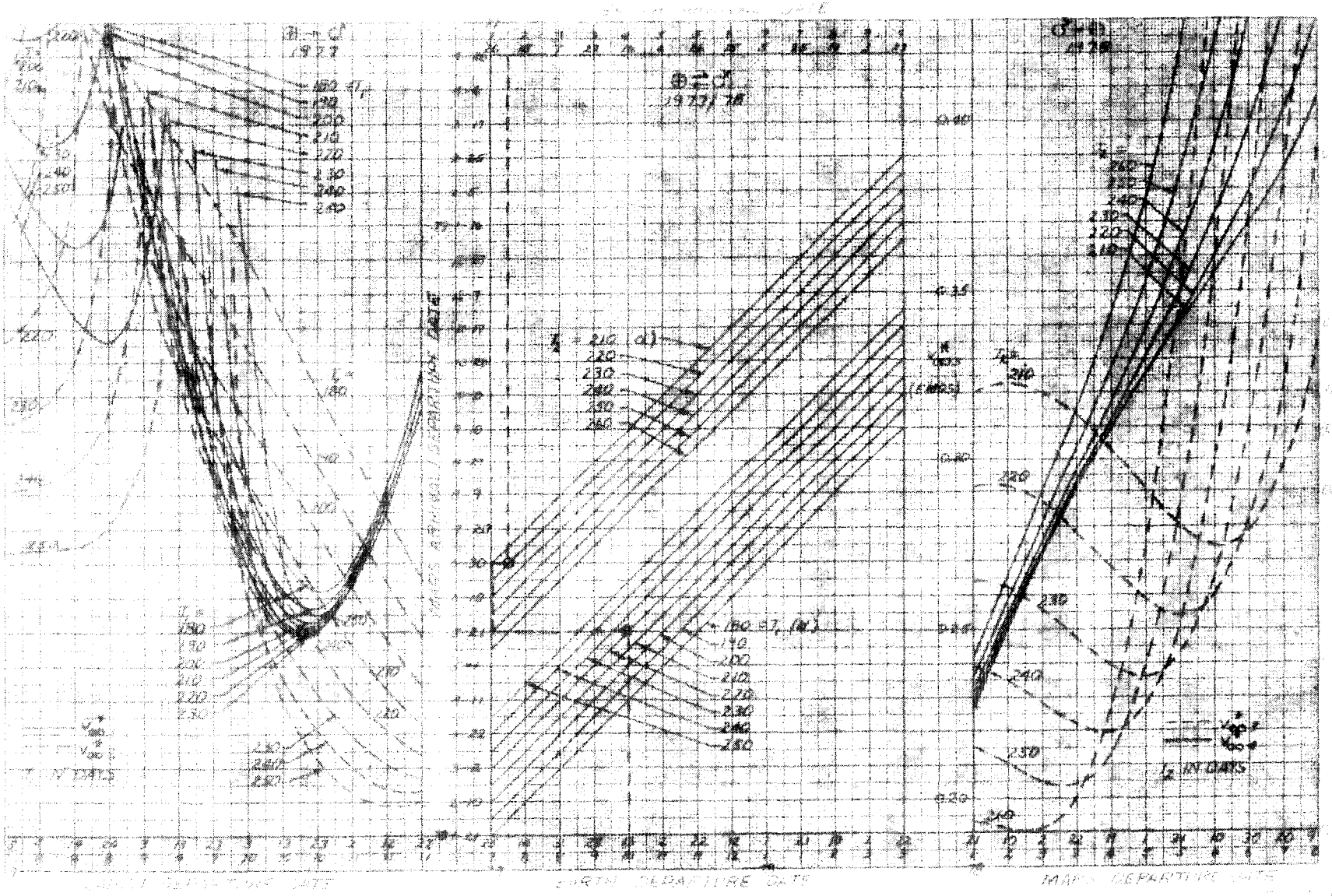
EARTH DEPARTURE DATE
MARS DEPARTURE DATE

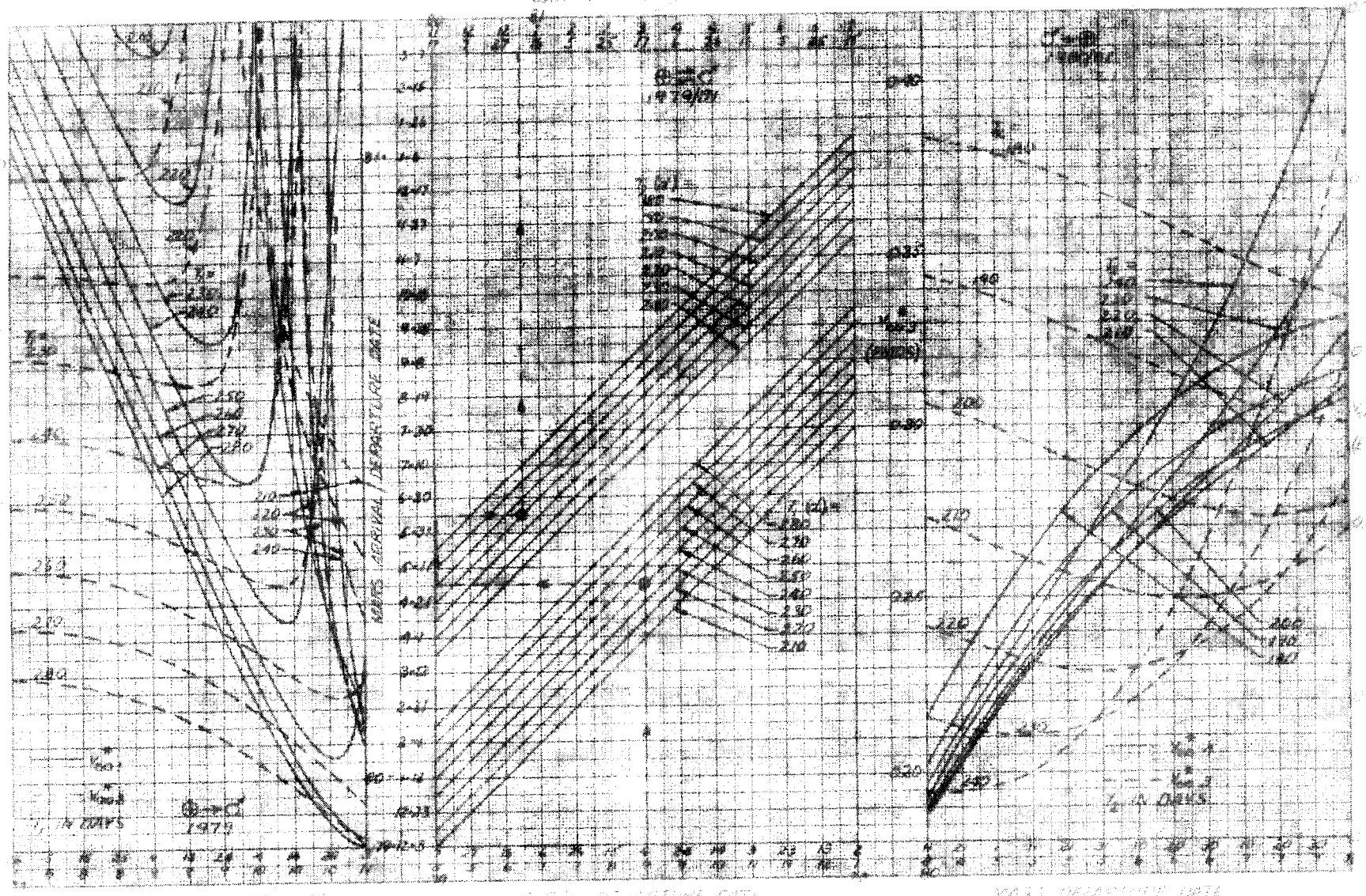
EARTH ARRIVAL DATE
MARS ARRIVAL / DEPARTURE DATE
1979
1979/80

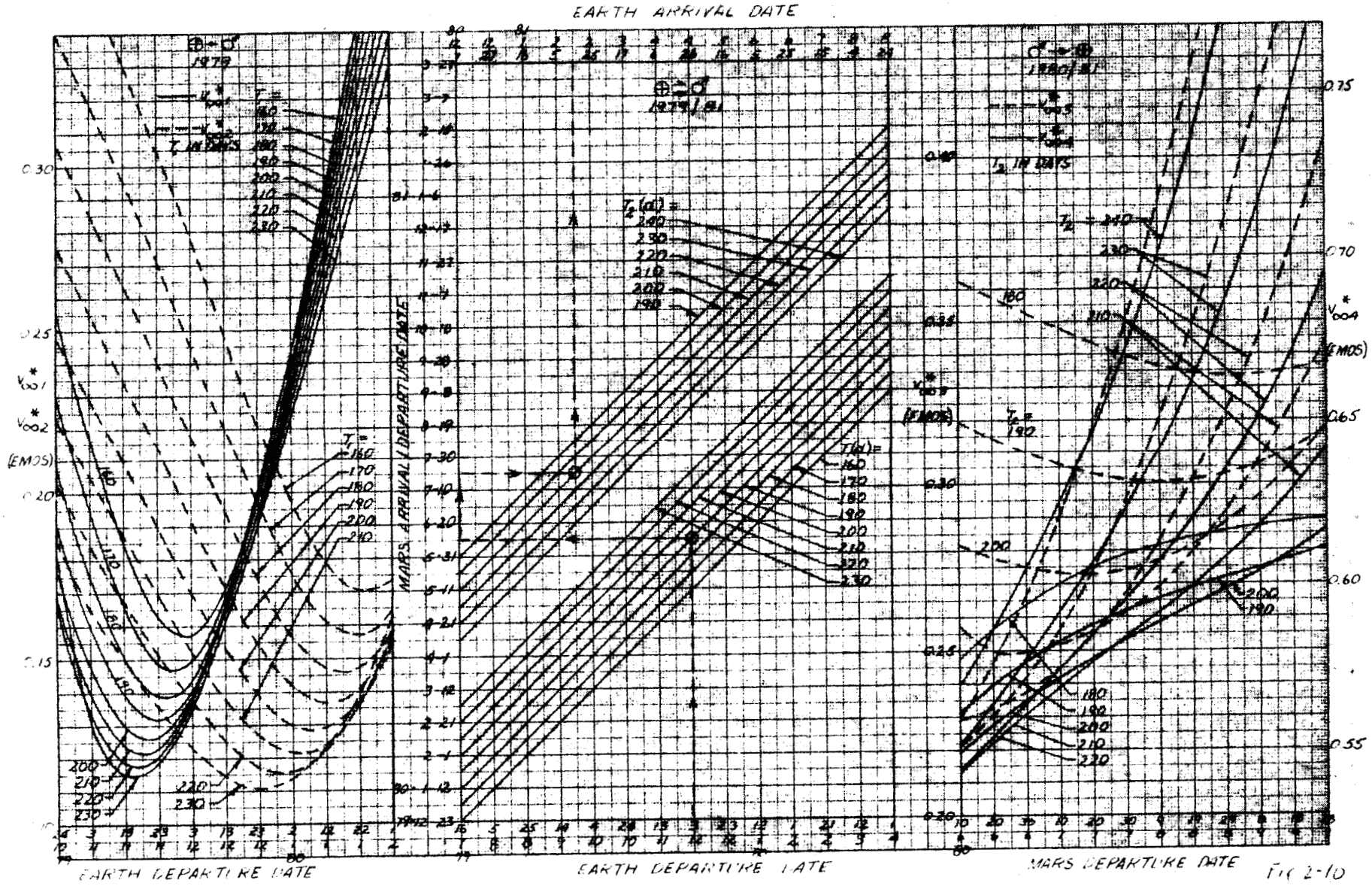
EARTH ARRIVAL DATE
EARTH DEPARTURE DATE
MARS ARRIVAL / DEPARTURE DATE
EARTH DEPARTURE DATE
MARS DEPARTURE DATE
(EMOS)

Fig 2-10

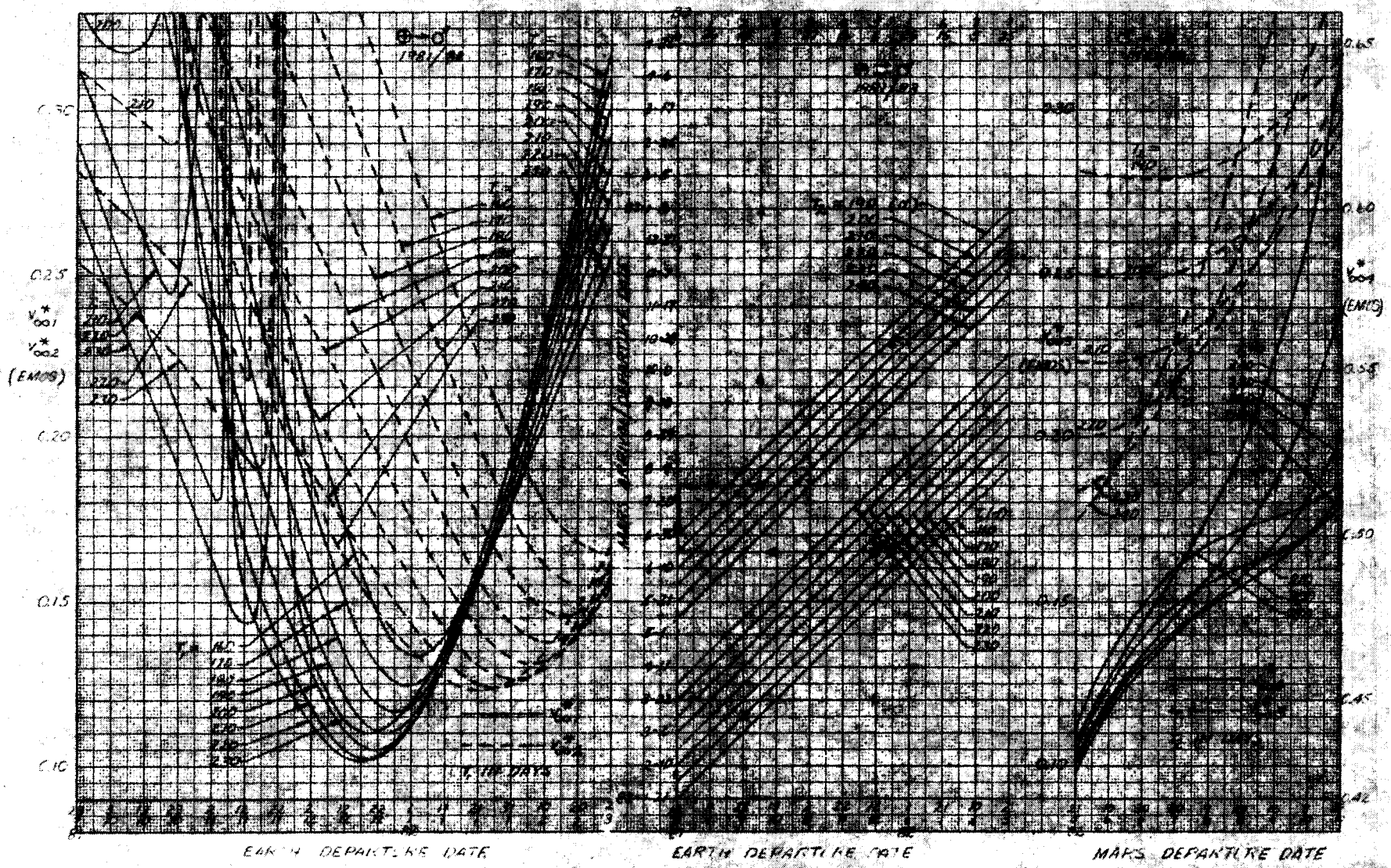
EARTH DEPARTURE DATE
EARTH DEPARTURE DATE
MARS DEPARTURE DATE
(EMIS)
(EMIS)

FIG. 2-11

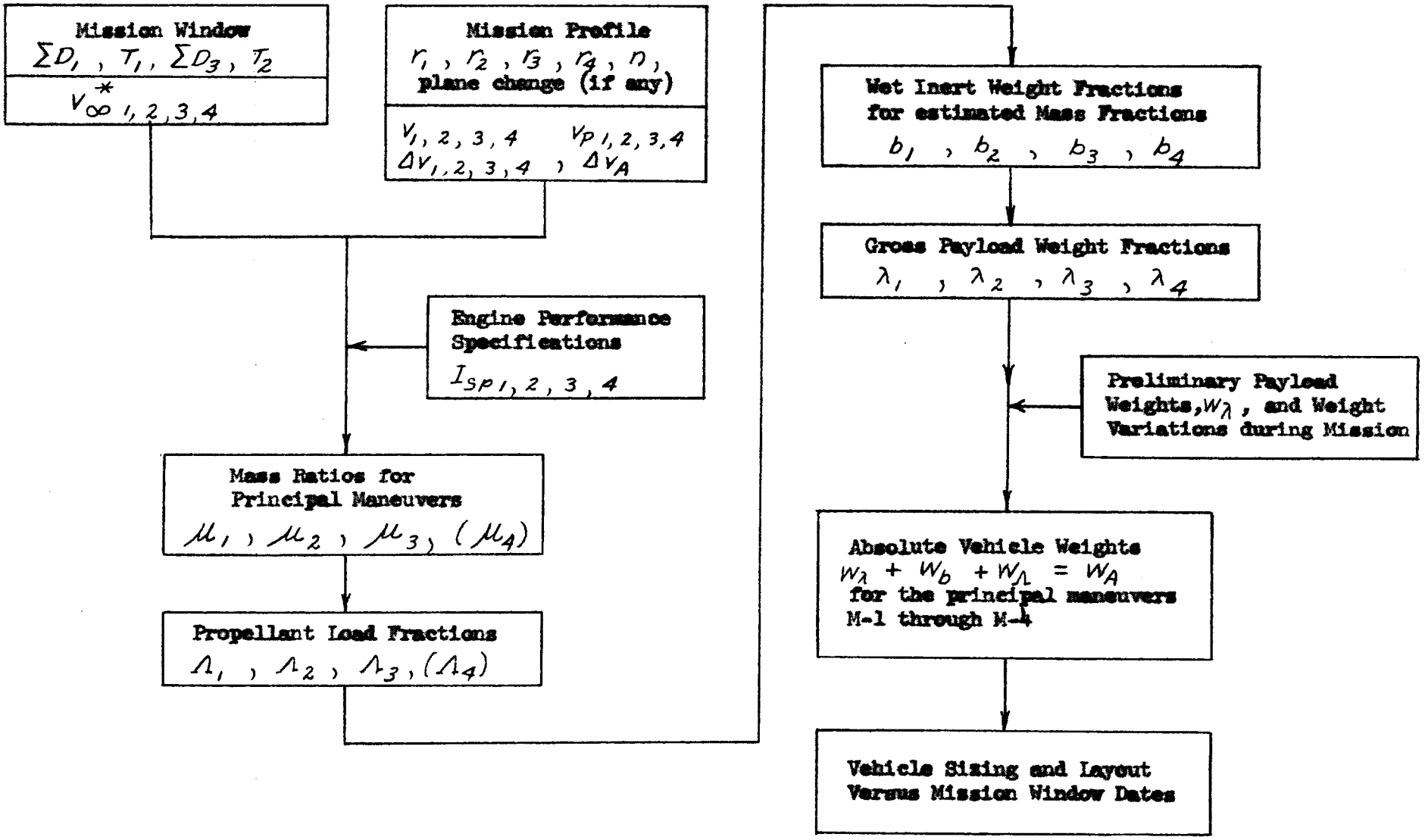

Fig. 4-1 Phase I Parametric Performance and Weight Estimates Using Mission Window Dates as Initial Independent Variable.

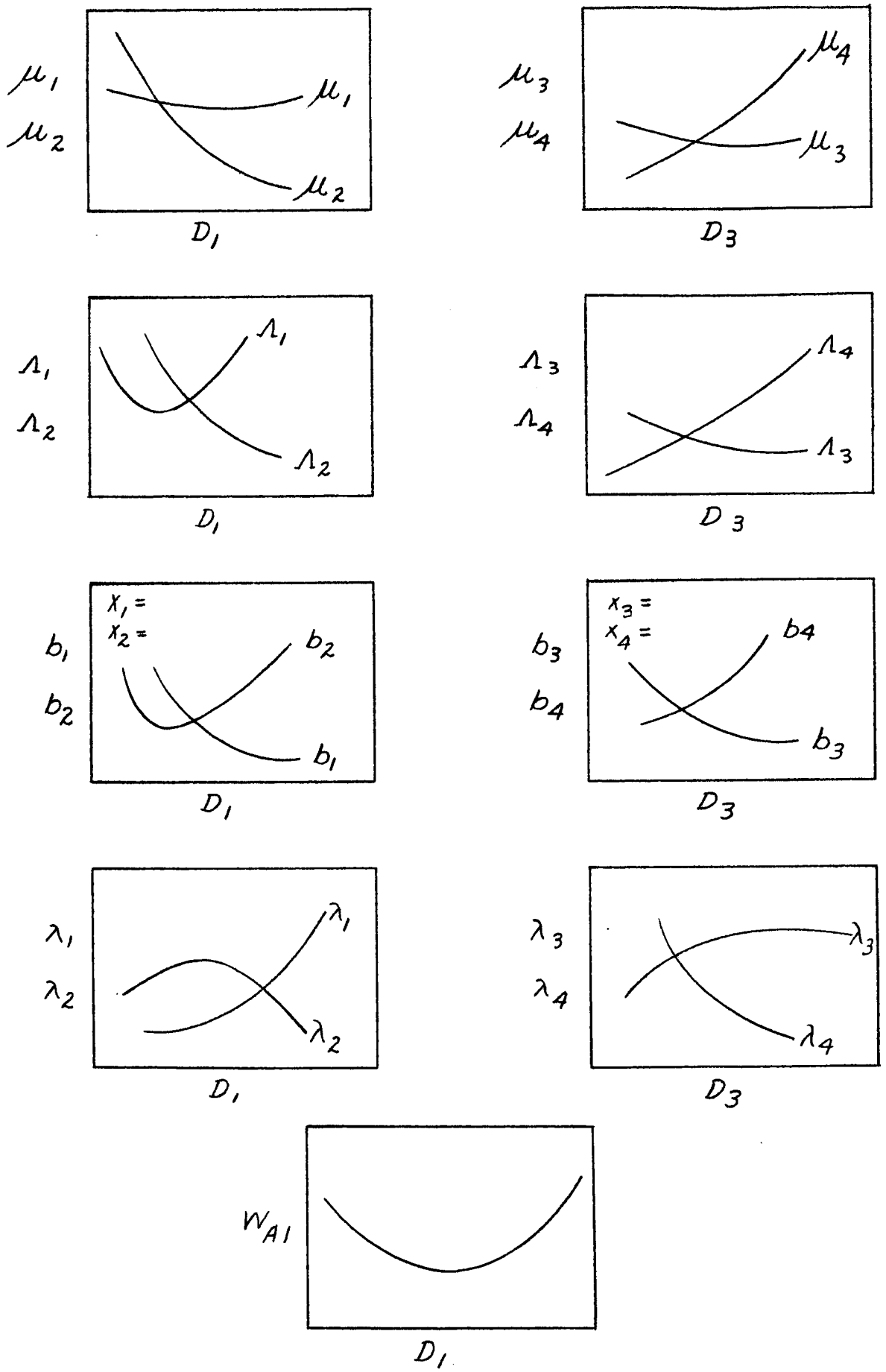

Fig. 4-2 Sequence of Graphs, Phase I

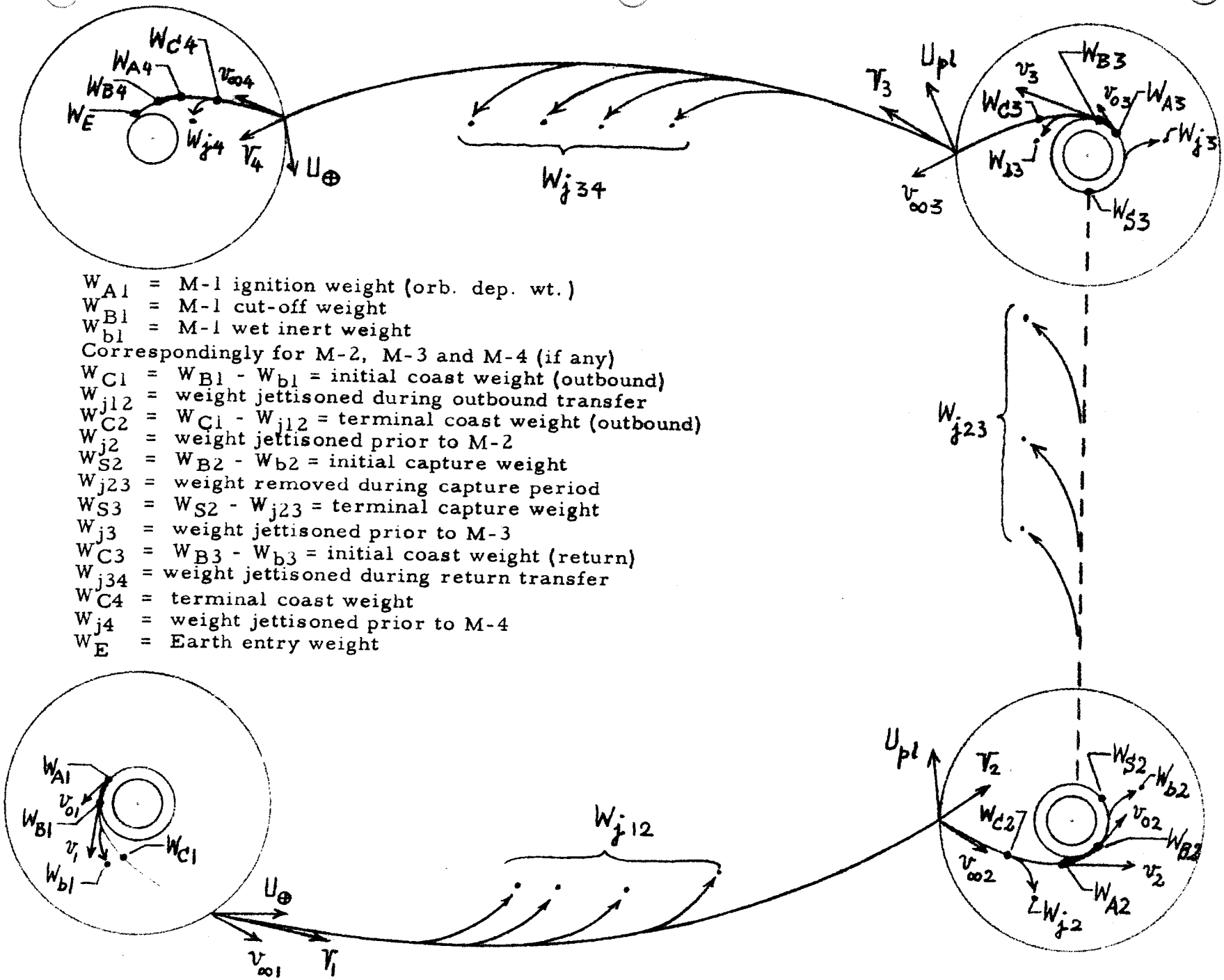

W_{A1} = M-1 ignition weight (orb. dep. wt.)
W_{B1} = M-1 cut-off weight
W_{b1} = M-1 wet inert weight
Correspondingly for M-2, M-3 and M-4 (if any)
W_{C1} = $W_{B1} - W_{b1}$ = initial coast weight (outbound)
W_{j12} = weight jettisoned during outbound transfer
W_{C2} = $W_{C1} - W_{j12}$ = terminal coast weight (outbound)
W_{j2} = weight jettisoned prior to M-2
W_{S2} = $W_{B2} - W_{b2}$ = initial capture weight
W_{j23} = weight removed during capture period
W_{S3} = $W_{S2} - W_{j23}$ = terminal capture weight
W_{j3} = weight jettisoned prior to M-3
W_{C3} = $W_{B3} - W_{b3}$ = initial coast weight (return)
W_{j34} = weight jettisoned during return transfer
W_{C4} = terminal coast weight
W_{j4} = weight jettisoned prior to M-4
W_E = Earth entry weight

Figure 4-3. Nomenclature of Weight and Velocity Terms

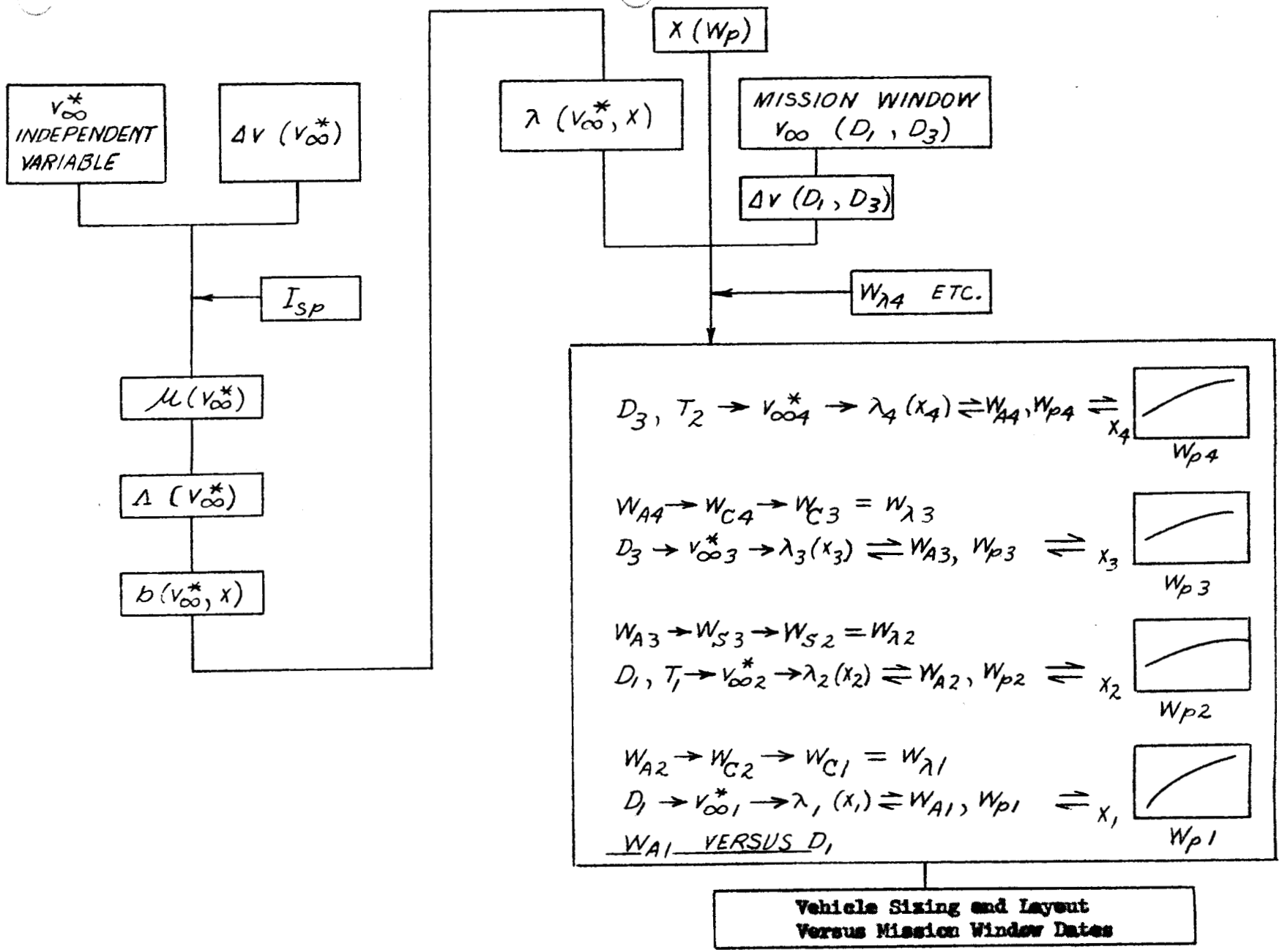

Fig. 4-4 **Phase I Parametric Performance and Weight Estimates Using Hyperbolic Excess Velocity as Initial Independent Variable.**

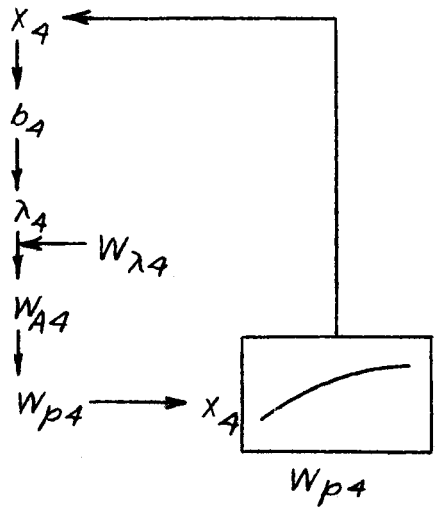

Iteration Cycle of Fig.

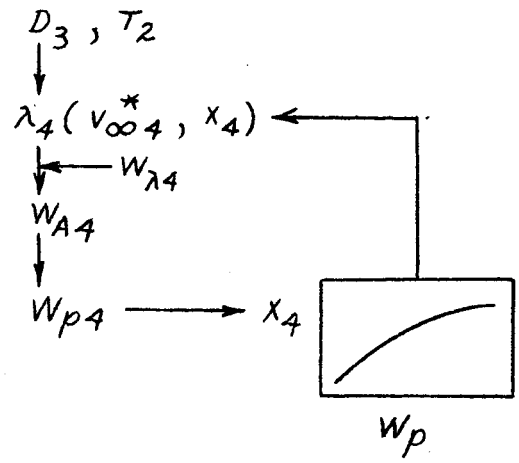

Iteration Cycle of Fig.

Fig. 4-5 Comparison of Iteration Cycles of the Two Methods of Phase I.

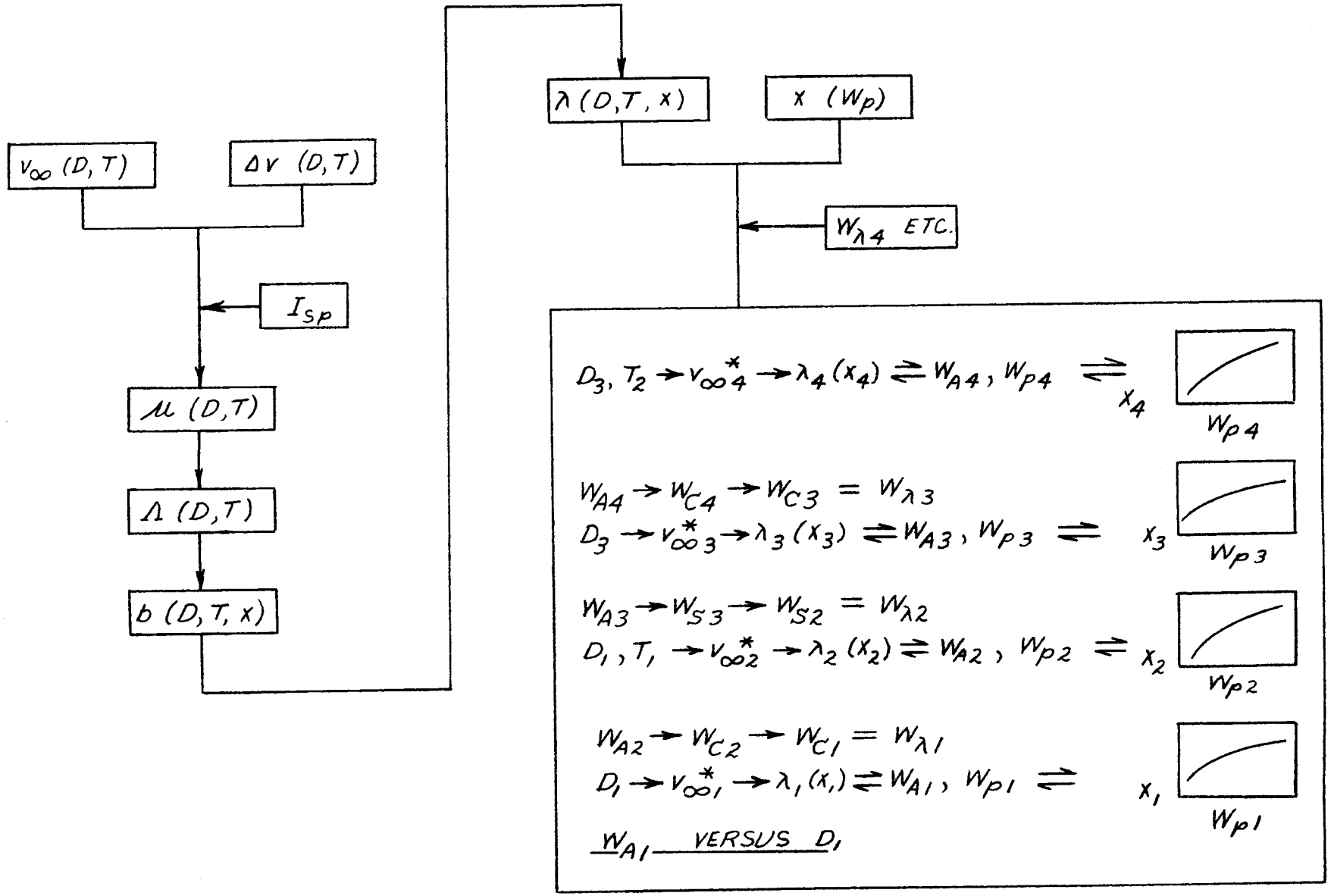

Fig. 4-6 Performance and Weight Estimates Using Mission Window Dates as Independent Variable with Parametric Variation of the Mass Fraction

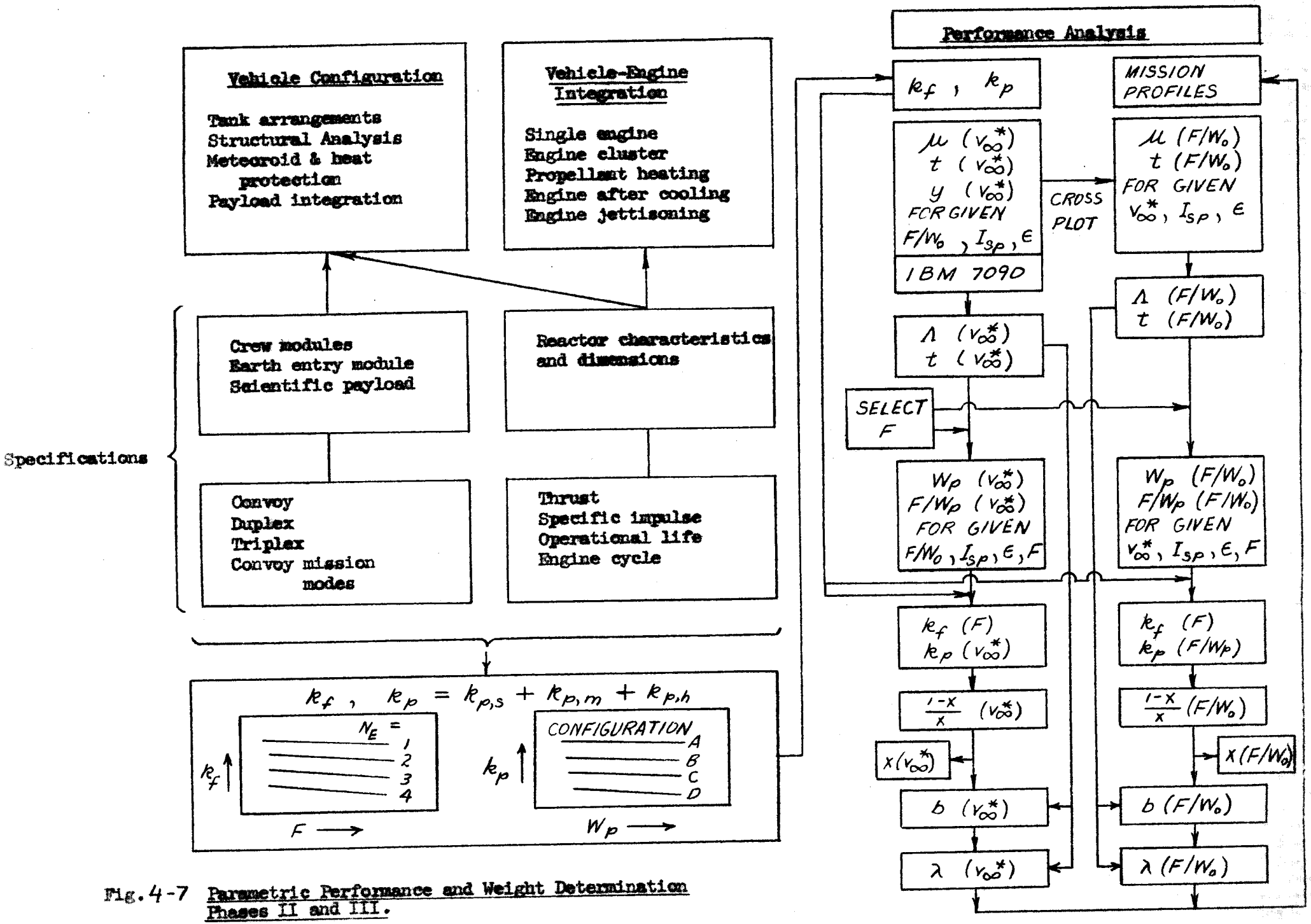

Fig. 4-7 Parametric Performance and Weight Determination Phases II and III.

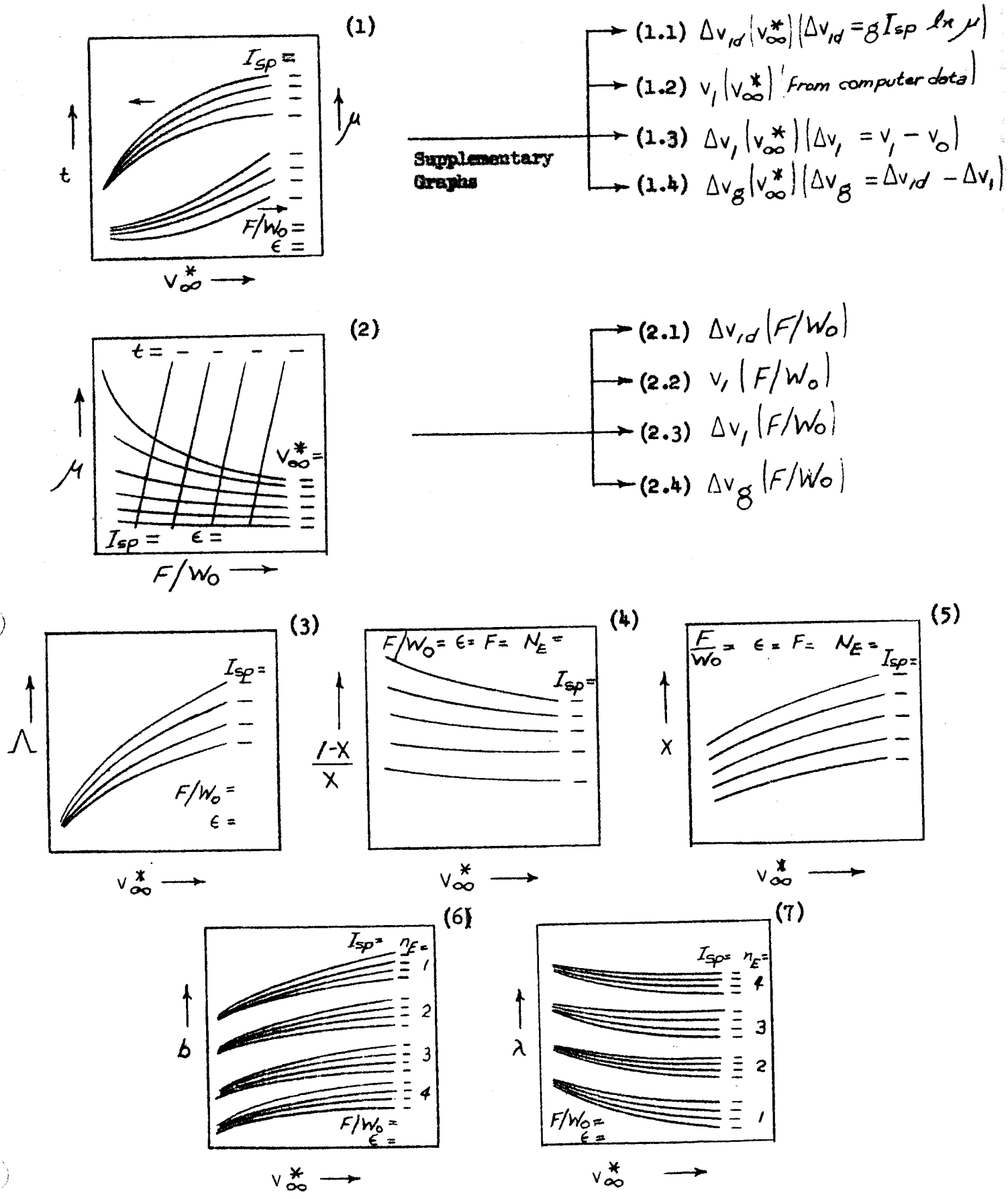

Fig. 4-8a Sequence of Charts, Phase II and III

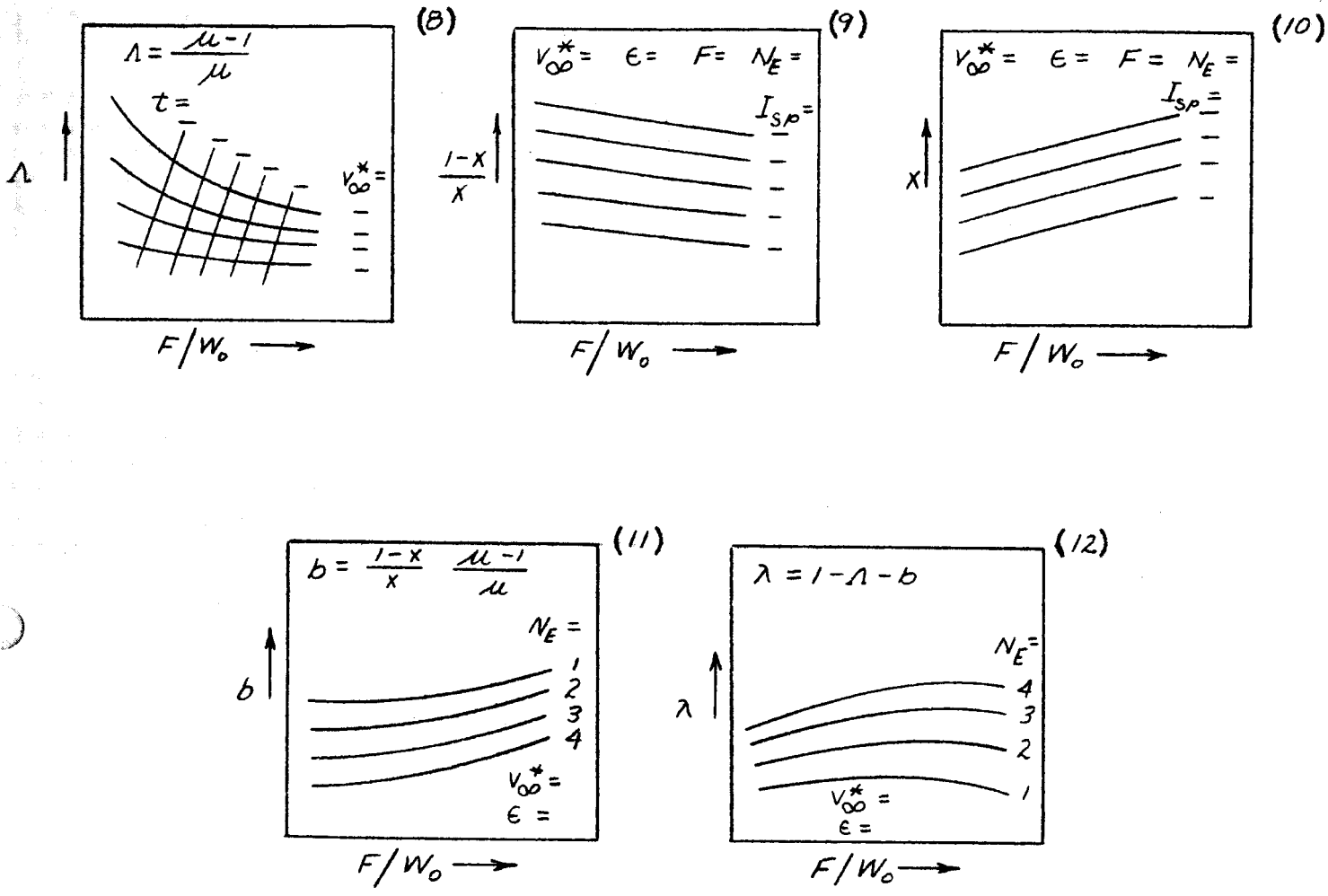

Fig. 4-8b Fig. 4-8a Concluded

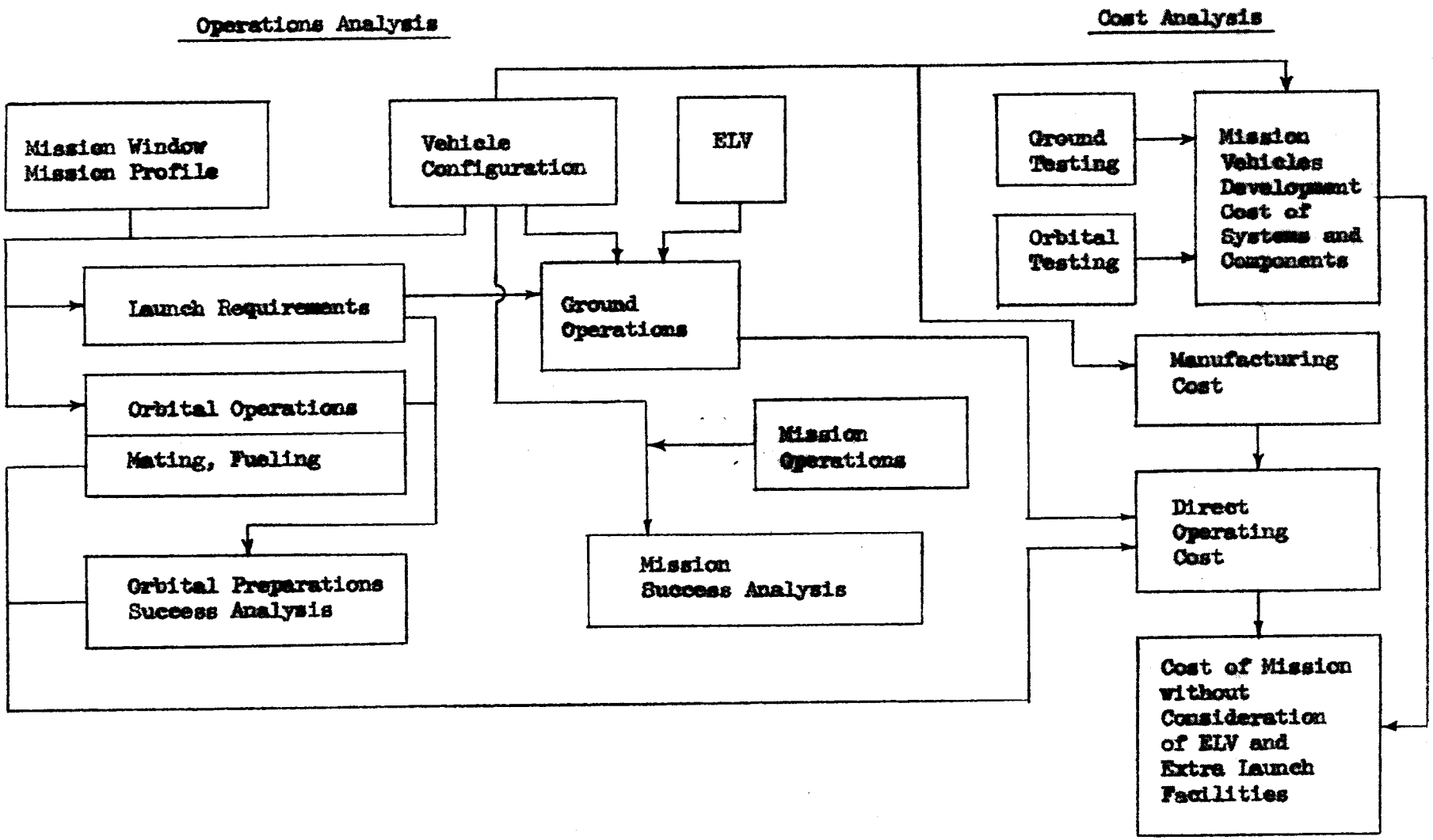

Fig. 4-9 Integration of Operations and Cost Analysis

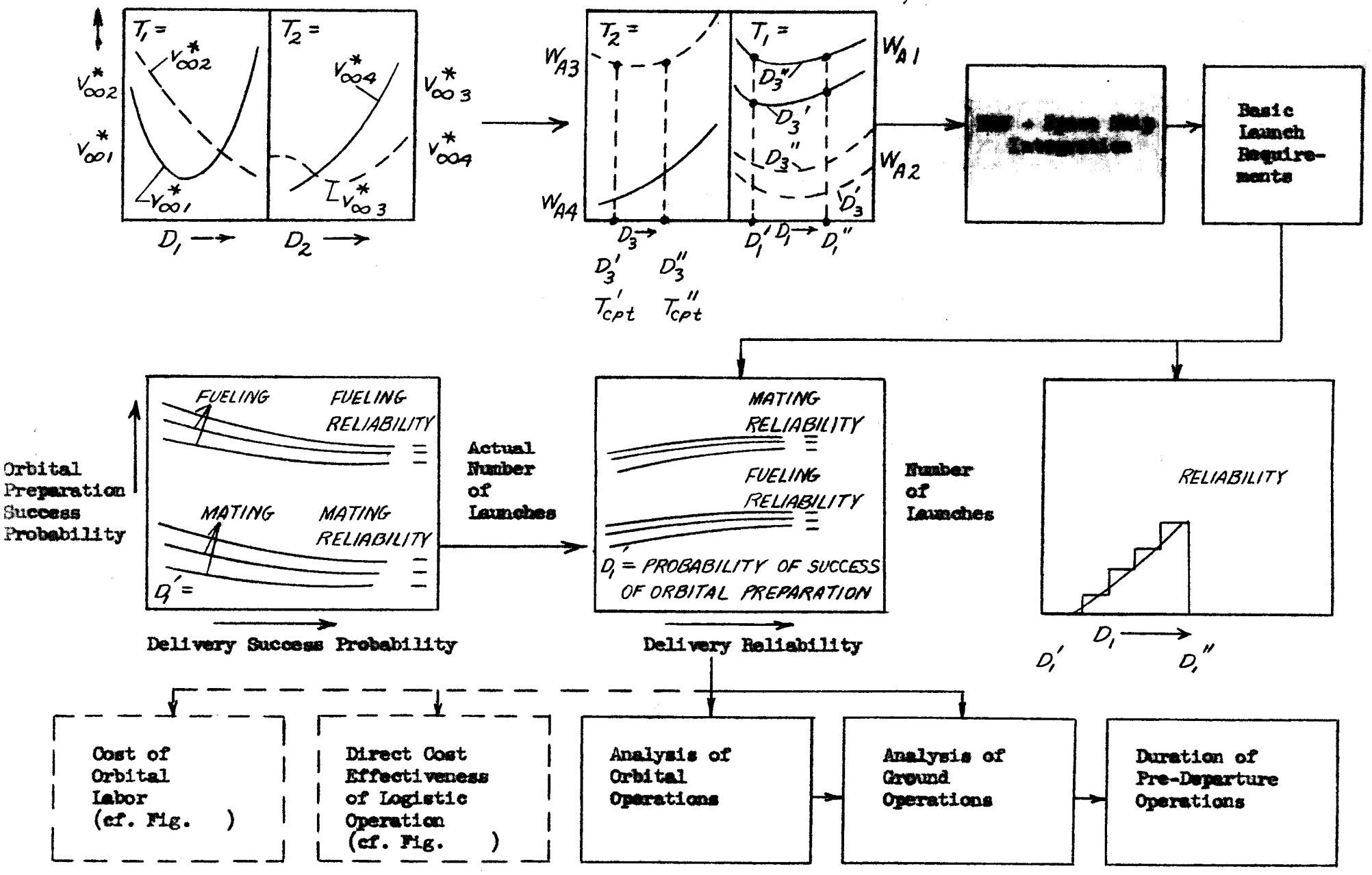

Fig. 4-10 Operations Analysis Flow Chart

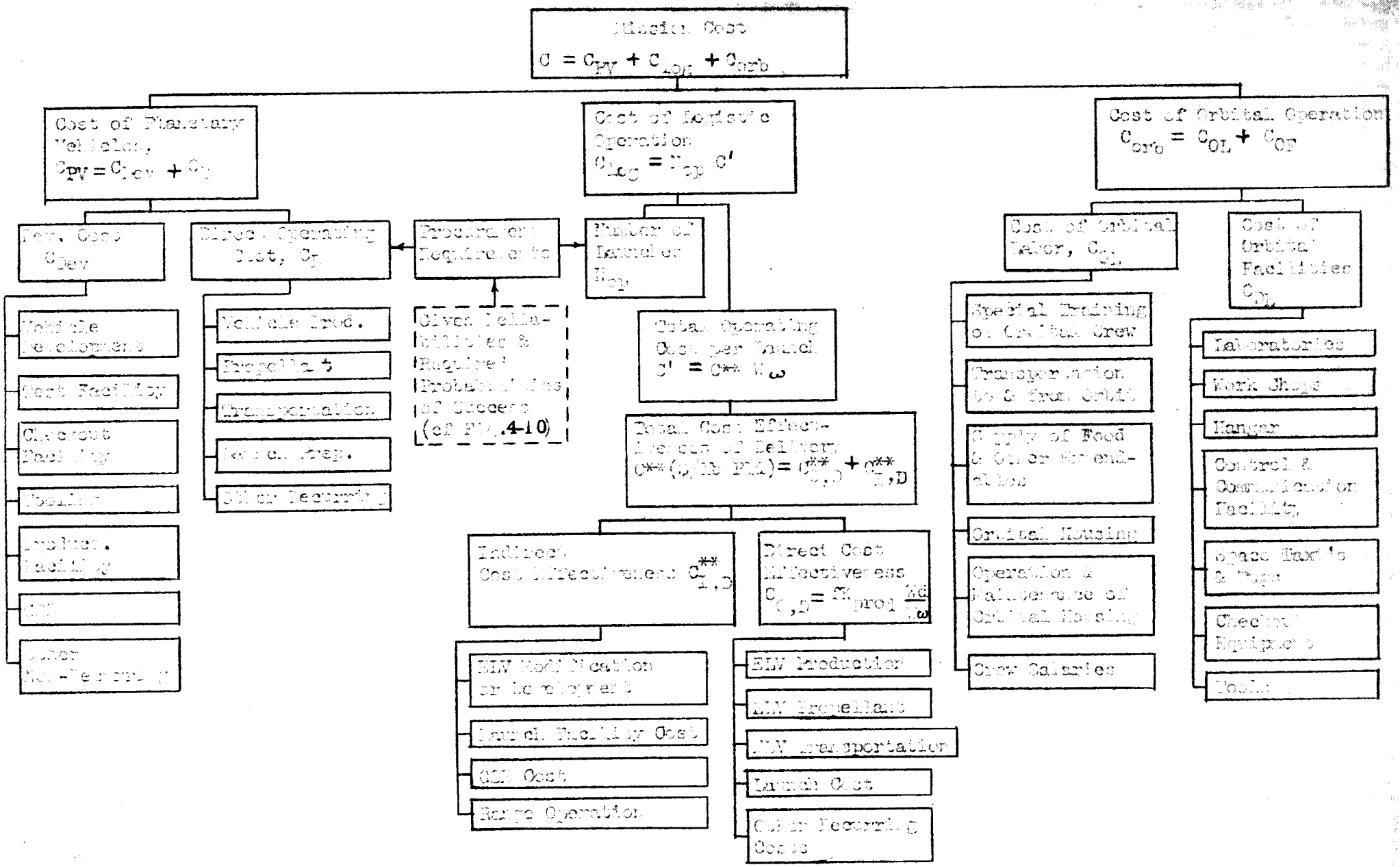

Fig. 4-11 Cost Analysis Breakdown

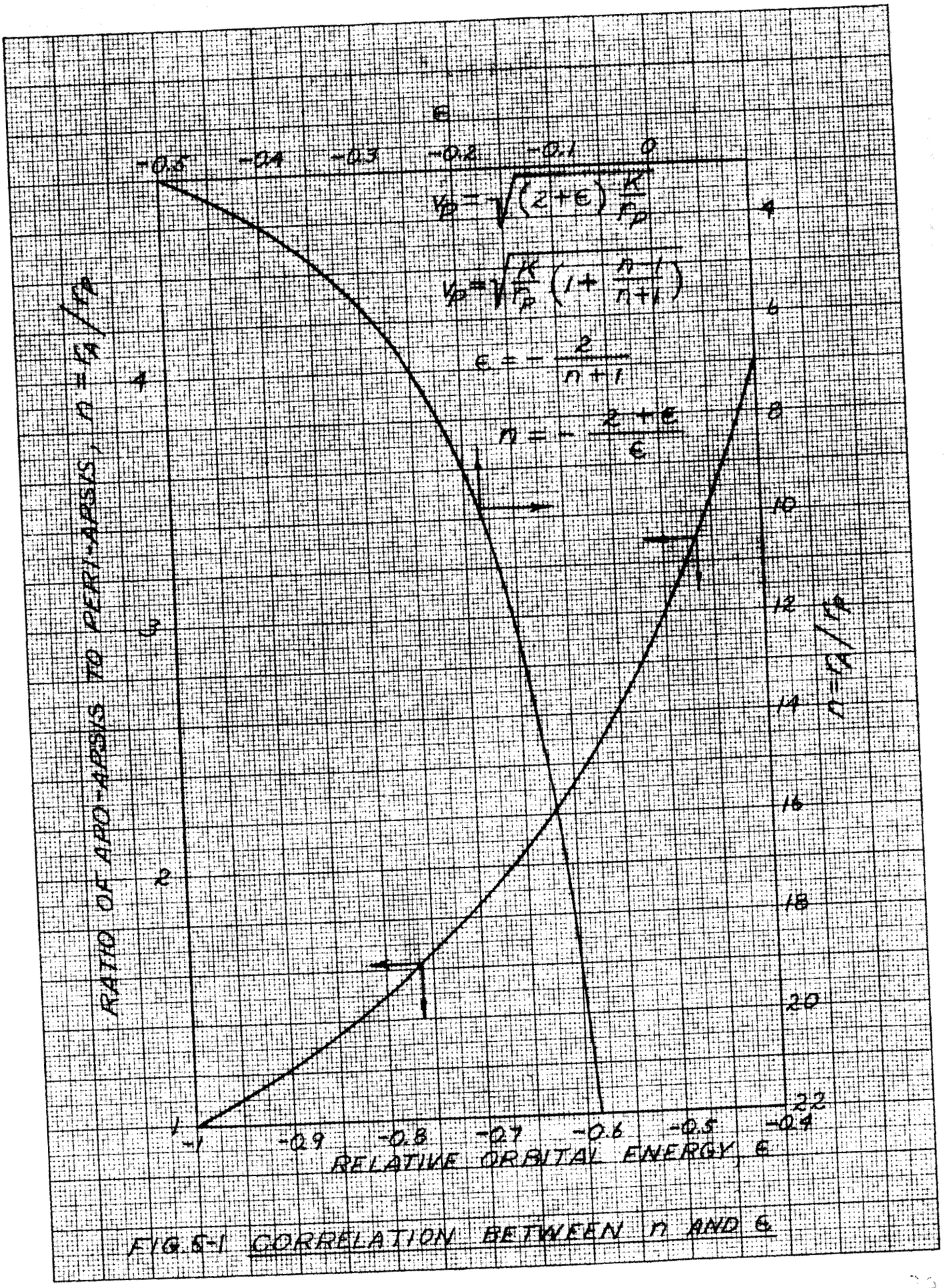

FIG. 6-1 CORRELATION BETWEEN n AND ε

K+E 10 X 10 TO THE CM. 359T-14G KEUFFEL & ESSER CO. ALBANENE

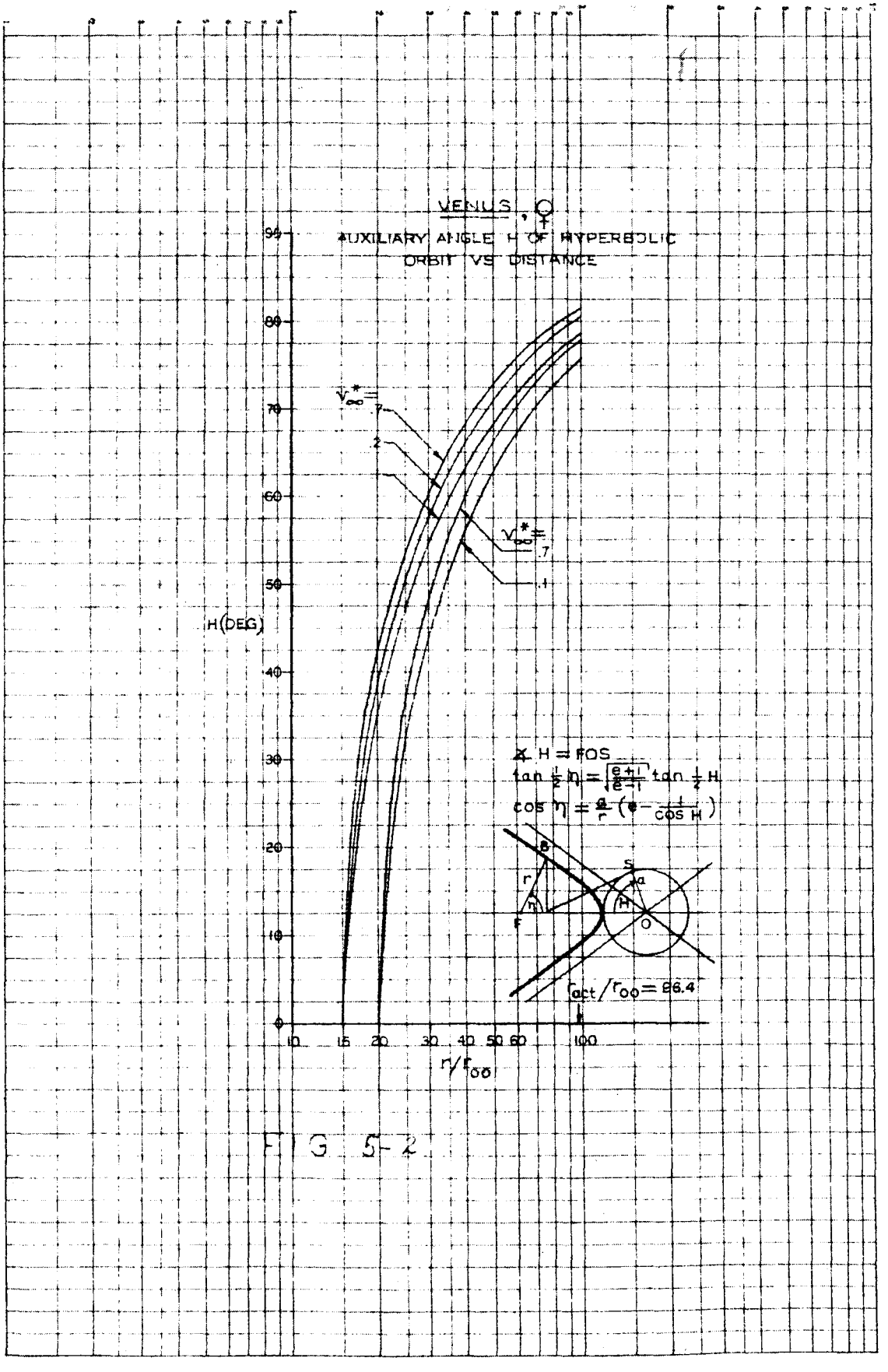
VENUS, ♀
AUXILIARY ANGLE H OF HYPERBOLIC ORBIT VS DISTANCE
H (DEG)
$V_\infty^* = 7$
2
$V_\infty^* = .7$
.1
∡ H = FOS
$\tan \frac{1}{2}\eta = \sqrt{\frac{e+1}{e-1}} \tan \frac{1}{2} H$
$\cos \eta = \frac{a}{r}\left(e - \frac{1}{\cos H}\right)$
$r_{act}/r_{\infty} = 86.4$
r/r_{∞}

FIG 5-2

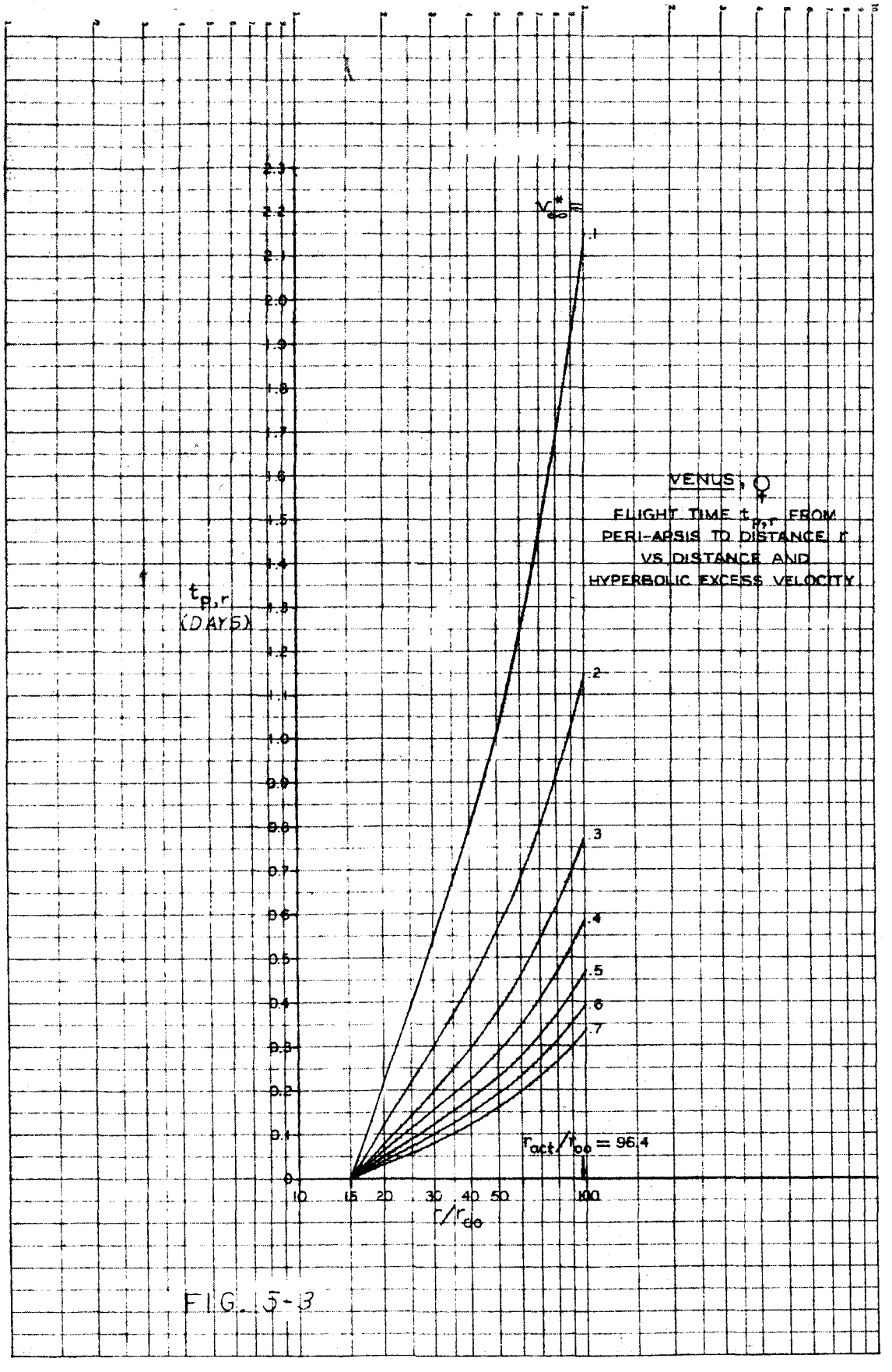
VENUS, ♀
FLIGHT TIME $t_{p,r}$ FROM PERI-APSIS TO DISTANCE r VS DISTANCE AND HYPERBOLIC EXCESS VELOCITY
V^*_{∞} =
.1
.2
.3
.4
.5
.6
.7
$t_{p,r}$ (DAYS)
r_{act}/r_{∞} = 96.4
r/r_{∞}
10
15
20
30
40
50
100
0
0.1
0.2
0.3
0.4
0.5
0.6
0.7
0.8
0.9
1.0
1.1
1.2
1.3
1.4
1.5
1.6
1.7
1.8
1.9
2.0
2.1
2.2
2.3

FIG. 5-3

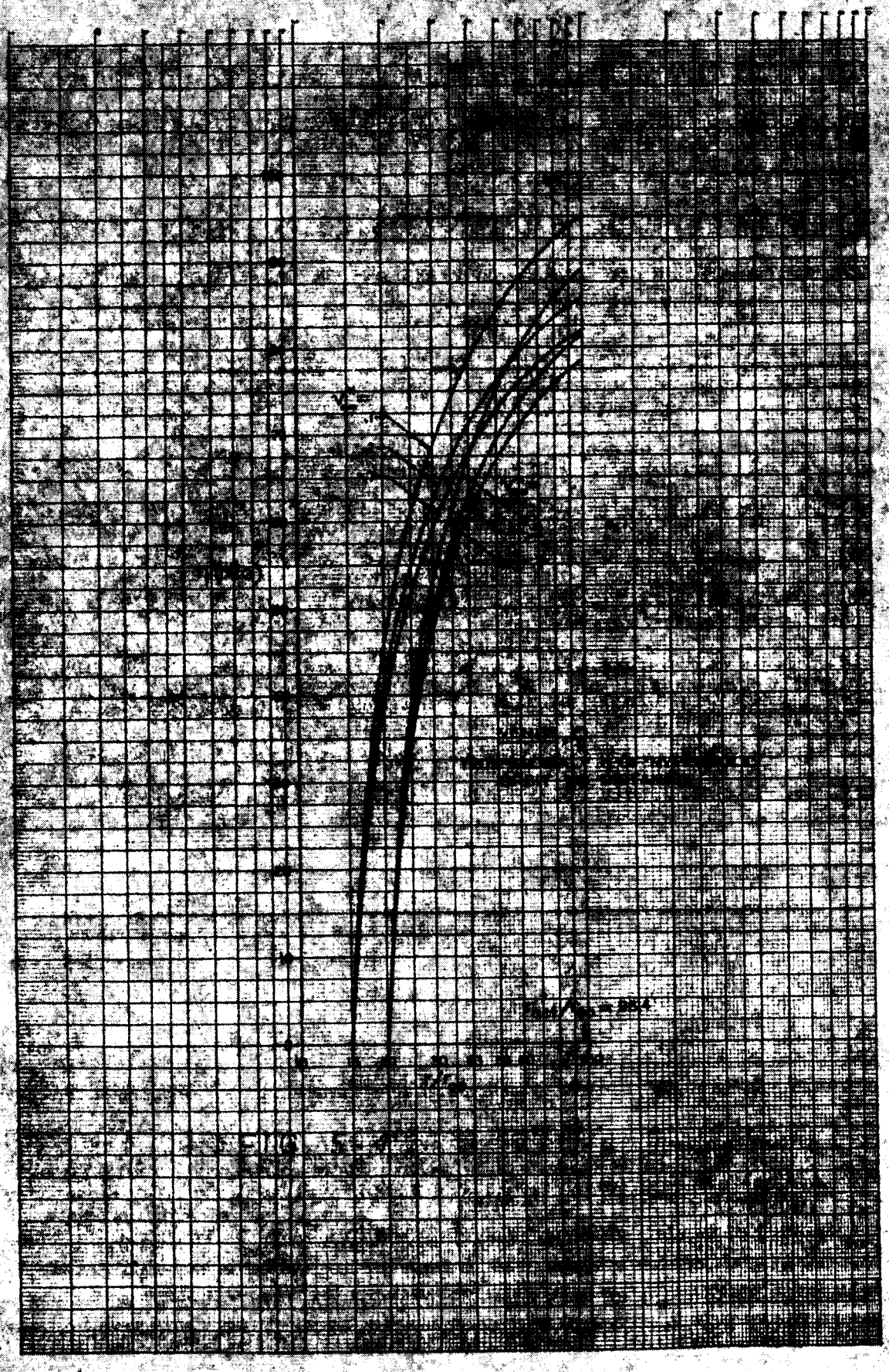

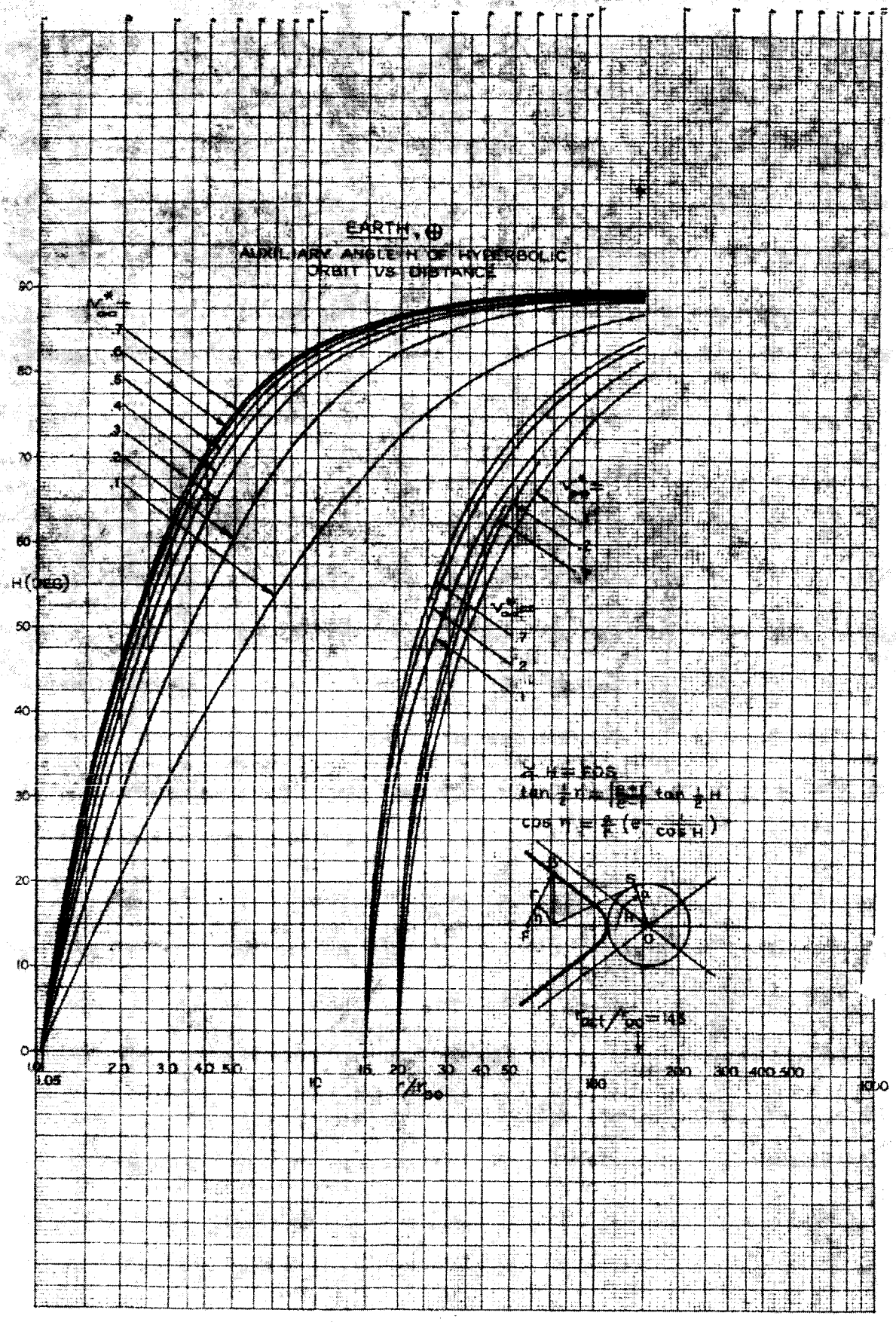
EARTH, ⊕
AUXILIARY ANGLE H OF HYPERBOLIC ORBIT VS DISTANCE
H (DEG)
r/r_SOI
1.05
2.0
3.0
4.0
5.0
10
15
20
30
40
50
100
200
300
400
500
1000
0
10
20
30
40
50
60
70
80
90

Fig. 3-5

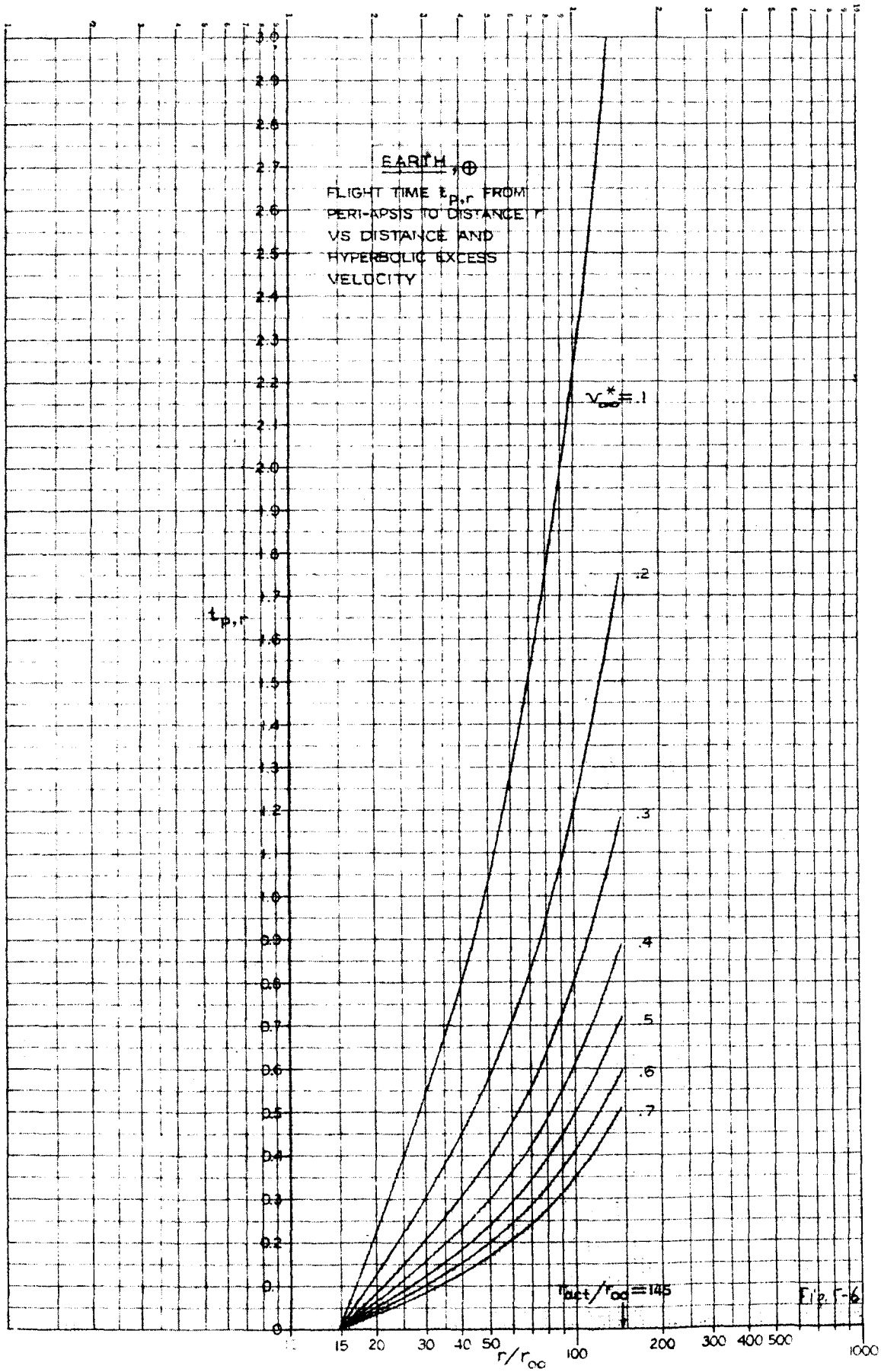
EARTH, ⊕
FLIGHT TIME $t_{p,r}$ FROM PERI-APSIS TO DISTANCE r VS DISTANCE AND HYPERBOLIC EXCESS VELOCITY
$V_{\infty}^{*} = .1$
.2
.3
.4
.5
.6
.7
$t_{p,r}$
$r_{act}/r_{\infty} = 145$
r/r_{∞}
15 20 30 40 50 100 200 300 400 500 1000
0 0.1 0.2 0.3 0.4 0.5 0.6 0.7 0.8 0.9 1.0 1.1 1.2 1.3 1.4 1.5 1.6 1.7 1.8 1.9 2.0 2.1 2.2 2.3 2.4 2.5 2.6 2.7 2.8 2.9 3.0

Fig. 5-6

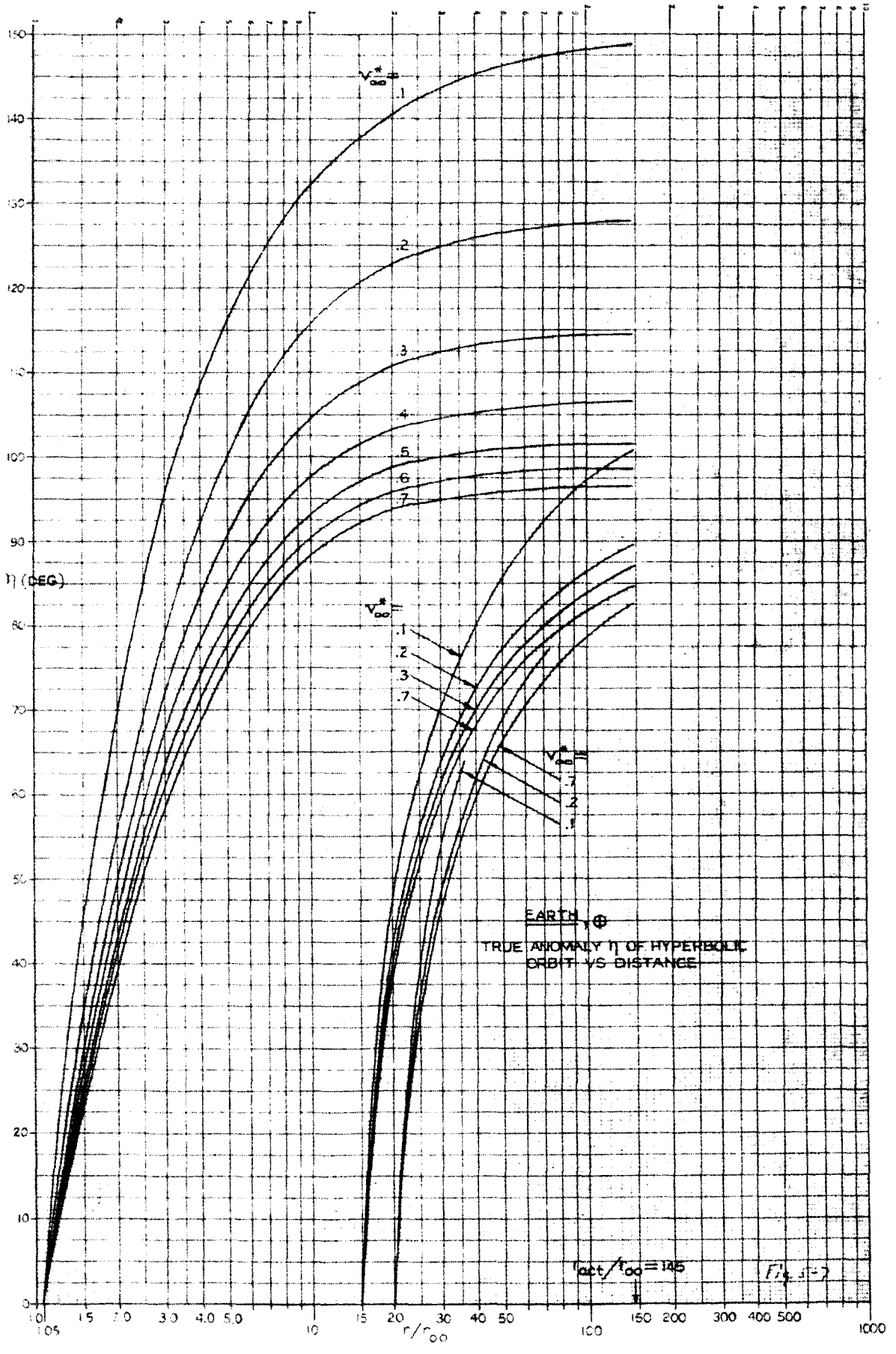
$V^*_{\infty}=$
.1
.2
.3
.4
.5
.6
.7
$V^*_{\infty}=$
.1
.2
.3
.7
$V^*_{\infty}=$
.7
.2
.1
η (DEG)
EARTH ⊕
TRUE ANOMALY η OF HYPERBOLIC ORBIT VS DISTANCE
$r_{act}/r_{\infty}=145$
r/r_{∞}

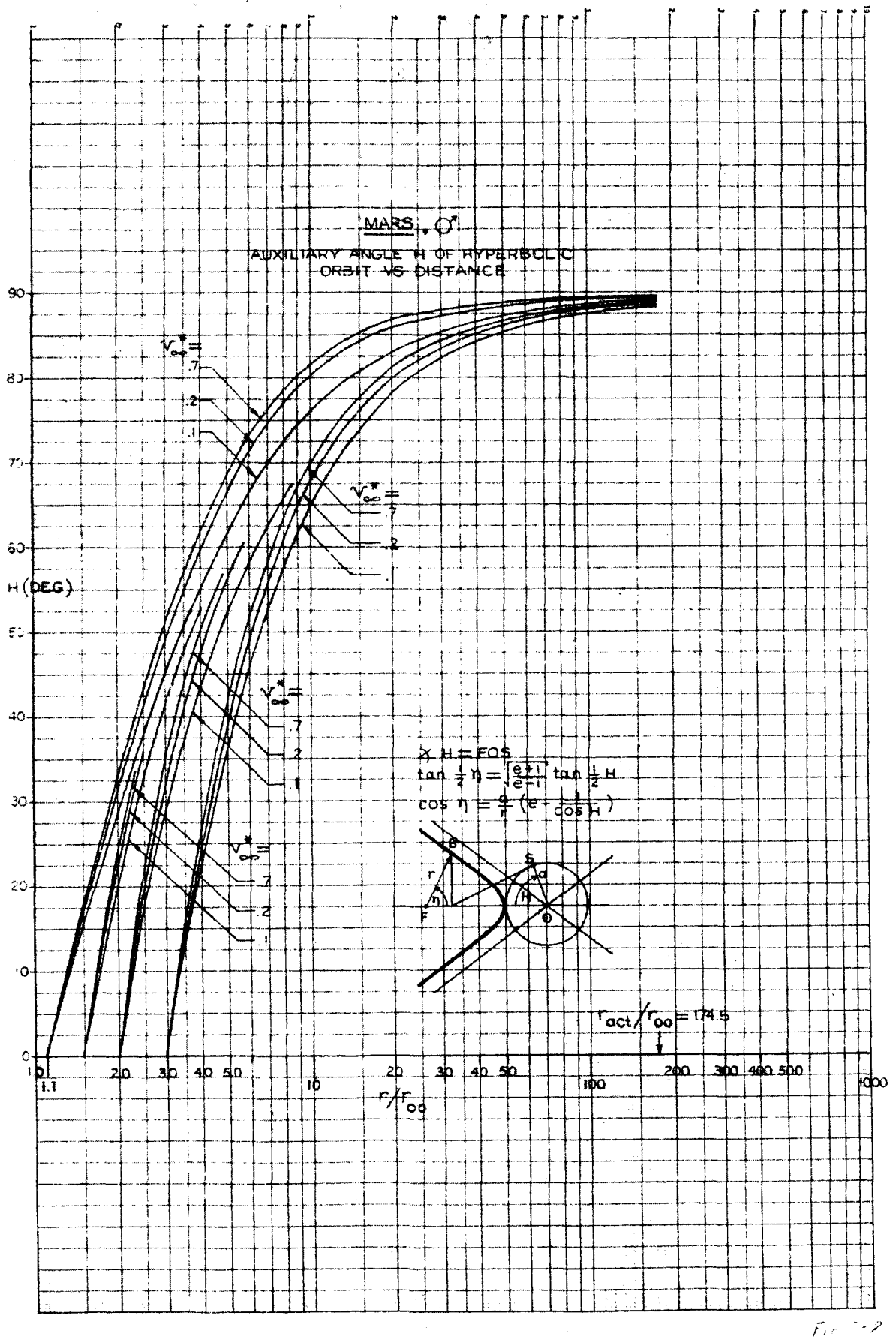
MARS ♂
AUXILIARY ANGLE H OF HYPERBOLIC ORBIT VS DISTANCE
H (DEG)
r/r_oo
r_act/r_oo = 174.5
V*_∞ = .7
.2
.1
∡ H = FOS
tan ½ η = √((e+1)/(e−1)) tan ½ H
cos η = a/r (e − 1/cos H)

Fig. 2

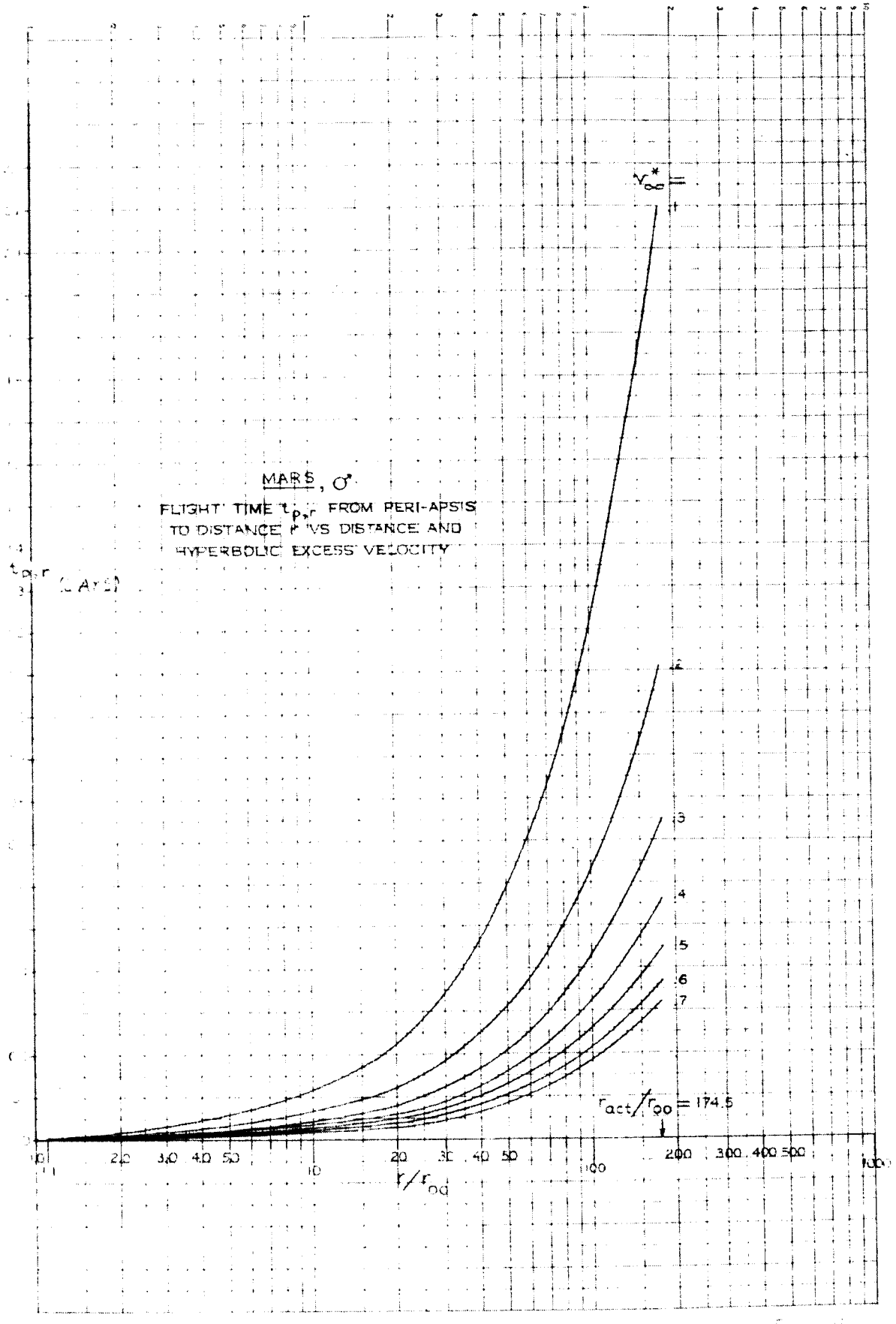
MARS, ♂
FLIGHT TIME $t_{p,r}$ FROM PERI-APSIS
TO DISTANCE r VS DISTANCE AND
HYPERBOLIC EXCESS VELOCITY
$t_{p,r}$ (DAYS)
$v_\infty^* =$
1
2
3
4
5
6
7
$r_{act}/r_{oo} = 174.5$
r/r_{oo}
1.0
2.0
3.0
4.0
5.0
10
20
30
40
50
100
200
300
400
500
1000

Fig. 7

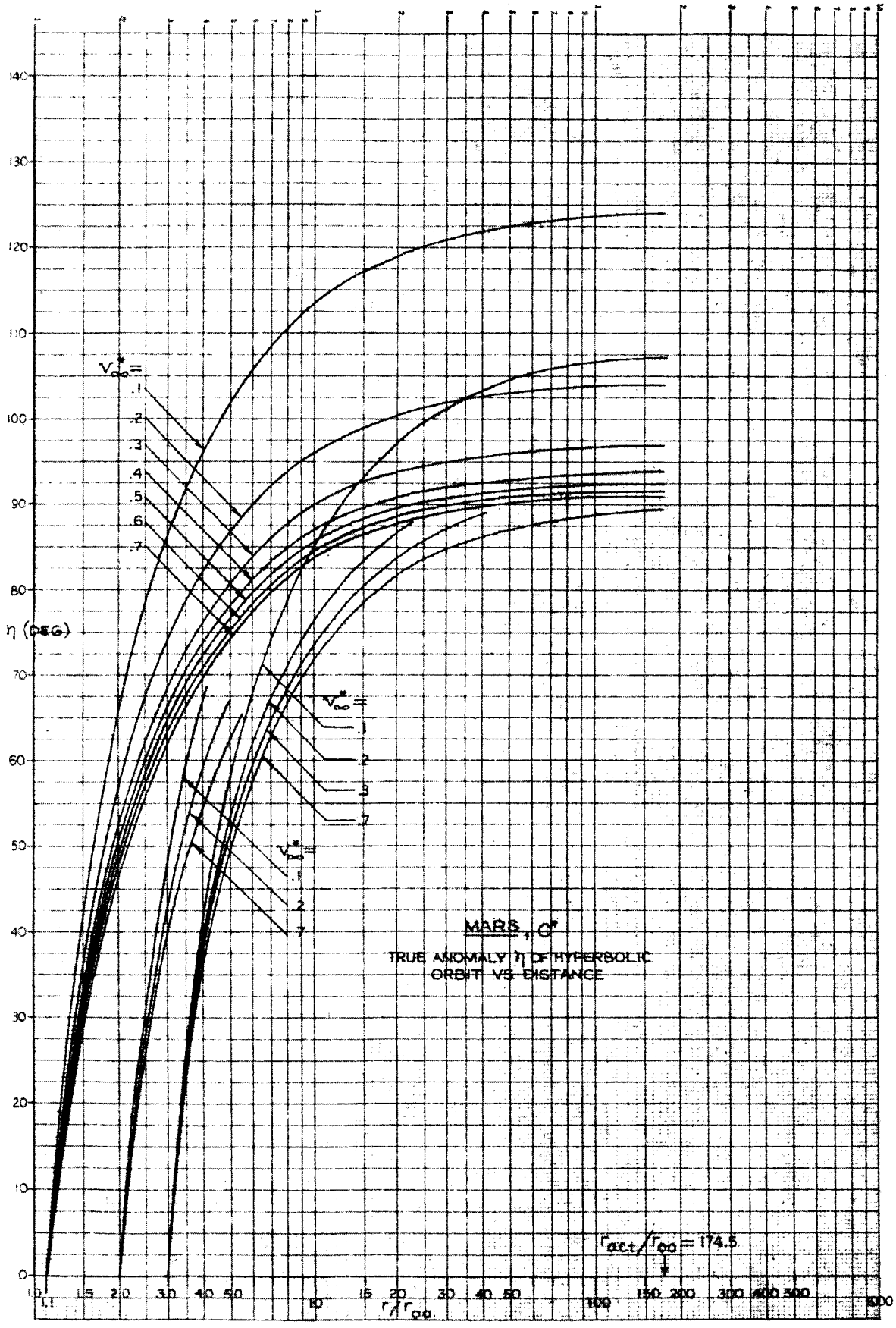
MARS, O*
TRUE ANOMALY η OF HYPERBOLIC ORBIT VS DISTANCE
η (DEG)
r/r∞
V*∞ = .1 .2 .3 .4 .5 .6 .7
V*∞ = .1 .2 .3 .7
V*∞ = .1 .2 .7
r act/r∞ = 174.5

Fig. 5-10

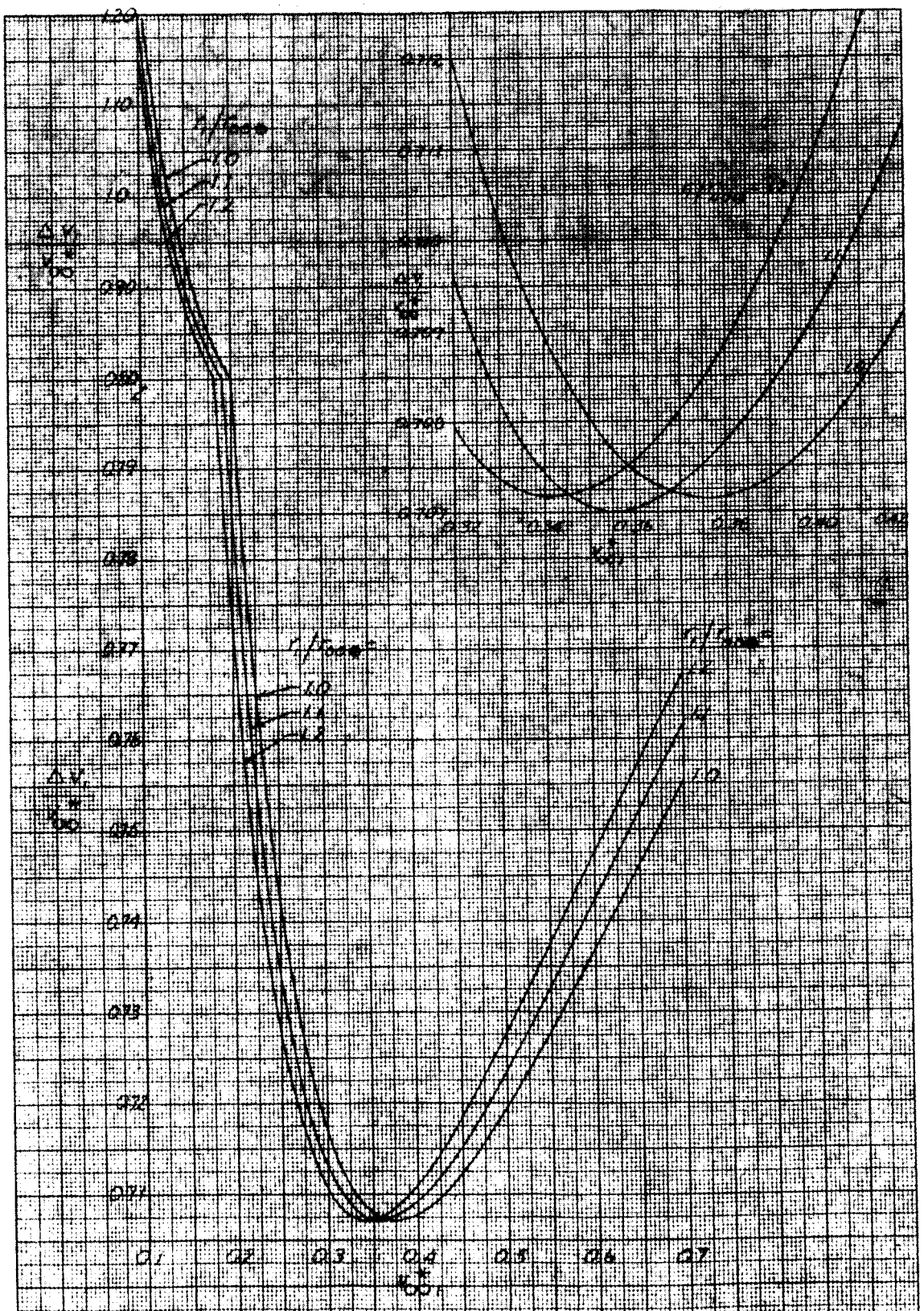

FIG 5-11 NON-DIMENSIONAL EARTH DEPARTURE VELOCITY INCREMENT VS. HYPERBOLIC EXCESS VELOCITY FOR SEVERAL EARTH ORBIT DISTANCES

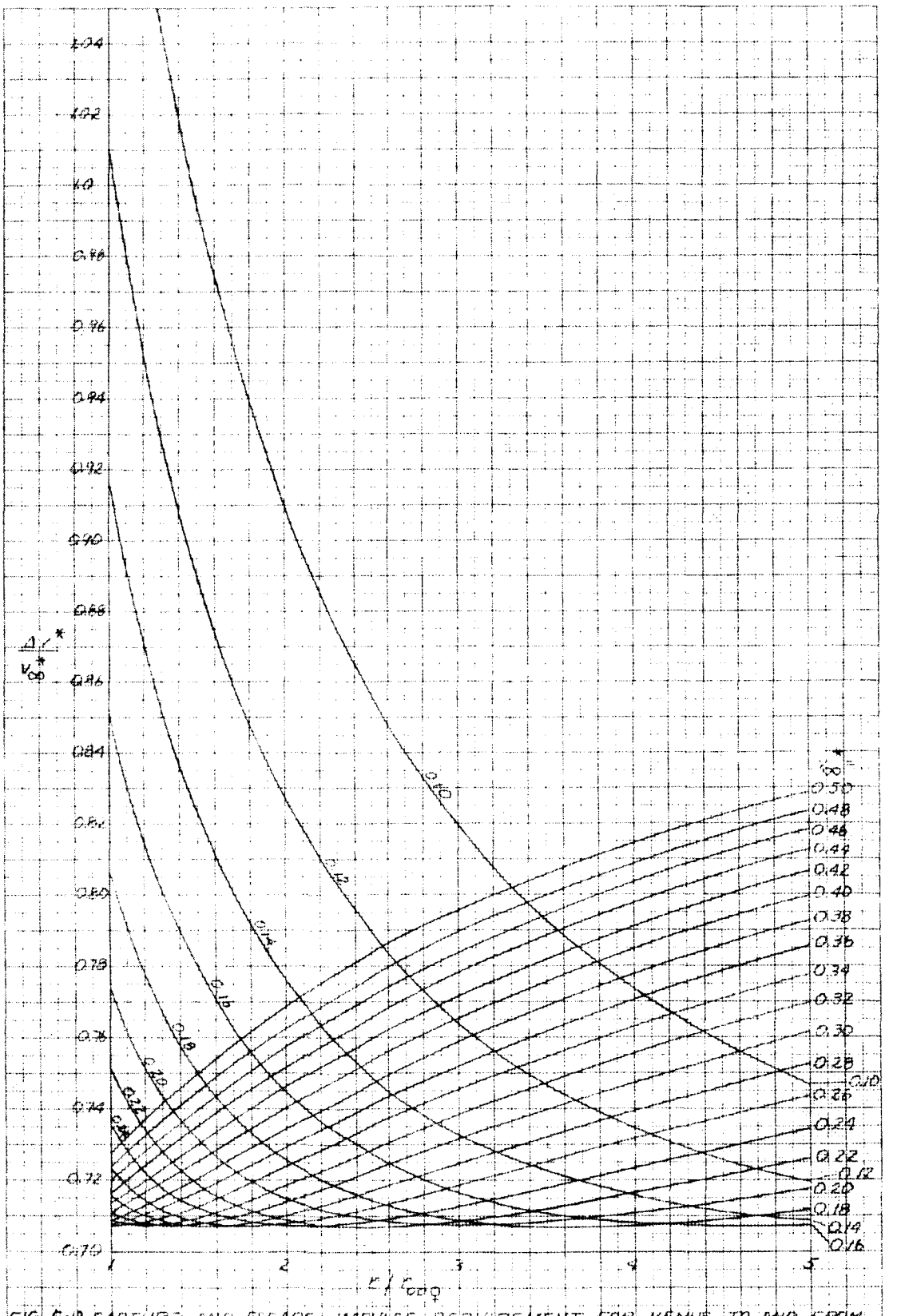

FIG. 5-12 CAPTURE AND ESCAPE IMPULSE REQUIREMENT FOR VENUS TO AND FROM CIRCULAR SATELLITE ORBITS AS A FUNCTION OF ORBIT DISTANCE AND HYPERBOLIC EXCESS VELOCITY

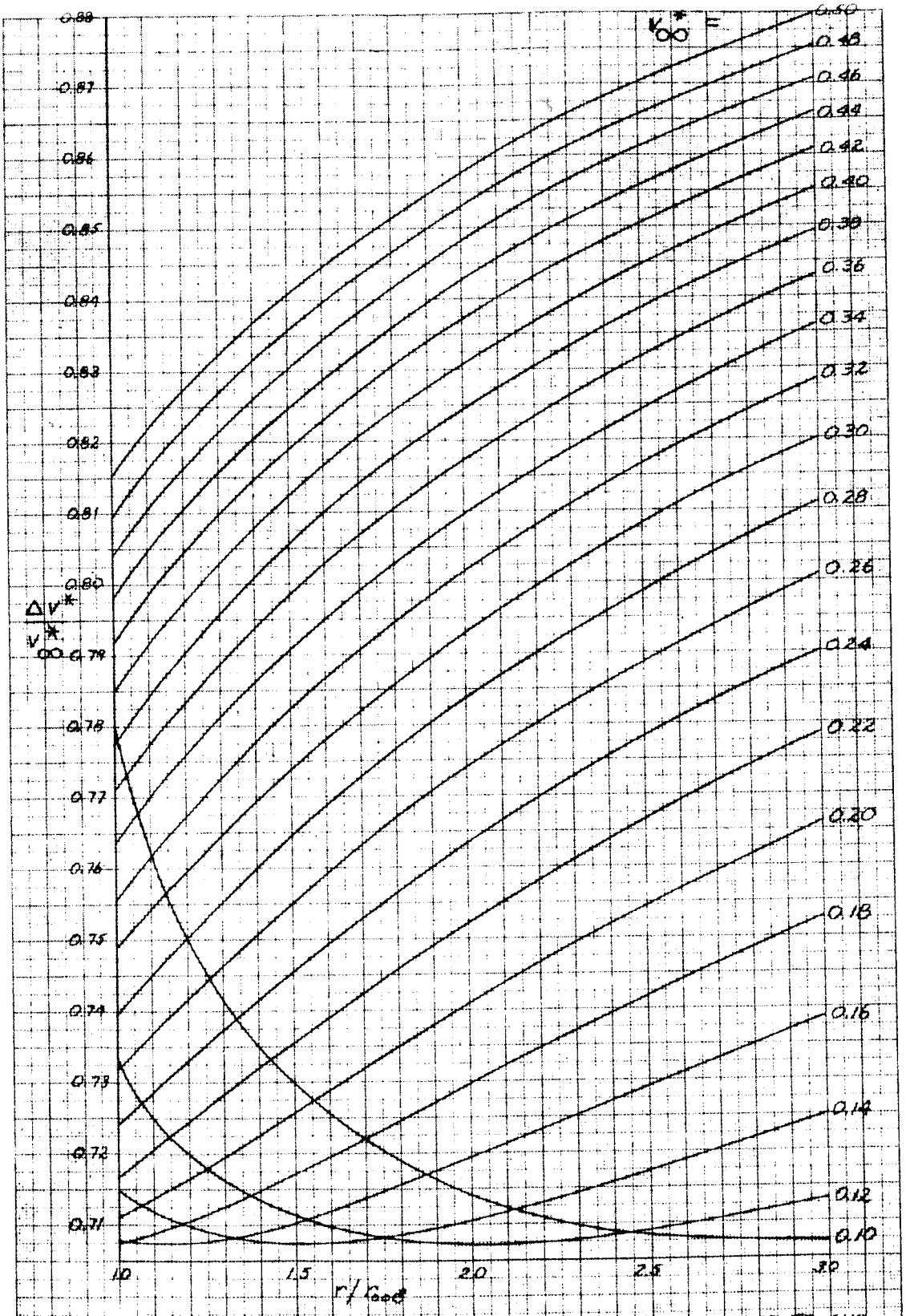

FIG. 5-13 CAPTURE AND ESCAPE IMPULSE REQUIREMENT FOR MARS TO AND FROM CIRCULAR SATELLITE ORBITS AS A FUNCTION OF ORBIT DISTANCE AND HYPERBOLIC EXCESS VELOCITY

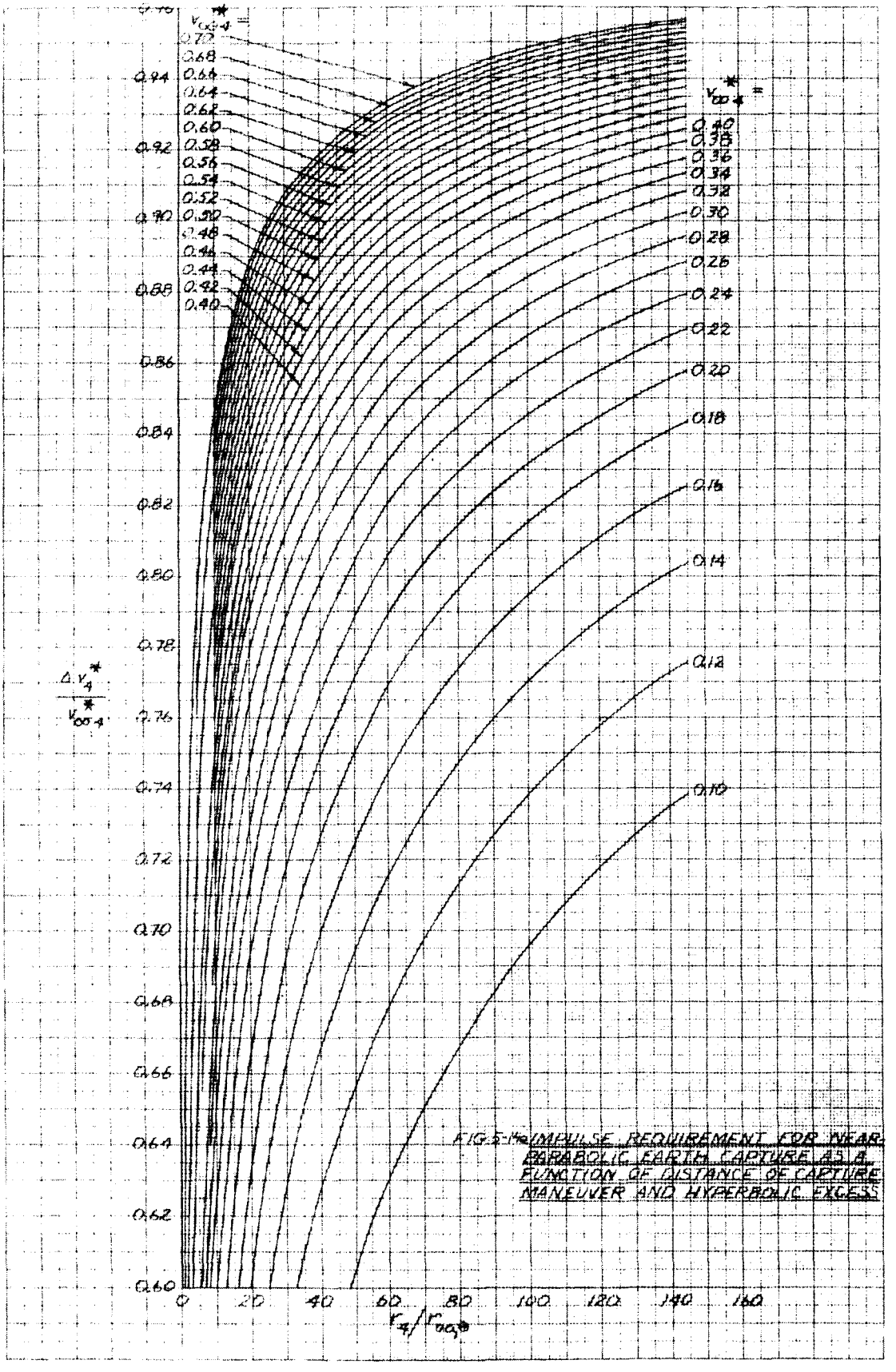

FIG. 5-14 IMPULSE REQUIREMENT FOR NEAR-PARABOLIC EARTH CAPTURE AS A FUNCTION OF DISTANCE OF CAPTURE MANEUVER AND HYPERBOLIC EXCESS

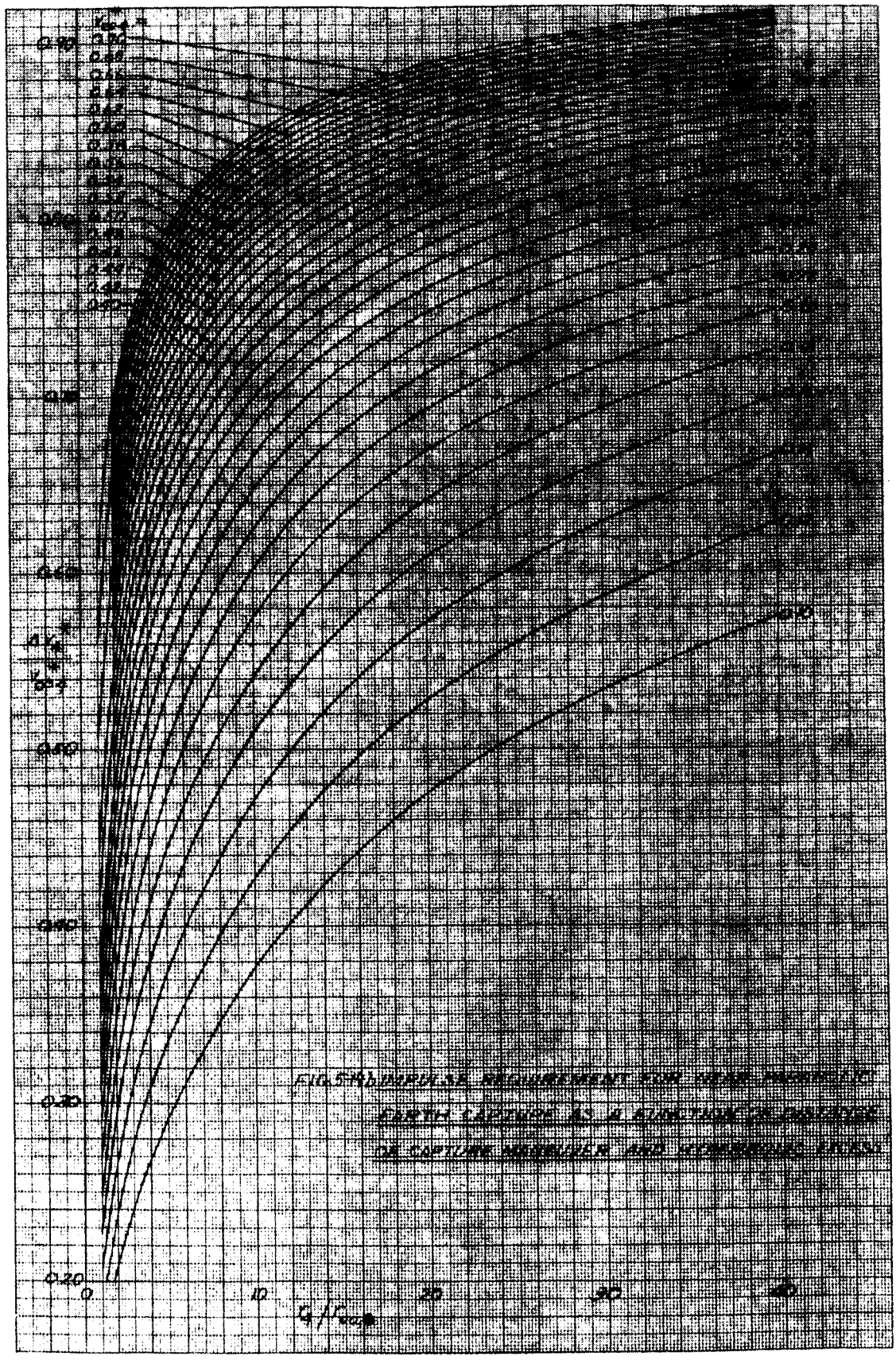

FIG. 5-4b IMPULSE REQUIREMENT FOR OPEN-PROGRADE EARTH CAPTURE AS A FUNCTION OF PARAMETER OF CAPTURE HYPERBOLA AND HYPERBOLIC EXCESS

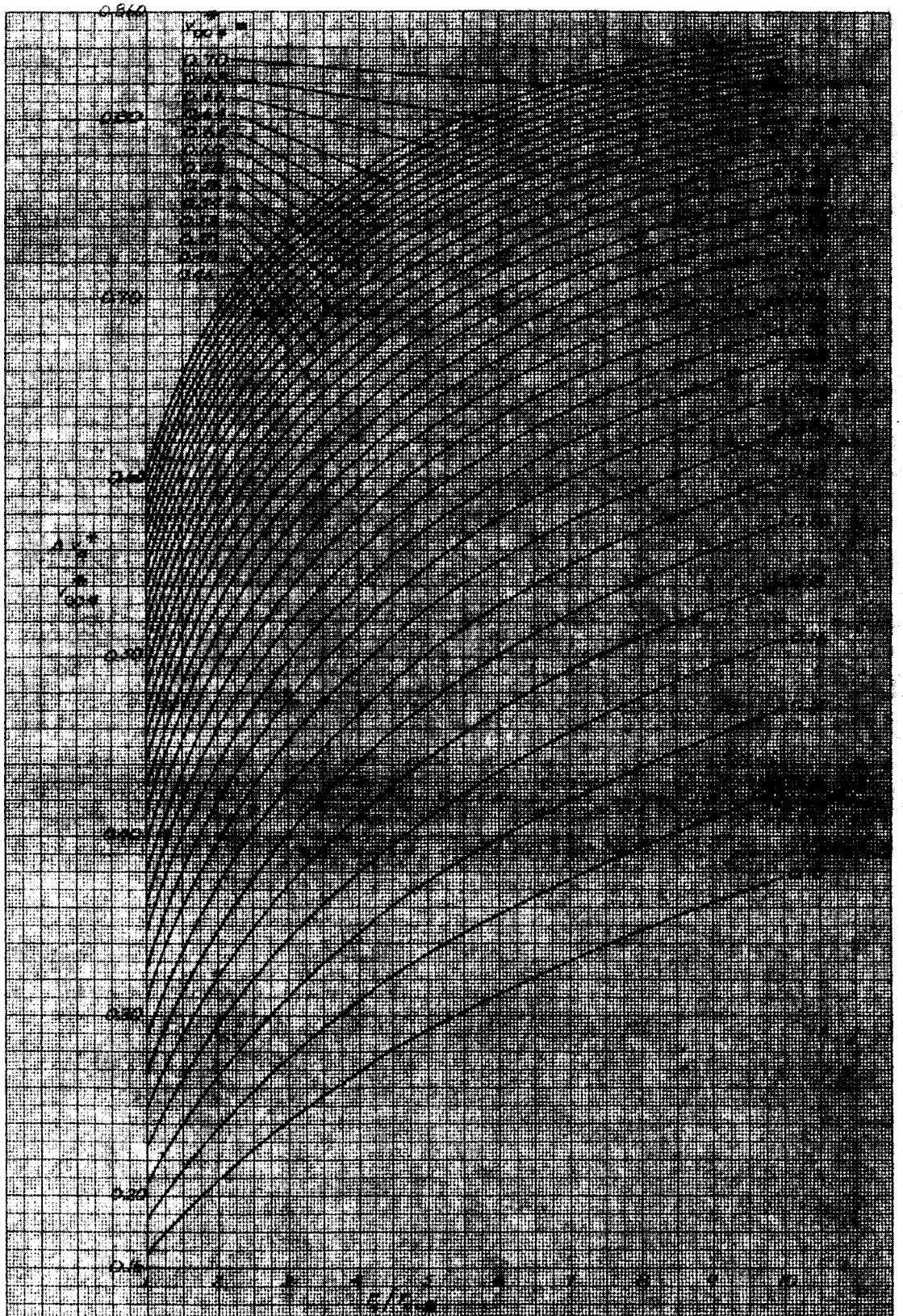

FIG. 5-4. IMPULSE PROPORTIONAL TO ANGULAR MOMENTUM AS A FUNCTION OF DISTANCE IN GRAZING TRAJECTORY AND RETROGRADE PROCESS

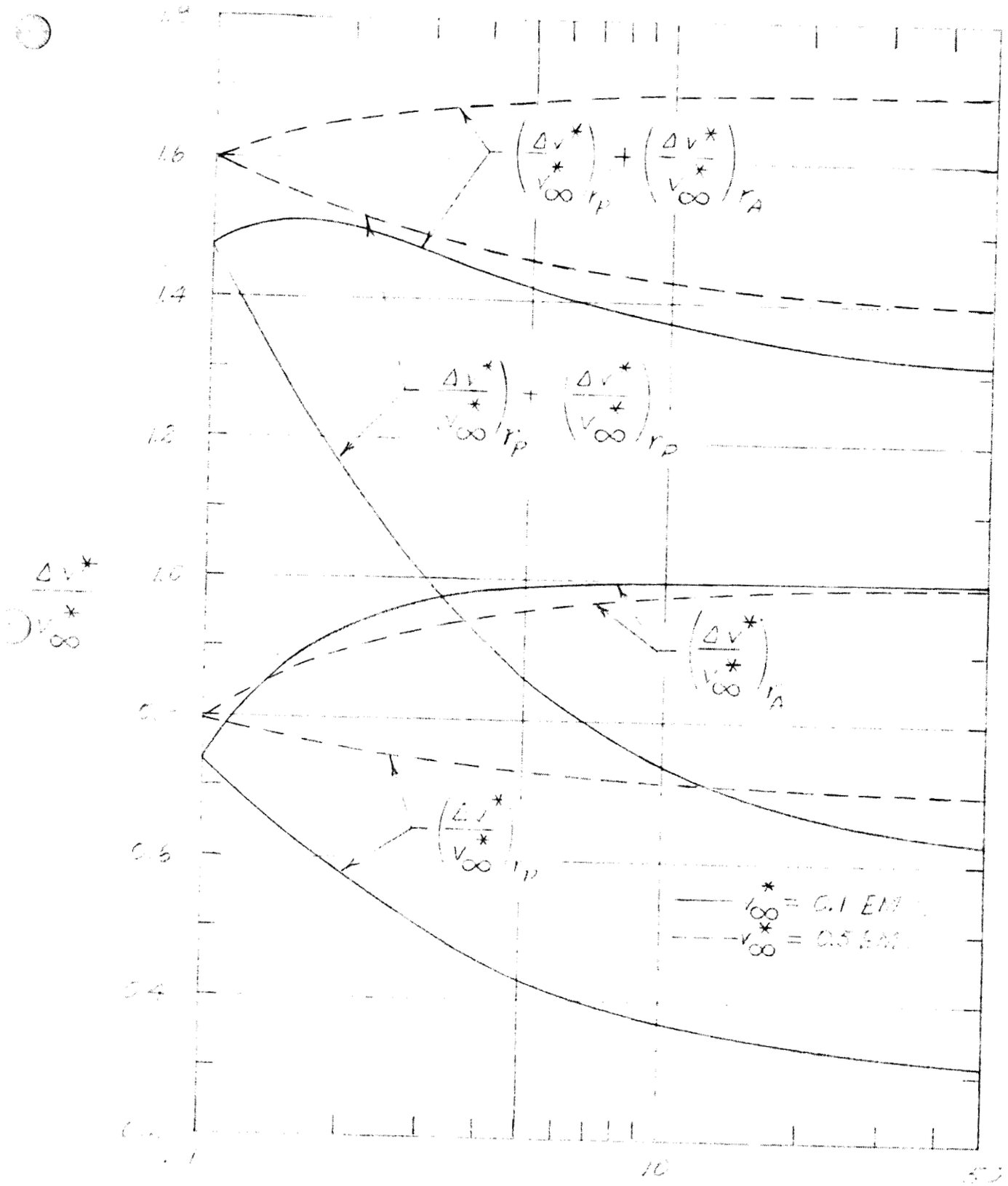

Fig. 5-15 Perigee and Apogee Impulses in an Elliptic Orbit for Capture or Escape Versus v_∞^* for two Values of v_∞^*

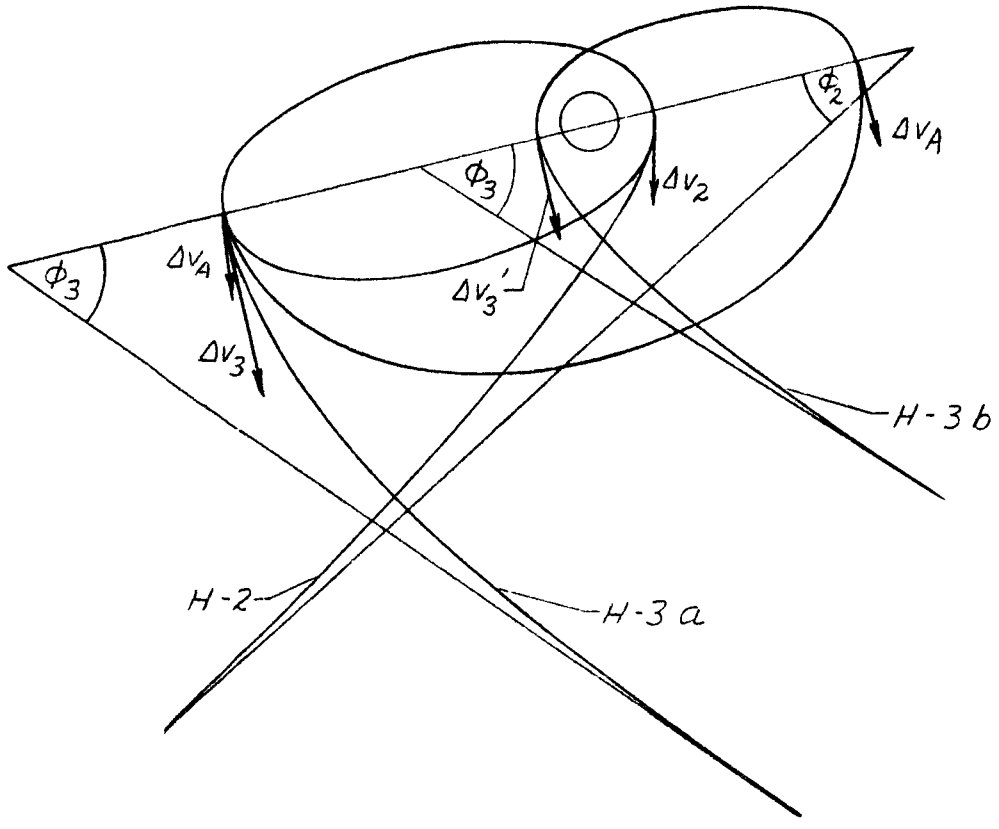

Fig. 5-16 Adjustment of Periapsis for Departure from Elliptic Capture Orbit

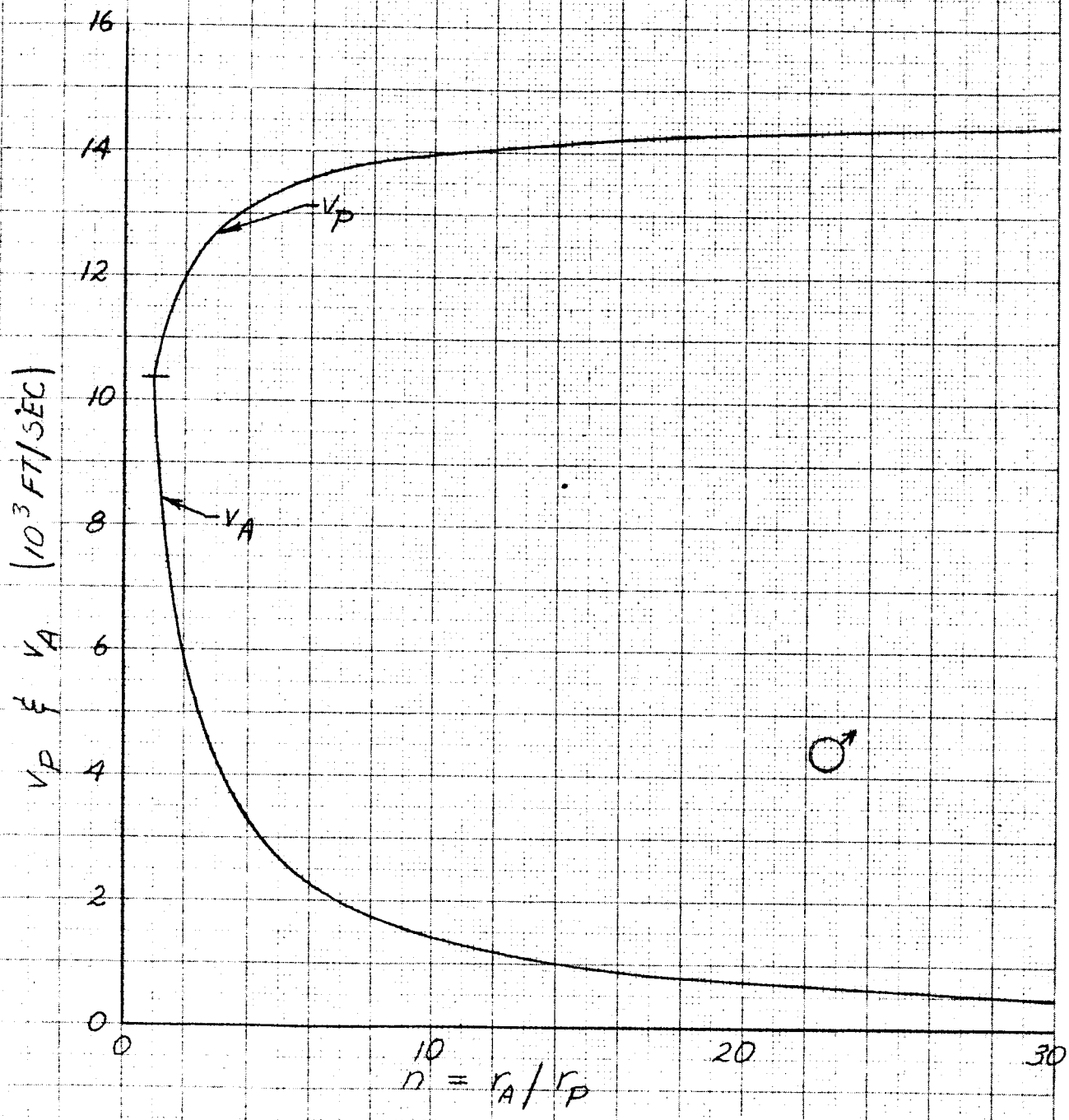

FIG. 5-17 PERIAPSIS AND APOAPSIS VELOCITY IN CIRCUM-MARTIAN ELLIPTIC ORBITS ($r_P = 1.3\, r_{00}$)

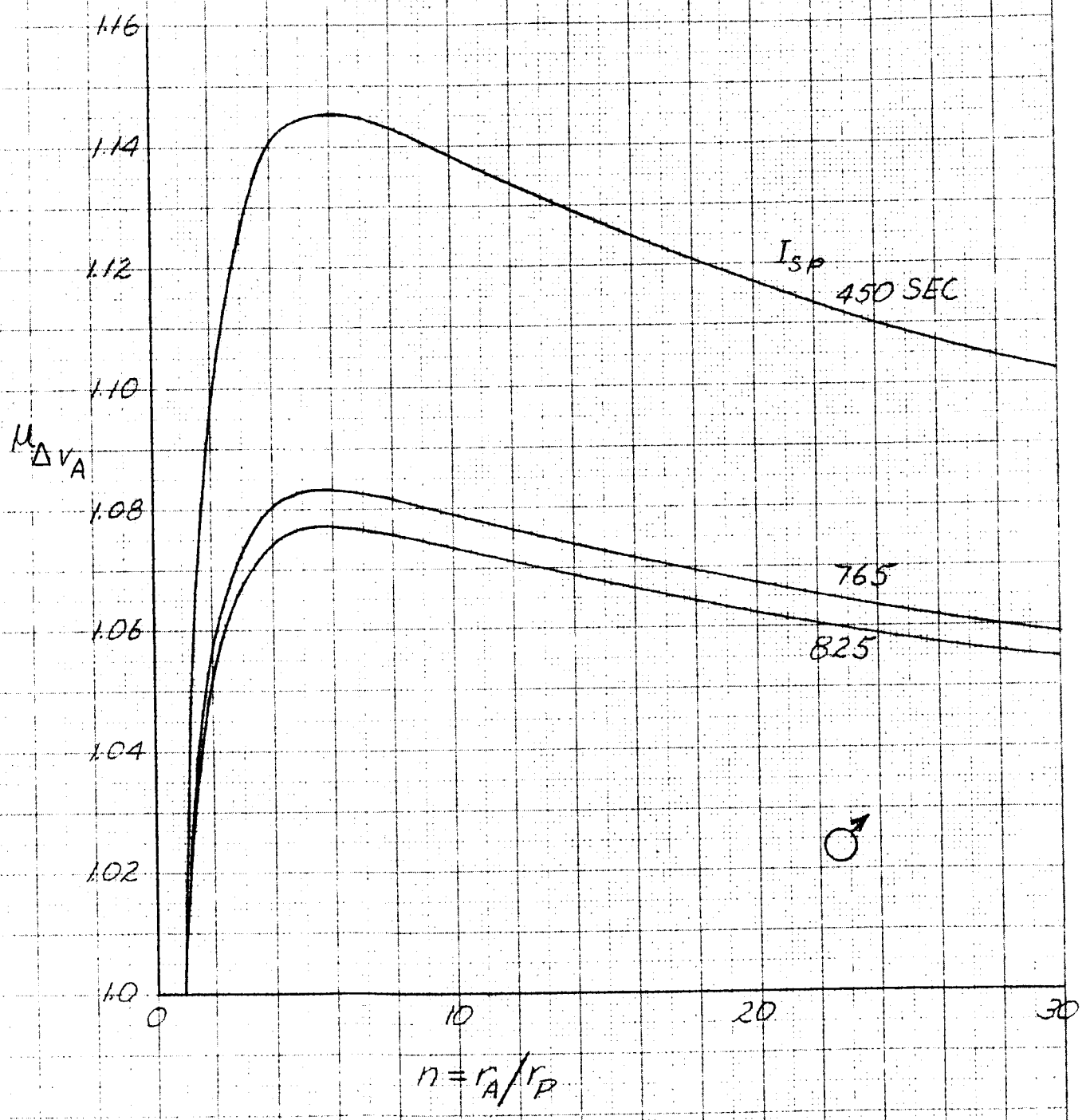

FIG. 5-19 MASS RATIO FOR CHANGE FROM ELLIPTIC TO CIRCULAR ORBIT AT PERIAPSIS DISTANCE

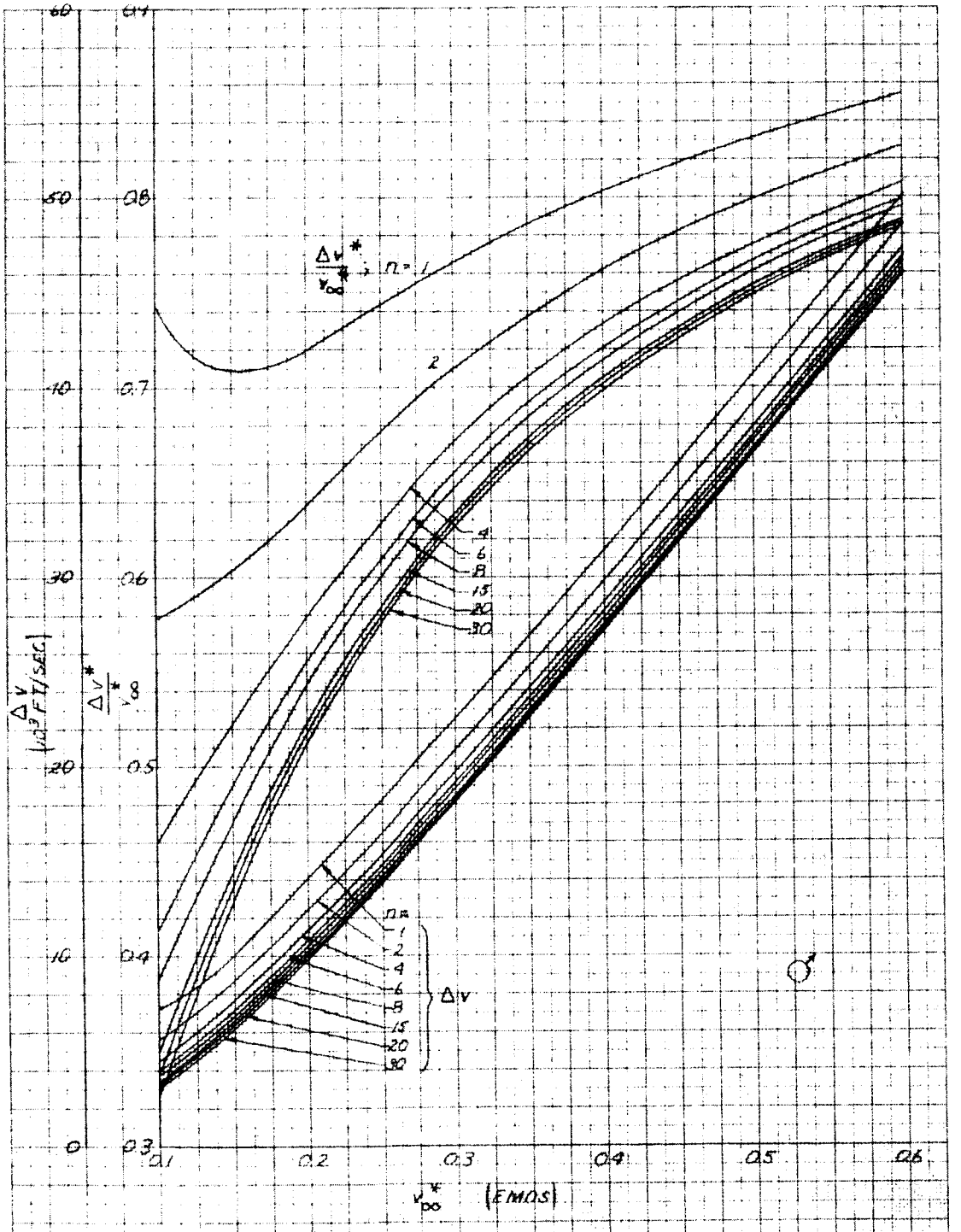

FIG. 5-20 VARIATION OF $\frac{\Delta v^*}{v_\infty^*}$ AND Δv VERSUS v_∞^*

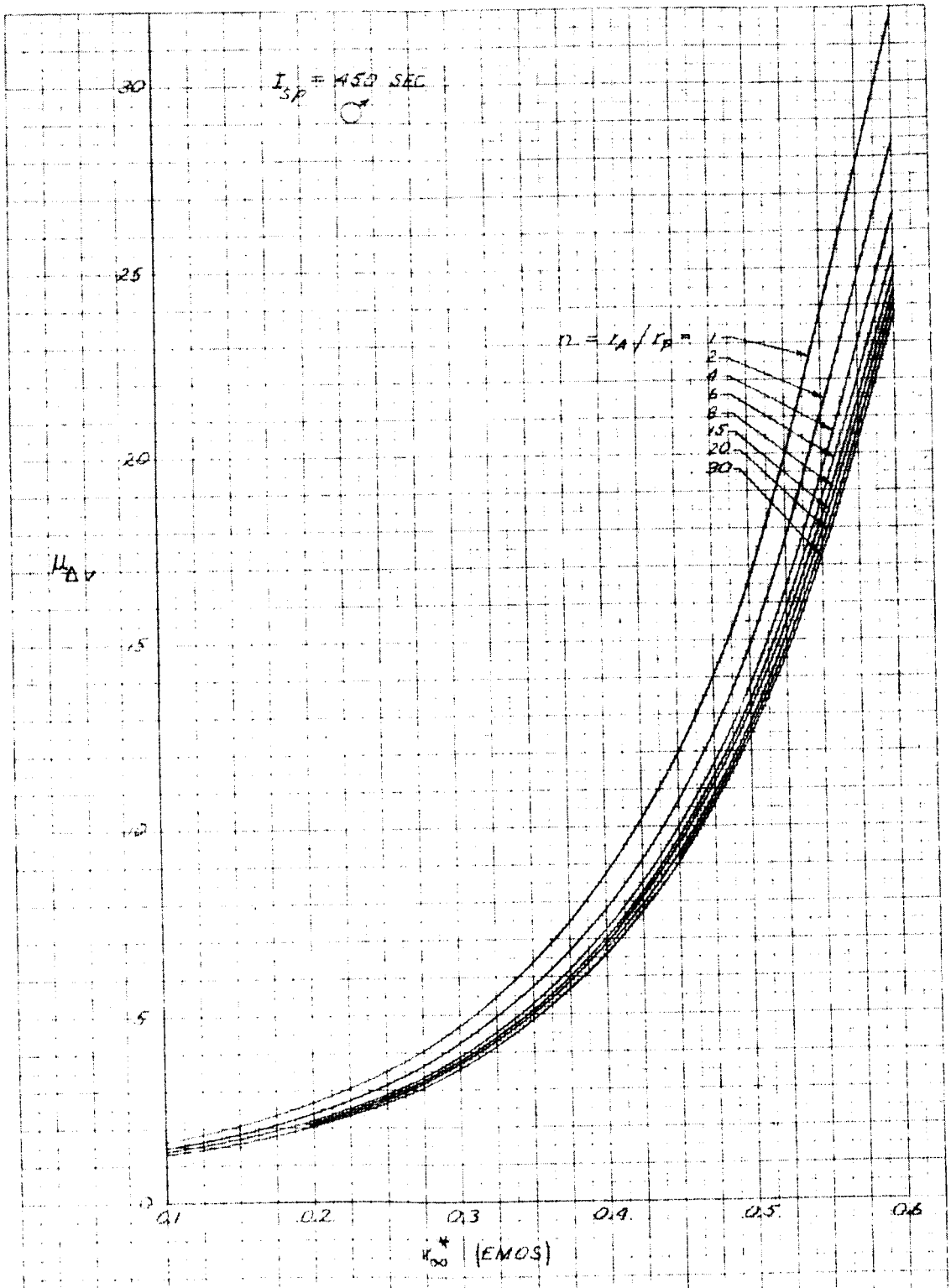

FIG. 5-21 VARIATION OF MASS RATIO FOR CAPTURE MANEUVER VERSUS V_∞^* AND n FOR I_{sp} = 450 SEC

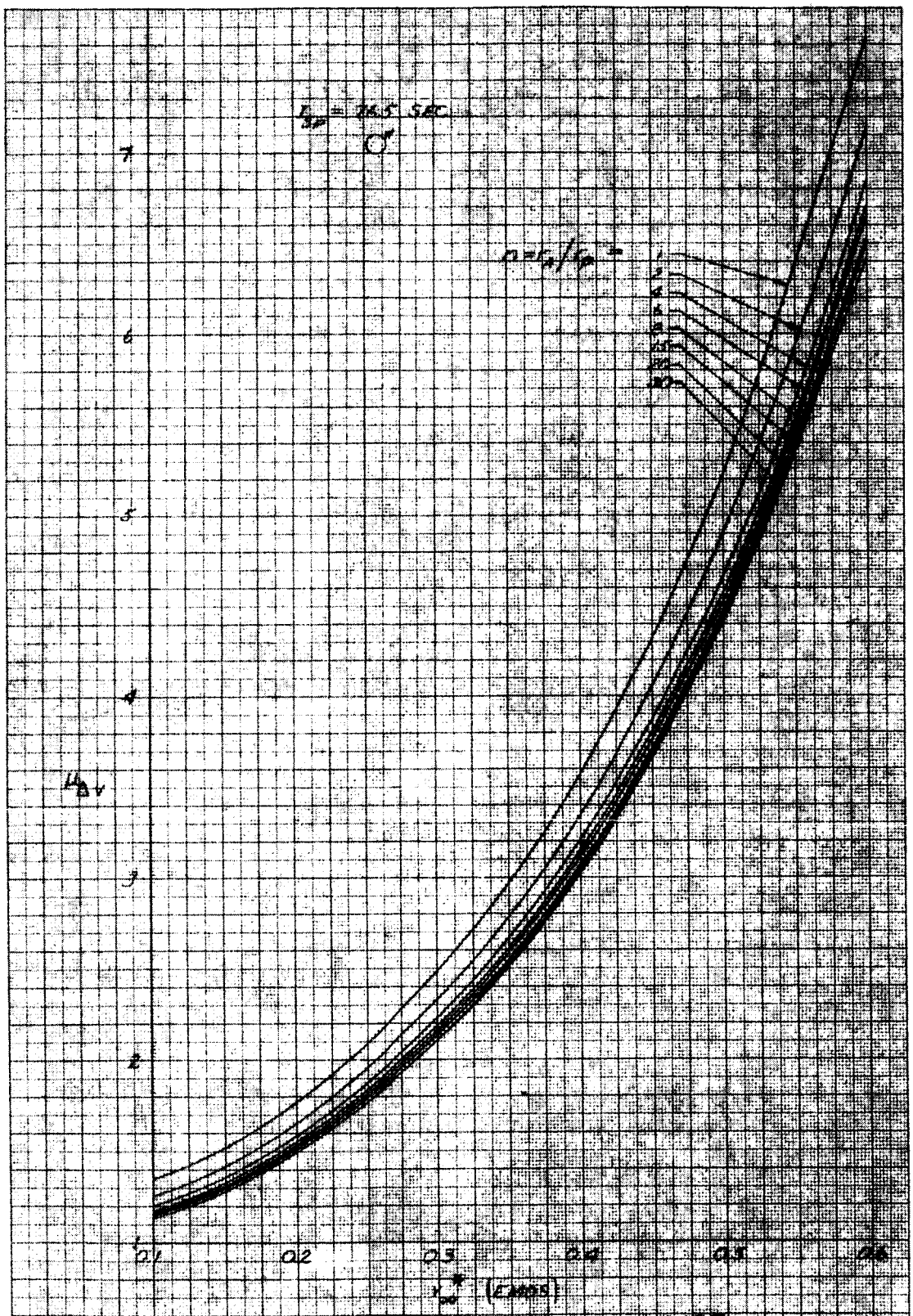

FIG 5-22 VARIATION OF MASS RATIO FOR CAPTURE MANEUVER VERSUS V_∞^* AND n FOR I_{sp} = 76.5 SEC

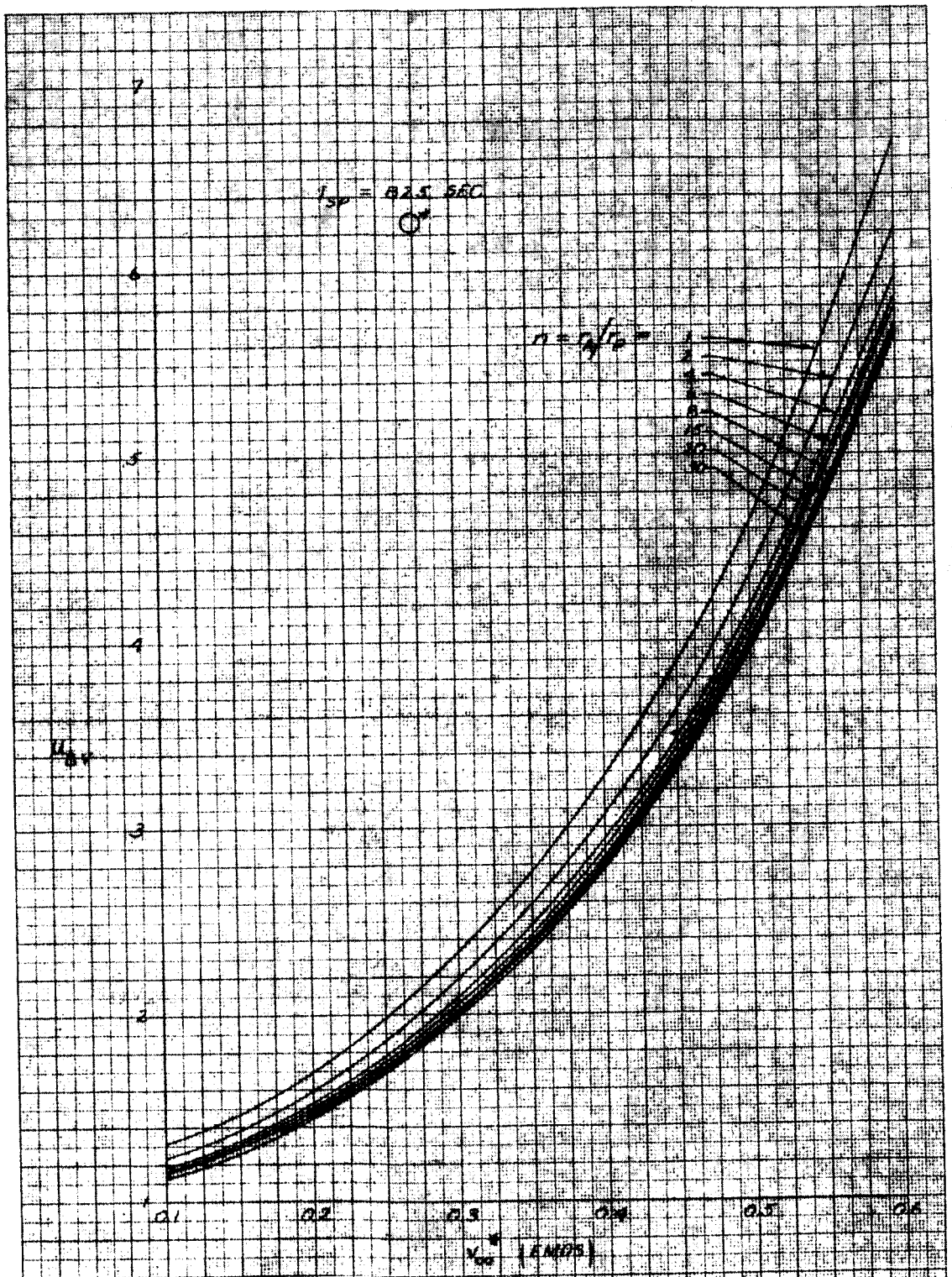

FIG. 5-23 VARIATION OF MASS RATIO FOR CAPTURE MANEUVER VERSUS V_∞^* AND n FOR I_{sp} = 825 SEC

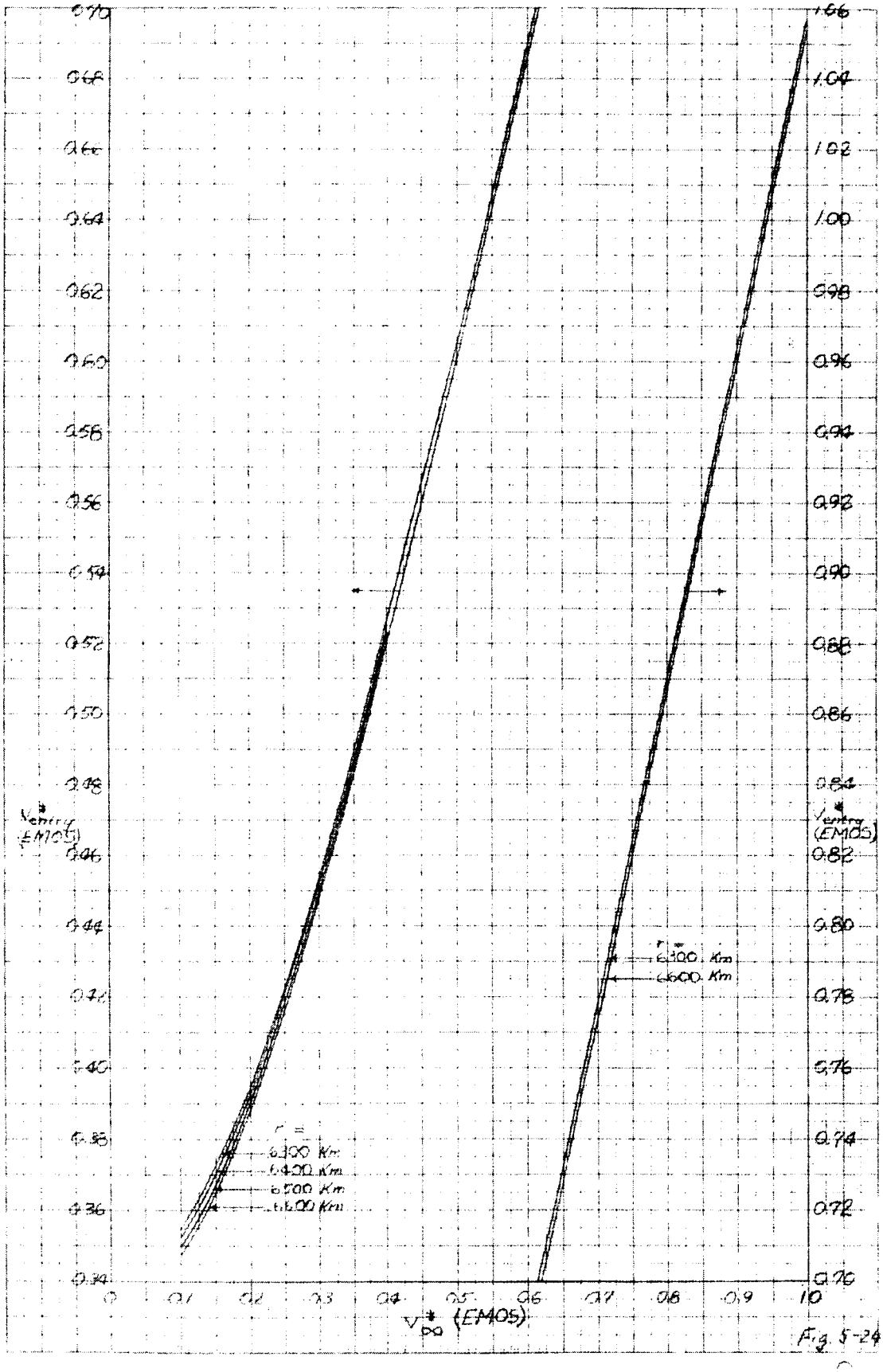
V^*_{entry} (EM05)
V^*_{∞} (EM05)
r =
6100 Km
6200 Km
6300 Km
6400 Km
6500 Km
6600 Km

Fig. 5-24

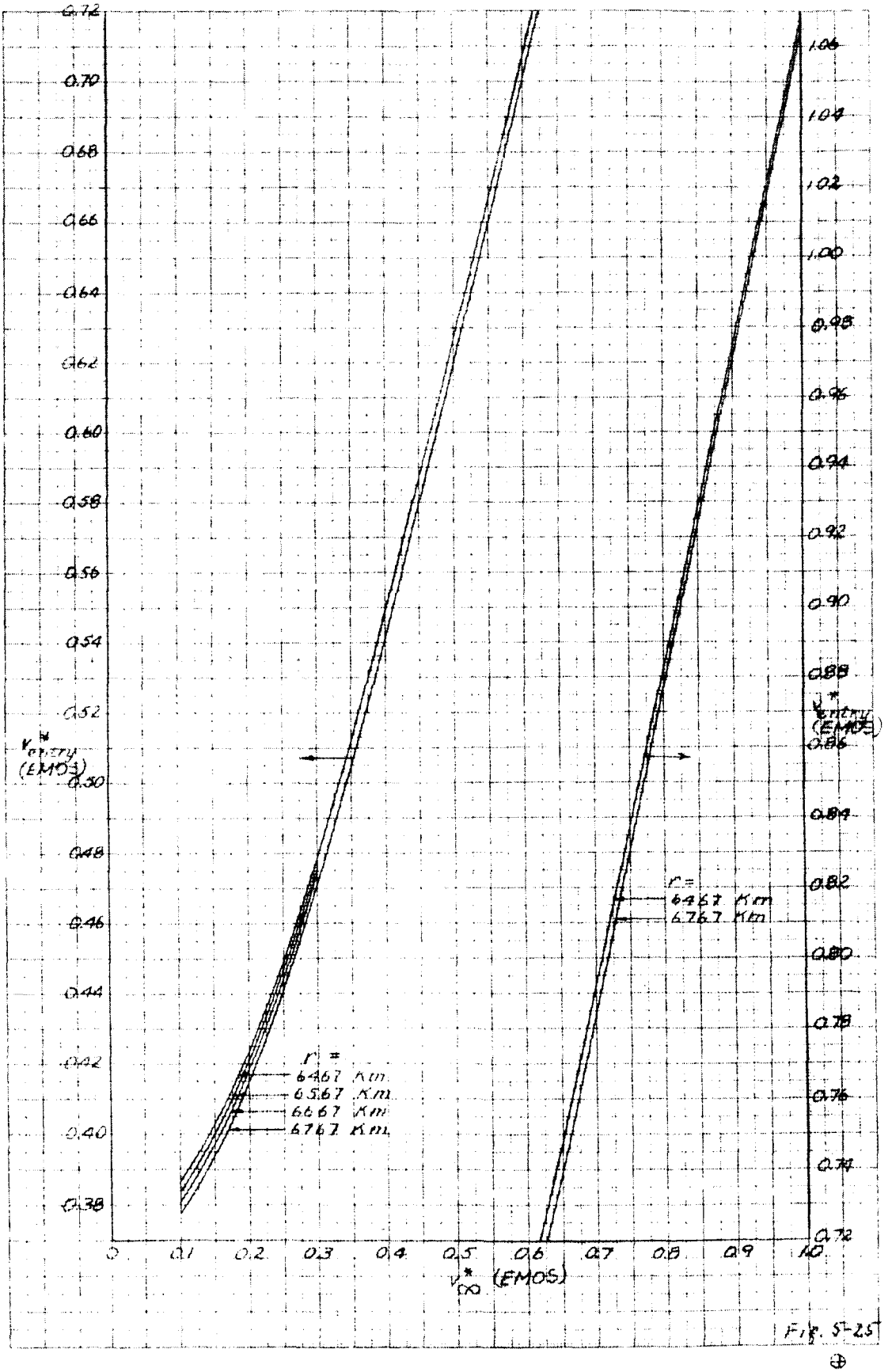
0.72
0.70
0.68
0.66
0.64
0.62
0.60
0.58
0.56
0.54
0.52
0.50
0.48
0.46
0.44
0.42
0.40
0.38
V^*_{entry} (EMOS)
1.06
1.04
1.02
1.00
0.98
0.96
0.94
0.92
0.90
0.88
0.86
0.84
0.82
0.80
0.78
0.76
0.74
0.72
V^*_{entry} (EMOS)
r =
6467 Km
6567 Km
6667 Km
6767 Km
r =
6467 Km
6767 Km
0
0.1
0.2
0.3
0.4
0.5
0.6
0.7
0.8
0.9
1.0
V^*_∞ (EMOS)

Fig. 5-25

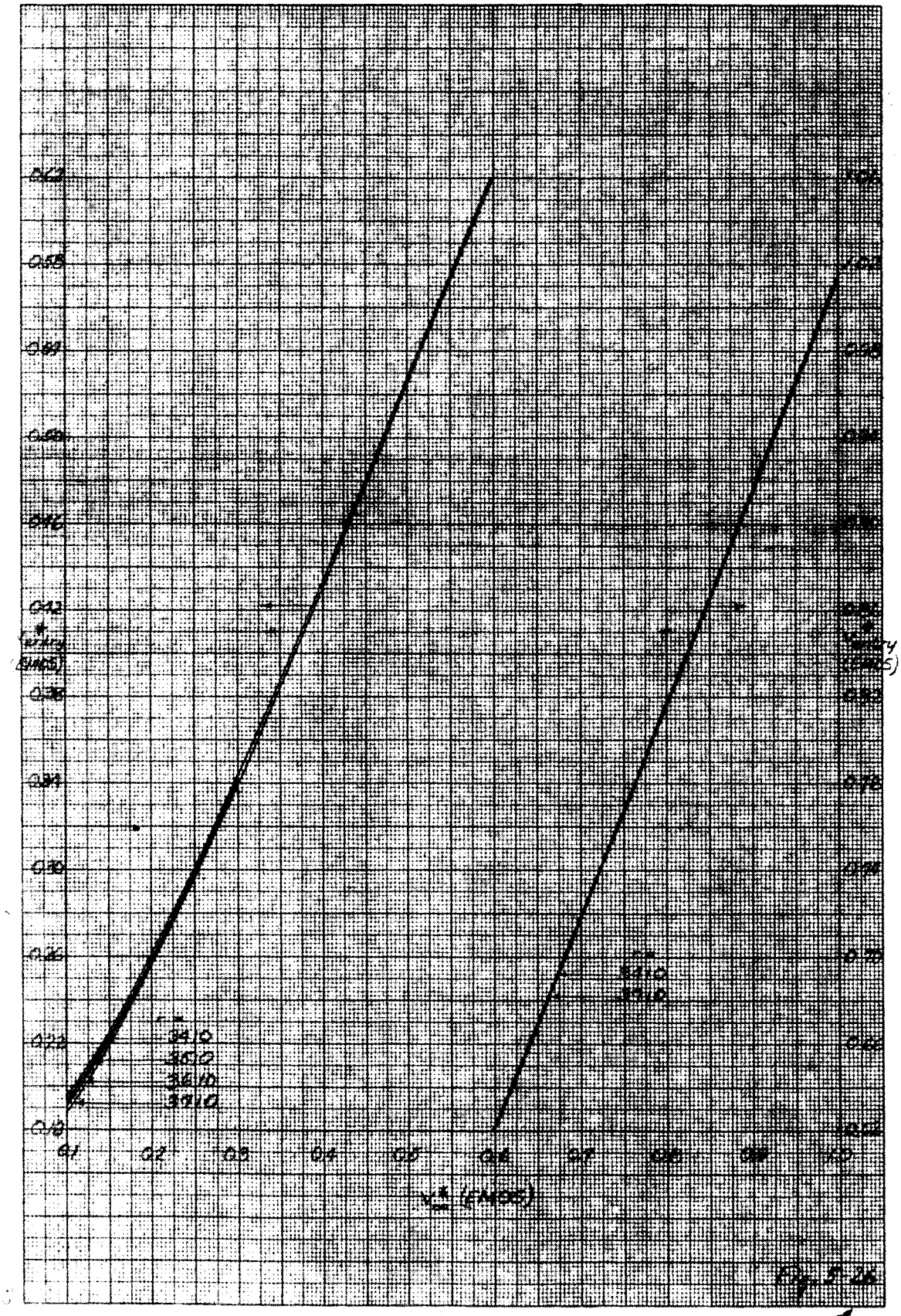

Fig. 5.26

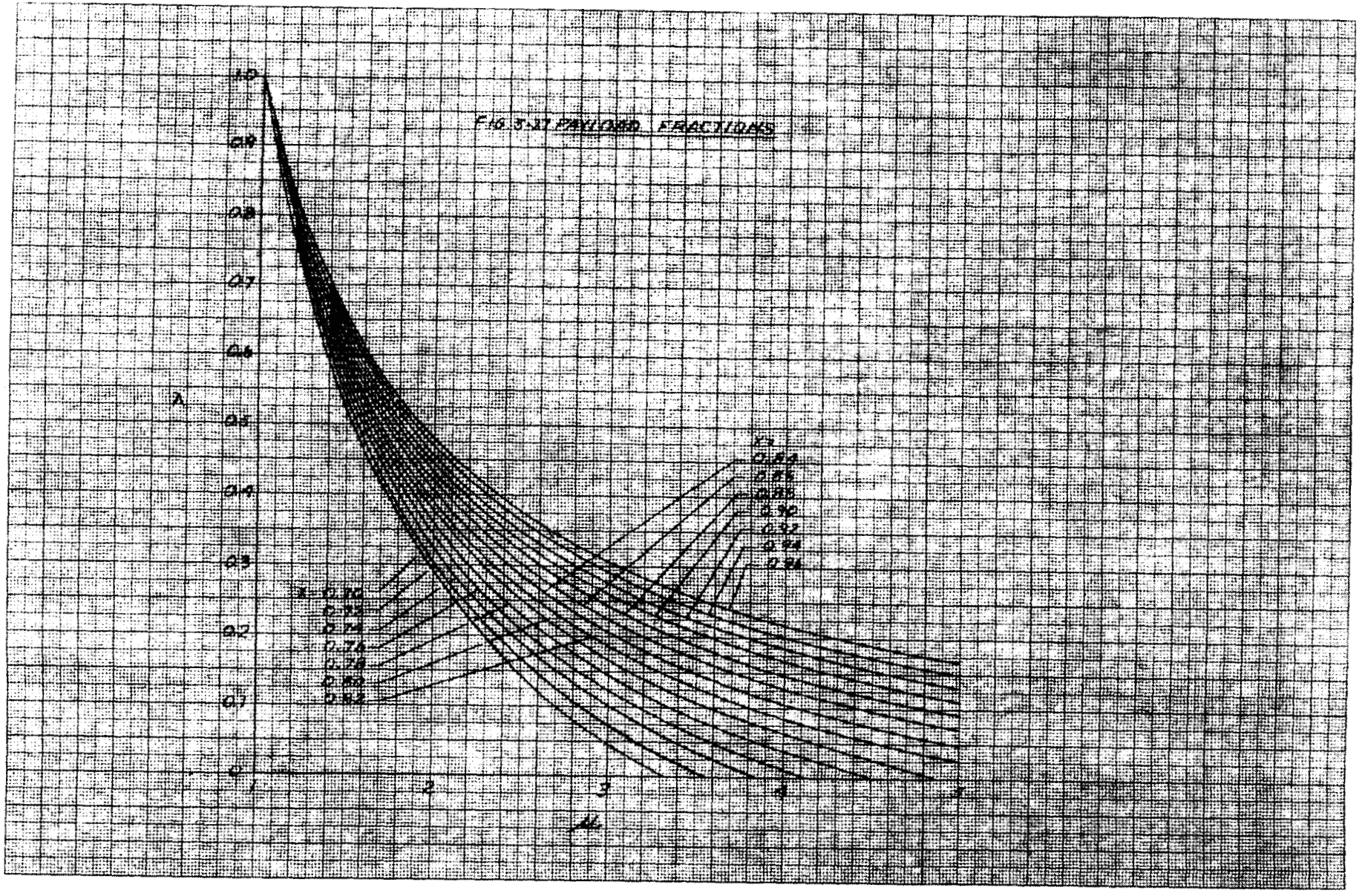

FIG 3-27 PAYLOAD FRACTIONS

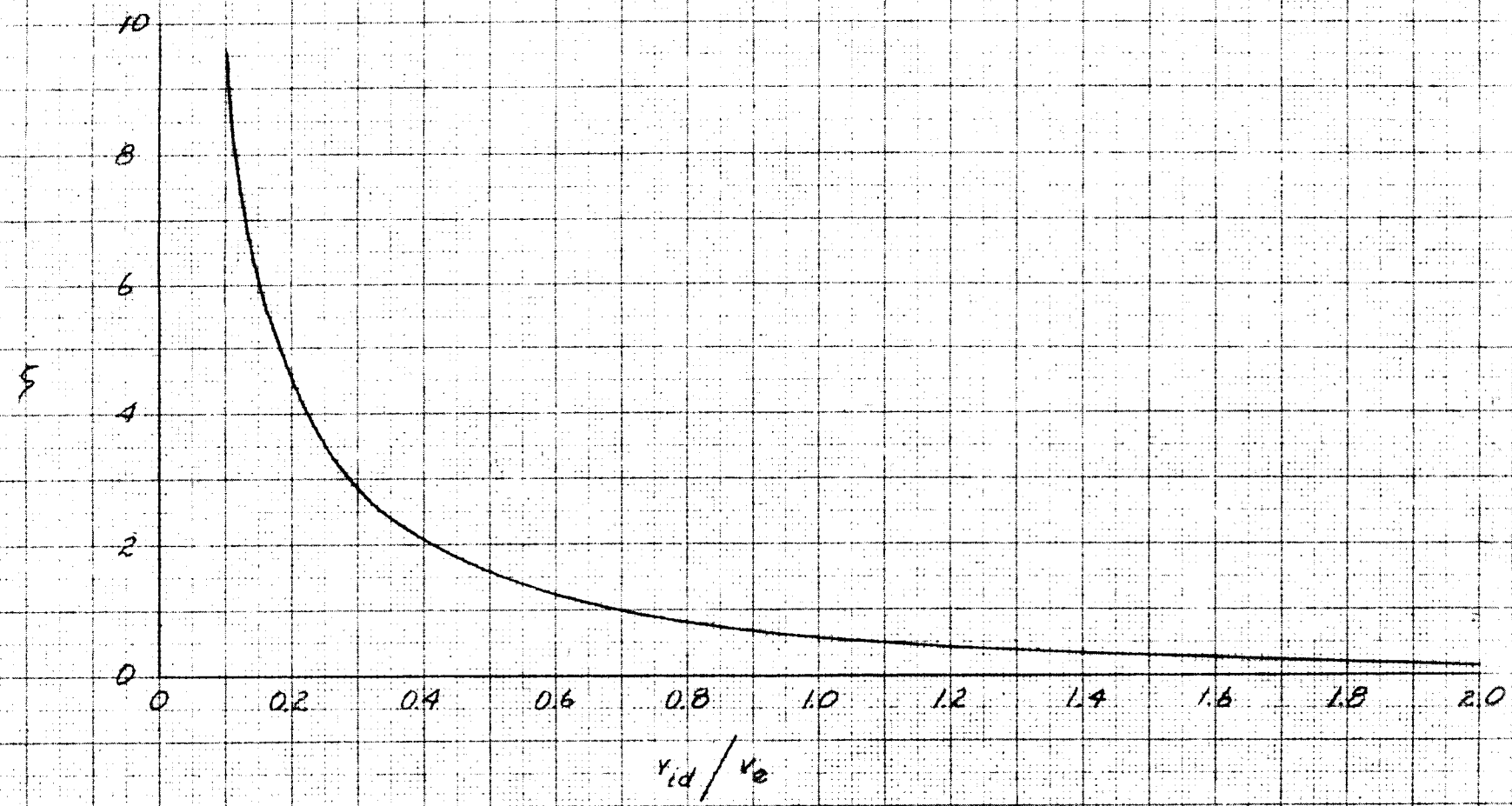

FIG. 5-28 RATIO ζ OF BURNOUT WEIGHT TO IMPULSE PROPELLANT WEIGHT VERSUS RATIO OF IDEAL VELOCITY TO EXHAUST VELOCITY FOR A SINGLE STAGE

10 X 10 TO THE 1/2 INCH 359T-11
KEUFFEL & ESSER CO. MADE IN U.S.A.
ALBANENE

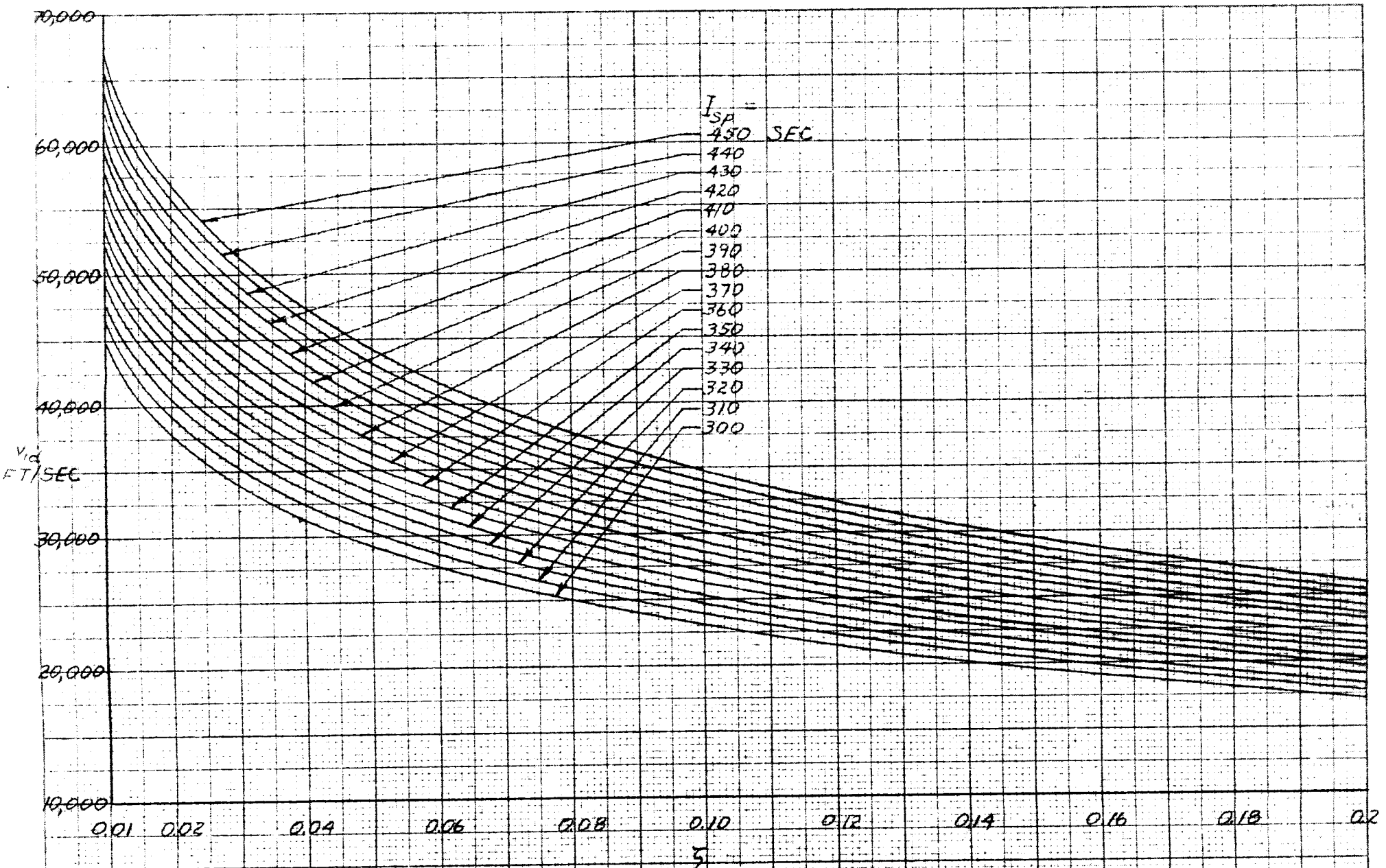

FIG. 5-19 IDEAL VELOCITY VERSUS RATIO ζ OF BURNOUT WEIGHT TO IMPULSE PROPELLANT WEIGHT FOR VARIOUS SPECIFIC IMPULSE VALUES ($300 \leq I_{SP} \leq 450$ SEC)